

Solving Problems of the Standard Model Through Scale Invariance, Dark
Matter, Inflation and Flavor Symmetry

Raymundo Alberto Ramos

Colima, Colima, Mexico

Master of Science, College of William and Mary, 2013
Bachelor of Science, Universidad de Colima, 2010

A Dissertation presented to the Graduate Faculty
of the College of William and Mary in Candidacy for the Degree of
Doctor of Philosophy

Department of Physics

The College of William and Mary
August 2016

©2016
Raymundo Alberto Ramos
All rights reserved.

APPROVAL PAGE

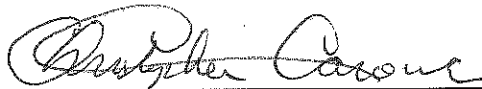
This Dissertation is submitted in partial fulfillment of
the requirements for the degree of

Doctor of Philosophy



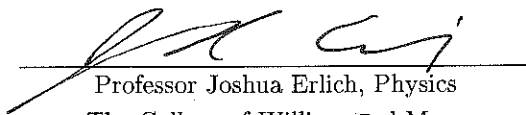
Raymundo Alberto Ramos

Approved by the Committee, May, 2016

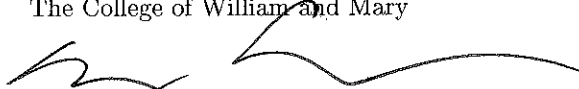


Committee Chair

Professor Christopher D. Carone, Physics
The College of William and Mary



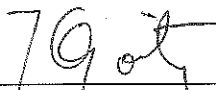
Professor Joshua Erlich, Physics
The College of William and Mary



Professor Marc Sher, Physics
The College of William and Mary



Associate Professor Patricia Vahle, Physics
The College of William and Mary



Professor José Goity, Physics
Hampton University

ABSTRACT

Through beyond standard model formulations we are able to suggest solutions to some of the current shortcomings of the standard model. In this thesis we focus in particular on inflation, the hierarchy of fermion masses, scale invariant extensions and dark matter candidates. First we present a model of hybrid natural inflation based on the discrete group S_3 , the smallest non-Abelian group. The S_3 potential has an accidental symmetry whose breaking results in a pseudo-Goldstone boson with the appropriate potential for a slow-rolling inflaton. The hybrid adjective comes from the fact that inflation is ended by additional scalar fields interacting with the inflaton. At some point during inflation, this interaction forces the additional scalars to develop vacuum expectation values, then they fall to a global minimum and inflation ends. We continue with another inflation model, in this case involving a two-field potential. This potential comes from the breaking of a flavor symmetry, the one that yields the hierarchy of fermion masses. Depending on the choice of parameters, the path followed by the inflaton may or not reach a point where inflation ends by a hybrid mechanism. For every model presented we study the field content and the parameters to demonstrate that there are solutions that follow the constraints from current experimental observations. Then we move to classically scale invariant extensions of the standard model. We proceed with a model where one-loop corrections break a non-Abelian gauge symmetry in a dark sector. This breaking provides an origin for the electroweak scale and gives mass to the gauge multiplet. For some parameter regions this massive gauge boson is a dark matter candidate. To finish, we also develop a model where we employ strong interactions in the dark sector. The particular dynamics of this model set the electroweak scale and generate a massive pseudo-Goldstone boson appropriate for dark matter.

TABLE OF CONTENTS

Acknowledgments	iv
Dedication	v
List of Tables	vi
List of Figures	vii
Chapter	
1 Introduction	1
1.1 The Standard Cosmology	5
1.1.1 Dynamics of the FRW Metric	7
1.1.2 The Cosmic Microwave Background	9
1.2 Inflation	10
1.2.1 The Horizon Problem	10
1.2.2 The Flatness Problem	13
1.2.3 Inflation by Slow-Rolling Fields	14
1.3 Dark Matter	18
1.3.1 WIMP Dark Matter	19
1.3.2 Annihilation in the Early Universe	20
1.3.3 Freeze-Out	22
1.3.4 Direct Detection	25
2 A Permutation on Hybrid Natural Inflation	27
2.1 Introduction	28
2.2 The Group S_3	31

2.3	The Model	33
2.4	Inflation Parameters	37
2.5	Numerical Analysis	39
2.6	Enhancing Primordial Gravity Waves	42
2.7	Inflation Shut-off and Reheating	46
2.8	Conclusions	48
3	Flavored Axion-Monodromy inflation	50
3.1	Introduction	51
3.2	Inflationary Trajectories	57
3.2.1	Termination Without a Waterfall.	57
3.2.2	Termination With a Waterfall.	63
3.3	Models	65
3.3.1	Origin of the Potential	65
3.3.2	Standard Model Flavor	69
3.4	Conclusions	72
4	Classical Scale-Invariance, the Electroweak Scale and Vector Dark Mat- ter	73
4.1	Introduction	74
4.2	The Model	78
4.3	Phenomenological Constraints	81
4.4	Vector Dark Matter	86
4.5	Conclusions	90
5	Dark Chiral Symmetry Breaking and the Origin of the Electroweak Scale	92
5.1	Introduction	93
5.2	The Model	95

5.3	Phenomenological Constraints	100
5.4	Dark Matter	104
5.5	Conclusions	107
Appendix A		
	RGEs	108
Appendix B		
	Discrete Gauge Symmetries, Briefly	110
Vita	128

ACKNOWLEDGMENTS

First, I would like to thank my adviser Dr. Christopher D. Carone for all the helpful discussions, guidance and confidence. I would like to thank all the professors in the high-energy theory group, Dr. Joshua Erlich and Dr. Marc Sher for their contributions to this work and my formation as a scientist.

I would like to say thanks to Dr. Alfredo Aranda, who introduced me to the theory of particles and fields. His teaching and enthusiasm for physics started me in this path.

I wish to extend my gratitude to my parents, Rafaela and Raymundo, for providing me with unconditional support and being always attentive, even when they were not clear about my future and when harder times befell us. Finally, I thank my wife Jazmín; her support and constant cheering have certainly helped me to get to this point.

To the loving memory of Rafaela Anguiano.

LIST OF TABLES

3.1	\mathbf{Z}_{21}^Φ charge assignments q , where the group transformation is defined by $\exp(2i\pi q/21)$. The Higgs doublet is a singlet under the flavor symmetry.	70
4.1	Sample points with $\Omega_D h^2 = 0.1138$, the central WMAP value [10] used in Fig. 4.3. All points shown have an elastic scattering cross section $\sigma(AN)$ below the current Xenon100 direct detection bounds [21].	90

LIST OF FIGURES

1.1	Effective interaction between dark matter and nucleons caused by the Higgs coupling with dark matter.	25
2.1	The Lyth bound is evaded if the inflaton slowly rolls from a steep point in the potential to near the minimum before the waterfall fields turn on.	44
3.1	Path followed by the inflaton during 60 e-folds of inflation corresponding to the solution of Sec. 3.2.1, in units where $M_* = 1$. The background is a density plot where darker zones have lower values of the potential than lighter ones.	62
3.2	Inflaton trajectory, in ρ - θ space, overlaid on a contour plot of the potential, in units where $M_* = 1$. The bottom of the trench is indicated by the thick red line while the inflation trajectory is denoted by the thin green line.	66
4.1	Regions of the g_D - λ_p plane that are consistent with the perturbativity and vacuum stability constraints discussed in the text. In (a), $m_\eta < m_h$, while in (b), $m_\eta > m_h$. The regions above and to the right of the dashed line in (a) and above the dashed line in (b) correspond to $\sin^2 \theta > 0.1$	83
4.2	Dark gauge boson annihilation diagrams included in the relic density estimate presented in the text.	87
4.3	Band where the dark gauge multiplet provides the dark matter relic density within $\pm 2\sigma$ experimental uncertainty.	88

- 5.1 Regions of the parameter space consistent with perturbativity and stability constraints, as well as $\sin^2 \theta < 0.1$. Points above the solid black line are consistent with approximate dark sector chiral symmetry. Two branches of points correspond to $m_\eta > m_{h_0}$ (upper branch) and $m_\eta < m_{h_0}$ (lower branch). The triangular points in the upper branch are consistent with current dark matter constraints. 103
- 5.2 Dark pion-nucleon elastic scattering cross section for the points within the dark-matter-preferred band of Fig. 5.1. The current bounds from LUX [20] and XENON100 [21] are also shown. . . . 106

Chapter 1

Introduction

The current scientific consensus is that the universe started with the Big Bang. According to the 2015 results from the Planck satellite, the universe is 13.8 billion years old [1]. It is well known that the universe has been subject of study through history. However, modern cosmology started to take shape with the development of general relativity, by Albert Einstein in 1917. A number of later events shaped cosmology as we know it. In 1927, George Lemaître proposed that the universe may have originated in a violent explosion, called the *Big Bang*. This explosion would result in an universe where objects keep moving apart from each other. Such a movement would be observable as a shift to the red color in the light we receive from astronomical objects. The analysis of data on several galaxies allowed Edwin Hubble to discover this red shift in 1929. More evidence in favor of the Big Bang came in 1965 with the discovery of the cosmic microwave background radiation (CMB) by Arno Penzias and Robert Woodrow Wilson [2]. The CMB is a prediction of the Big Bang theory. It is made up of the photons that scattered at the time neutral atoms started to form.

The CMB study raised a number of new questions. Observations found that the CMB is homogeneous to a high degree of precision. However, as we will see in this chapter, big bang cosmology (BBC) indicates that the different regions of the CMB were causally disconnected at the time it formed. We call this the *horizon problem*. Moreover, measurements indicate that the current universe is nearly flat [1], while predictions indicate that its curvature should have deviated to an open or a closed universe over time. The observed flatness requires an extremely fine-tuned initial total density. This is what we know as the *flatness problem*. In 1980, Alan Guth [3] proposed a solution to these problems. His idea was to include an epoch of exponential growth of the universe. This inflationary universe would put regions in causal contact at the time the CMB was formed and would naturally lead to a flat universe. Guth's original idea was that the universe supercooled in a false vacuum state and after sometime it tunneled to the true vacuum. However, this formulation does not allow for appropriate reheating, the mechanism by which the standard model particles come to fill the universe. A solution to this problem was later presented by Andrei Linde [4] and independently by Andreas Albrecht and Paul Steinhardt [5]. The new approach was to have a scalar field, the *inflaton*, spend some time rolling slowly towards a minimum of its potential. This is known as *slow-roll inflation*. The clearest indication of inflation would be the presence of effects from the big bang's gravitational waves on the CMB. Although typical gravitational wave effects are small, in this case, the exponential growth during inflation should boost their presence. The search for this effects is still active. In Sec. 1.2 we will discuss more about the BBC problems, their solution and some more details about inflation.

In Chapters 2 and 3 we will formulate models of slow-roll inflation, with focus on a particular formulation called natural inflation. In this type of inflation, an accidental symmetry naturally creates a flat potential. Explicit breaking of the symmetry results in an axion with an effective potential appropriate for slow rolling inflation. The success of this type of inflation is the natural appearance of a flat potential. The complication comes from the fact that a very high scale for the symmetry breaking may be required to achieve enough inflation. We alleviate this by considering extra scalar fields that interact with the axion, modifying its dynamics. The extra fields create a waterfall potential that interferes with the rolling and ends inflation.

In Chapter 2 we will present a model based on the discrete symmetry group S_3 , the smallest non-Abelian discrete group. This will result in an accidental $SO(2)$ symmetry, broken by small S_3 invariant terms. The presence of extra fields will end inflation by waterfaling. In Chapter 3 we will move further and propose a way to embed inflation in a flavor symmetry model. Flavor symmetries attempt to explain the patterns displayed by the Yukawa couplings of fermions. The flavons, the fields responsible for the flavor symmetry breaking, will yield two Goldstone bosons giving rise to an axion-monodromy potential. A linear combination of the two bosons will act as the slow-rolling inflaton. Interestingly, in this model we will have both waterfaling and non-waterfaling solutions, depending on the choice of parameters.

A different problem in BBC that has not yet been resolved is the nature of *dark matter*. In 1937, Fritz Zwicky studied the Coma cluster [6] and found that luminosity and internal rotations were unreliable indicators for the determination of cluster mass. He proposed new methods to determine cluster masses that

allowed one to estimate the contribution from a new component of matter called dark matter.

The current standard model fails to explain the presence of dark matter in the universe, hence the need for propositions beyond the standard model. Weakly interacting massive particles are among the most popular hypothetical candidates for dark matter [7]. They self-annihilate with a strength typical of the weak interaction, for a sufficiently massive particle, this gives the right abundance of dark matter.

In this thesis, we will relate the problem of dark matter to another very well known shortcoming of the standard model: the hierarchy problem. In the current standard model, the radiative corrections to the Higgs boson mass should add up to a very huge mass, with the order of the cutoff of the theory. To obtain the measured ~ 125 GeV the calculation requires fine tuning order-by-order in perturbation theory. Going beyond the standard model provides different solutions to this problem, *e.g.* the presence of partners to cancel the divergences. We will concentrate our efforts on the classically scale invariant option. A classically scale invariant extension of the standard model requires that we forbid all dimensionful terms of the standard model Lagrangian, as well as any higher mass scales. Now the extension should be free of quadratic divergences, provided none originate from Planck-scale physics. In this approach, we still require a way to generate the electroweak scale and the Higgs boson mass.

In Chapters 4 and 5 we use different mechanisms to provide an origin for the electroweak scale and Higgs mass. Both require the addition of new fields, singlets under the standard model that communicate with it through Higgs portal interactions. The two cases provide a dark matter candidate. We will present how

dark matter arises in each model as well as results for their relic abundance and direct detection. In Chapter 4 we will use the Coleman-Weinberg mechanism to break an $SU(2)_D$ gauge symmetry in a dark sector. This results in a non-zero vacuum expectation value for a dark scalar giving mass to the $SU(2)_D$ vector bosons, which are the dark matter candidates of this model. In Chapter 5 we employ chiral symmetry breaking in a dark sector to generate a linear term for a dark scalar in the scalar potential, together with three composite states. One of the composite states is stable and electrically neutral, thus a dark matter candidate.

In the remainder of this chapter, we will present the basic setup needed to understand the part of cosmology relevant for this work. From there we will develop the main features of inflation with special interest in the solutions of the flatness and horizon problems. To finish the introduction on inflation, we will show some details of how scalar fields may drive inflation. Later we will introduce dark matter in a more technical level. We will explain how to calculate its evolution and the possible effects of a special type of dark matter, namely, weakly interacting massive particles. For a more detailed and complete treatment of cosmology and the evolution of the universe we suggest that the reader consult Refs. [8] and [9].

1.1 The Standard Cosmology

The standard model of cosmology assumes that the universe is homogeneous and isotropic on the largest measurable scales. Isotropy is backed by current observations of the temperature of the CMB. We can expect this isotropy to be observable at every other point since we are not at a spot specially favorable for

this measurement. This means that the universe looks the same from every point, thus we conclude that it is homogeneous.

These assumptions are encoded in the Friedmann-Robertson-Walker (FRW) (sometimes Friedmann-Lemaître-Robertson-Walker) metric

$$ds^2 = -dt^2 + a^2(t) \left[\frac{dr^2}{1 - kr^2} + r^2 (d\theta^2 + \sin^2 \theta d\phi^2) \right], \quad (1.1)$$

The spherical coordinates (r, θ, ϕ) are comoving coordinates. We can think about the comoving coordinates as the position objects hold while space stretches between them as the universe expands. The effects of this expansion are factored-out in the scale factor $a(t)$. The parameter k carries the sign of the curvature and it can have the following values

$$k = \begin{cases} 1 & \text{closed universe} \\ 0 & \text{flat universe} \\ -1 & \text{open universe.} \end{cases} \quad (1.2)$$

It is convenient to define the Hubble parameter

$$H \equiv \frac{\dot{a}}{a}, \quad (1.3)$$

which gives the expansion rate of the universe. The inverse of the Hubble parameter is the Hubble time, which sets the time scale for the expansion. A particularly useful definition is the comoving Hubble radius $(aH)^{-1}$, which we will be using later in this section. We can use H to relate the velocity of the most distant

galaxies relative to us with their distance as $v \approx Hd$. This is called the Hubble law.

As the universe expands, the physical distance gets scaled. It is useful to consider a time coordinate that scales by the same factor. Therefore, we define the conformal time as

$$\tau = \int \frac{dt}{a(t)}. \quad (1.4)$$

With this change, the FRW metric is rewritten to

$$ds^2 = a(t)^2 \left\{ -d\tau^2 + \left[\frac{dr^2}{1 - kr^2} + r^2 (d\theta^2 + \sin^2 \theta d\phi^2) \right] \right\}. \quad (1.5)$$

Furthermore, changing coordinates according to

$$r^2 = \Phi_k^2(\chi) \equiv \begin{cases} \sin^2 \chi & k = +1 \\ \chi^2 & k = 0 \\ \sinh^2 \chi & k = -1, \end{cases} \quad (1.6)$$

allows us to rewrite Eq. (1.5) as

$$ds^2 = a(\tau)^2 \left\{ -d\tau^2 + \left[d\chi^2 + \Phi_k^2(\chi) (d\theta^2 + \sin^2 \theta d\phi^2) \right] \right\}. \quad (1.7)$$

1.1.1 Dynamics of the FRW Metric

In the previous subsection we presented the FRW metric, a core component of the standard cosmology. General relativity gives us the tools to derive the

dynamics of the universe. Let's start with Einstein's equations

$$R_{\mu\nu} - \frac{1}{2}Rg_{\mu\nu} = 8\pi GT_{\mu\nu} \quad (1.8)$$

where G is Newton's gravitational constant, $g_{\mu\nu}$ is the metric tensor with μ, ν running over the time-space coordinates, $R_{\mu\nu}$ is the Ricci tensor, R is the Ricci scalar and $T_{\mu\nu}$ is the energy-momentum tensor with elements $T_{00} = \rho$, the energy density; $T_{i0} = T_{0j} = 0$, $T_{ij} = pg_{ij}$, where p is the pressure and g_{ij} is the spatial metric with i, j running over the three spatial coordinates.

With these pieces in hand, two coupled equations can be extracted from Eq. (1.8)

$$H^2 \equiv \left(\frac{\dot{a}}{a}\right)^2 = \frac{8\pi G}{3} \sum_i \rho_i - \frac{k}{a^2}, \quad (1.9)$$

$$\frac{\ddot{a}}{a} + \frac{1}{2} \left(\frac{\dot{a}}{a}\right)^2 = -4\pi G \sum_i p_i - \frac{k}{2a^2}, \quad (1.10)$$

where the i runs over all types of energy and the number of dots denotes the order of the derivatives with respect to physical time. Combining these equations results in the acceleration equation

$$\frac{\ddot{a}}{a} = -\frac{4\pi G}{3} \sum_i (\rho_i + 3p_i). \quad (1.11)$$

Equations (1.9) and (1.11) are known as the Friedmann equations. Note that Eq. (1.9) contains the rate of increase of the scale factor on the left-hand side, relating it to the total density of energy in the universe.

1.1.2 The Cosmic Microwave Background

We call the radio waves that fill the universe cosmic microwave background (CMB). This background is what remains of the original heat of the big bang. When the formation of electrically neutral atoms started, photons were able to travel free across the universe. This event is called recombination. The CMB is the radiation that arrives to us from this moment in the life of the universe. Its spectrum matches that of a thermal black body with a temperature of ~ 2.72 K. Analysing the features of the CMB spectrum such as peaks heights and their positions allows us to find properties of the universe as relevant as the curvature, the inflationary parameters and the density of baryonic matter.

Precise measurement of the CMB temperature is therefore relevant to cosmology in general. Specialized observatories, pointed at deep space, measure radiation intensity and polarization at microwave frequencies. One of the most known efforts to measure and map the CMB is the *Wilkinson Microwave Anisotropy Probe* (WMAP)[10], a NASA explorer mission that started in 2001. This apparatus scanned the sky during 9 years. The *Planck* satellite was another space observatory dedicated to map the CMB. It was operated by the European Space Agency and was active from 2009 to 2013. Their latest results to date of writing were published in 2015 [1, 11]. Another experiment dedicated to observe the CMB is the *Background Imaging of Cosmic Extragalactic Polarization* (BICEP). This experiment consists of a telescope near the South Pole and is now in its third iteration (BICEP3)[12].

1.2 Inflation

Measurements suggest that the current standard model of big bang cosmology is still incomplete. Data from the CMB indicate that we live in a very flat universe. As we will see later, a flat universe in the present corresponds to a very fine-tuned set of initial conditions. This is known as the *flatness problem*. Moreover, the CMB is homogeneous to a high degree of precision, even at regions very far from each other. At earlier times, these regions should have been causally disconnected. Yet the homogeneity of the CMB suggests that there should be a mechanism that coordinated their evolution. This is called the *horizon problem*. It is possible to solve these problems by extending the BBC to include an epoch of inflation.

1.2.1 The Horizon Problem

To better understand what is the problem with the horizon in standard cosmology let's make some definitions and calculate some relevant quantities. First, define the particle horizon, the maximum comoving distance light can travel between two times t_1 and t_2

$$\chi_p(\tau) = \tau_2 - \tau_1 = \int_{t_1}^{t_2} \frac{dt}{a(t)}. \quad (1.12)$$

The particle horizon is converted to a physical quantity by multiplying by the scale factor

$$d_p(t) = a(t)\chi_p. \quad (1.13)$$

The age of the universe, the time from the big bang singularity until today, is finite. Therefore, the distance photons can travel is limited by this finite time.

Assuming a flat universe, with the scale factor for today defined as $a_0 \equiv a(t_0) = 1$, consider a photon moving in a radial path since the big bang during a time t_* . To simplify the calculation let's assume a matter-dominated universe with

$$a(t) = \left(\frac{t}{t_0}\right)^{2/3} \Rightarrow H = \frac{2}{3}t^{-1} = a^{-3/2}H_0, \quad (1.14)$$

where $H_0 = H(t_0)$. From Eq. (1.12) we can calculate the comoving distance traveled by the photon since the big bang and until the scale factor reaches $a_* = a(t_*)$. With this, it is easy to calculate the physical distance d_*

$$\chi_* = 2H_0^{-1}\sqrt{a_*}, \quad d_* = 2H_0^{-1}a_*^{3/2} = 2H_*^{-1}, \quad (1.15)$$

where $H_* = H(t_*)$. Now we are ready to truly understand the problem. The CMB as measured currently is isotropic to a high degree of precision. It corresponds to the universe with a scale factor $a_{\text{CMB}} \approx 1/1200$. Using this value we can calculate the comoving distance for the photons reaching the Earth from the CMB

$$\chi_{\text{Earth}} - \chi_{\text{CMB}} = 2H_0^{-1}(1 - \sqrt{a_{\text{CMB}}}) \approx 2H_0^{-1}. \quad (1.16)$$

The comoving horizon for the same photons at the time they were emitted is

$$\chi_{\text{CMB}} = 2H_0^{-1}\sqrt{a_{\text{CMB}}} \approx 6 \times 10^{-2}H_0^{-1}. \quad (1.17)$$

This means that in the CMB we observe regions separated enough to have non-overlapping horizons when they emitted radiation. They were causally disconnected at the time of creation of the first atoms, thus with no mechanism to syn-

chronize their properties. However, current measurements suggest that at that time the universe was homogeneous. This is known as the *horizon problem*.

Inflation solves this problem by changing how both the scale factor and the Hubble parameter develop after the big bang. First, let's rewrite Eq. (1.12) using the scale factor a as the integration variable

$$\chi_p = \int_{a(t_1)}^{a(t_2)} \frac{da}{a} \frac{1}{aH}. \quad (1.18)$$

In this way we introduce the comoving Hubble radius $(aH)^{-1}$ to the integral. The standard model of cosmology considers an ever growing comoving Hubble radius. Let's entertain the possibility that this was not true at some point in the early evolution of the universe: that there was a brief time where the comoving Hubble radius actually decreased.

Qualitatively, a decreasing Hubble radius means that aH increases over time

$$\frac{d}{dt}(aH) = \frac{d}{dt} \left(a \frac{da}{dt} a^{-1} \right) = \ddot{a} > 0. \quad (1.19)$$

This points at an accelerated expansion of the universe as the solution to the horizon problem. Assuming that inflation ends at the grand unification scale $T_{\text{GUT}} = 10^{16}$ GeV and neglecting the brief recent matter-dominated universe, *i.e.* assume that H is proportional to a^{-2} , we find

$$\frac{a_0 H_0}{a_E H_E} = a_E$$

where the E subscript indicates quantities at the end of inflation. The current temperature of the CMB is $T_0 \approx 2.7 \text{ K} \approx 10^{-13} \text{ GeV}$. This means that at the end

of inflation we require a decrease in the comoving Hubble radius of $a_E = T_0/T_E \approx 10^{-29}$. The lower number of e-foldings required to accommodate all currently visible regions of the CMB inside the same comoving Hubble radius at the end of inflation is

$$N = \ln \left(\frac{a_0}{a_E} \right) = \ln \left(\frac{T_E}{T_0} \right) \approx 67. \quad (1.20)$$

Since we assumed a radiation dominated universe we used $a \propto T^{-1}$. We can interpret Eq (1.20) as the minimum exponential growth required from inflation to solve the horizon problem. The case presented above is a rough estimate that illustrates the size of inflation. In fact, a widely accepted condition is that $N \approx 60$. This is the same we apply in the coming chapters.

1.2.2 The Flatness Problem

Assuming flat spatial sections ($k = 0$), the Friedmann Eq. (1.9) allows us to define a critical density

$$\rho_c \equiv \frac{3H^2}{8\pi G}. \quad (1.21)$$

Note that this quantity borrows its time dependence from $H = H(t)$. We use it to define the density parameter

$$\Omega_{\text{total}} \equiv \frac{\rho}{\rho_c}. \quad (1.22)$$

and rewrite Eq. (1.9) as

$$1 - \Omega_{\text{total}} = -\frac{k}{(aH)^2}. \quad (1.23)$$

In the standard model of cosmology $(aH)^{-1}$ is an ever growing quantity. This property of the comoving Hubble radius together with Eq. (1.23) indicate that

$|1 - \Omega_{\text{total}}|$ grows quadratically faster than the comoving Hubble radius, except for the special case $|\Omega_{\text{total}}| = 1$ ($k = 0$), corresponding to $\rho = \rho_c$.

Current measurements [1] point to a value of $\Omega_{\text{total}}(a_0) \approx 1$. We can see from Eq. (1.23) that this requires an extremely fine-tuned value for the total density at earlier times. To give an example, consider an universe made of radiation and dust. The observed range for the total density requires that we start with

$$0 \leq 1 - \Omega_{\text{total}} \leq 10^{-60}, \quad (1.24)$$

making our nearly flat universe a highly improbable result from the standard cosmology.

In a universe with an epoch of inflation, $|\Omega_{\text{total}}| = 1$ is a natural result. The acceleration of the scale factor $\ddot{a} > 0$ allows the comoving Hubble radius to shrink, naturally lowering the value of $|1 - \Omega_{\text{total}}|$, thus explaining why today we live in a flat universe.

1.2.3 Inflation by Slow-Rolling Fields

We start with a real scalar field ϕ , with a potential $V(\phi)$. This field is going to be responsible for driving inflation, therefore we call it the inflaton. The corresponding energy momentum tensor is

$$T_{\mu\nu} = \partial_\mu \phi \partial_\nu \phi - g_{\mu\nu} \left(\frac{1}{2} \partial^\alpha \phi \partial_\alpha \phi + V(\phi) \right), \quad (1.25)$$

Consider a flat universe, $k = 0$, and let's simplify the problem by assuming ϕ is a homogeneous field, *i.e.* it has only physical time t dependence. With these assumptions we extract the expressions for the energy density and pressure from

Eq. (1.25)

$$\rho_\phi = \frac{1}{2}\dot{\phi}^2 + V(\phi), \quad (1.26)$$

$$p_\phi = \frac{1}{2}\dot{\phi}^2 - V(\phi). \quad (1.27)$$

Using these expressions we can write Eqs. (1.9) and (1.11) with ϕ as the energy source

$$H^2 = \frac{8\pi G}{3} \left(\frac{1}{2}\dot{\phi}^2 + V(\phi) \right), \quad (1.28)$$

$$\dot{H} + H^2 = -\frac{8\pi G}{3} \left(\dot{\phi}^2 - V(\phi) \right). \quad (1.29)$$

Using Eq. (1.28) and its derivative in the left hand side of Eq. (1.29) allows us to find the equation of motion

$$\ddot{\phi} + 3H\dot{\phi} + \frac{dV}{d\phi} = 0, \quad (1.30)$$

where the effect of expansion in the universe appears as a friction term. Now let's make a few comments about the equations above before proceeding. First, note that in Eqs. (1.26) and (1.27) the potential energy can contribute dominantly to the energy density and the pressure, we just need $\dot{\phi}^2 \ll V(\phi)$, in other words, a scalar field that rolls very slowly towards the minimum of its potential. This will result in a equation of state $p \approx -\rho$. A slow-rolling field allows us to disregard terms involving the acceleration $\ddot{\phi}$, simplifying the equation of motion to

$$\dot{\phi} \approx -\frac{1}{3H} \frac{dV}{d\phi}. \quad (1.31)$$

In the case of Eq. (1.28), the term with $\dot{\phi}$ is negligible when compared to $V(\phi)$, this equation becomes

$$H^2 \approx \frac{8\pi G}{3} V(\phi). \quad (1.32)$$

To judge whether or not the field ϕ is a slow-rolling inflaton, it is conventional to define *slow-roll parameters* and set conditions over their values. The main slow-roll parameters are:

$$\epsilon = -\frac{\dot{H}}{H^2}, \quad (1.33)$$

$$\eta = -\frac{\ddot{\phi}}{H\dot{\phi}} + \epsilon. \quad (1.34)$$

Inflation is defined by an accelerated increase of the scale factor, $\ddot{a}/a = \dot{H} + H^2 > 0$. This means that when we have $\epsilon = -\dot{H}/H^2 < 1$ inflation occurs. The η parameter helps us ensure that the rolling is actually slow, a small η value is related to the negligible $\ddot{\phi}$ that we mentioned earlier. Using Eqs. (1.31) and (1.32) we can rewrite the slow-roll parameters in terms of the potential and its derivatives

$$\epsilon \equiv \frac{M_P^2}{16\pi} \left(\frac{V'}{V} \right)^2, \quad (1.35)$$

$$\eta \equiv \frac{M_P^2}{8\pi} \frac{V''}{V}, \quad (1.36)$$

where the primes indicate the number of derivatives with respect of ϕ and $M_P^2 = 1/G$ is the Planck scale. With the parameters in this form we can see that ϵ tells us how steep the potential is while η measures how curved it is. The conditions on the parameters to have slow-rolling inflation are $|\epsilon|, |\eta| \ll 1$. We take $\epsilon = 1$ to signal the end of inflation. The small value for η allows inflation to continue as

long as needed to solve the horizon problem. From the parameters ϵ and η we are able to find the slow-roll inflation parameters

$$n_s = 1 - 6\epsilon + 2\eta, \quad (1.37)$$

$$r = 16\epsilon, \quad (1.38)$$

$$n_r = 16\epsilon\eta - 24\epsilon^2 - 2\gamma, \quad (1.39)$$

$$\Delta_R^2 = \frac{V}{24\pi^2\epsilon}, \quad (1.40)$$

where $\gamma \equiv [M_P^2/(64\pi)]V'V'''/V^2$ is a higher order slow-roll parameter.

To measure the amount of inflation achieved from some initial t_i to t_{end} at the end of inflation, we define the number of *e-folds*, the exponential growth of the scale factor, as

$$N \equiv \ln \left(\frac{a(t_{\text{end}})}{a(t_i)} \right). \quad (1.41)$$

We can rewrite the number of e-folds as a function of the initial and final value of the scalar field, $\phi_i = \phi(t_i)$ and $\phi_{\text{end}} = \phi(t_{\text{end}})$, respectively. The result is an integral that can be written in terms of the potential $V(\phi)$ and its first derivative

$$N \equiv \ln \left(\frac{a(t_{\text{end}})}{a(t_i)} \right) = \int_{t_i}^{t_{\text{end}}} dt H = \frac{8\pi}{M_P^2} \int_{\phi_{\text{end}}}^{\phi_i} d\phi \frac{V}{V'}. \quad (1.42)$$

Alternatively, this can be written in terms of ϵ as

$$N = \frac{2\sqrt{\pi}}{M_P} \int_{\phi_{\text{end}}}^{\phi_i} \frac{d\phi}{\sqrt{\epsilon}}. \quad (1.43)$$

Recent and more detailed descriptions about inflation may be read in Refs. [13] and [14].

1.3 Dark Matter

To measure the density of matter in the universe first take a sample big enough for the universe to look homogeneous. The mass of the objects contained in that region can be determined by applying Kepler's third Law [8]

$$GM(r) = v^2 r \quad (1.44)$$

where G is Newton's gravitational constant, $M(r)$ is the mass contained within the radius r and v is the orbital velocity at r . Counting the number of galaxies per unit of volume gives us the number density of galaxies n_{GAL} . Once we determined the masses of the galaxies is easy to find the average galactic mass $\langle M_{\text{GAL}} \rangle$. The average density of the universe is

$$\langle \rho \rangle = n_{\text{GAL}} \langle M_{\text{GAL}} \rangle \quad (1.45)$$

from there, the density parameter is simply $\Omega_0 = \langle \rho \rangle / \rho_c$, the measured average density divided by the critical density. This technique applied to spiral galaxies with an r defined as the radius that contains most of the light emitted by the galaxy results in [8]

$$\Omega_{\text{LUM}} \approx 0.01 \quad (1.46)$$

at most. In other words, if we base our calculations on the light emitting matter only, we end accounting for 1% of the critical density.

Furthermore, considering r outside the luminous region of the galaxy, we expect the velocity to decrease as a function of $r^{-1/2}$, but observations [15, 16]

indicate that the velocity is constant, therefore $M(r) \propto r$. The missing matter has no measurable emission of radiation, we can say that it is *dark matter*.

The contribution from dark matter to the matter of spiral galaxies can be determined through rotation curve measurements. These observations indicate that spiral galaxies are covered by a diffuse halo of dark matter that contributes from 3 to 10 times the mass of the visible matter. Including these effect we have

$$\Omega_{\text{HALO}} \gtrsim 0.1 \approx 10 \Omega_{\text{LUM}}, \quad (1.47)$$

Indicating that most of the content of the galaxy is actually non luminous.

1.3.1 WIMP Dark Matter

The explanations to the mysterious dynamics of the luminous matter are diverse, including modifications to the basic dynamics of gravity [18]. In this case we will concentrate on the dark matter solutions, in particular the type of dark matter called weakly interacting massive particle (WIMP).

WIMP is a dark matter candidate believed to have a very weak interaction with ordinary matter, thus the name. A very massive particle interacting through a weak strength force yields the appropriate self-annihilation cross section for the measured relic abundance of dark matter [19]. This interaction, despite its weakness, has a very important experimental interest, since it provides the means to detect WIMP particles by their effects on a target in a detector, the weaker the interaction, the bigger the target required for detection.

At earlier times, when the WIMP mass was lower than the universe temperature, pairs of WIMP particles were able to convert to and from pairs of standard

model (SM) particles. As the universe expanded, the temperature decreased. When the expansion rate of the universe surpassed the rate of the annihilation of WIMP pairs into SM particles, the WIMP *froze out*. In other words, the expansion moved the dark matter particles far apart one from each other. This left a cosmological relic in equilibrium. The abundance of this relic can be calculated with the Boltzmann equation, something we will describe below.

1.3.2 Annihilation in the Early Universe

With the Boltzmann equation we can quantify the rate of change in the abundance for a species of particles. Let's start with a particle A with number density n_A and assume that the annihilation process with particles B , C and D goes as $A + B \leftrightarrow C + D$. The corresponding Boltzmann equation is

$$\begin{aligned}
a^{-3} \frac{d(n_A a^3)}{dt} = & \int \frac{d^3 p_A}{(2\pi)^3 2E_A} \int \frac{d^3 p_B}{(2\pi)^3 2E_B} \int \frac{d^3 p_C}{(2\pi)^3 2E_C} \int \frac{d^3 p_D}{(2\pi)^3 2E_D} \\
& \times (2\pi)^4 \delta^3(p_A + p_B - p_C - p_D) \delta(E_A + E_B - E_C - E_D) |\mathcal{M}|^2 \\
& \times \{f_C f_D [1 \pm f_A] [1 \pm f_B] - f_A f_B [1 \pm f_C] [1 \pm f_D]\} \quad (1.48)
\end{aligned}$$

where a is the expansion rate, p_j , $E_j = \sqrt{p_j^2 + m_j^2}$ and f_j are, respectively, momentum, energy and distribution for the corresponding particle, \mathcal{M} is the amplitude for the process, in most cases is the same for either direction $A + B \rightarrow C + D$ or $C + D \rightarrow A + B$. The \pm signs in the last line of Eq. (1.48) correspond to plus sign for bosons (Bose enhancement factor) and minus sign for fermions (Pauli blocking factor.)

We will be working with systems where the distribution typically has the form

$$f_j \rightarrow e^{(\mu_j - E_j)/T}, \quad (1.49)$$

and the factors $[1 \pm f]$ in Eq. (1.48) can be neglected. With these simplifications and applying conservation of energy ($E_A + E_B = E_C + E_D$), the last line of Eq. (1.48) can be rewritten as

$$\begin{aligned} f_C f_D [1 \pm f_A] [1 \pm f_B] - f_A f_B [1 \pm f_C] [1 \pm f_D] \\ \rightarrow e^{-(E_A + E_B)/T} \left\{ e^{(\mu_C + \mu_D)/T} - e^{(\mu_A + \mu_B)/T} \right\}. \end{aligned} \quad (1.50)$$

The number density can be written

$$n_i = g_i e^{\mu_i/T} \int \frac{d^3 p}{(2\pi)^3} e^{-E_i/T} \quad (1.51)$$

where g_i is the degeneracy factor for the corresponding particle. The equilibrium density for each particle is defined as

$$n_i^{(0)} \equiv g_i \int \frac{d^3 p}{(2\pi)^3} e^{E_i/T} = \begin{cases} g_i \left(\frac{m_i T}{2\pi} \right)^{3/2} e^{-m_i/T} & m_i \gg T, \\ g_i \frac{T^3}{\pi^2} & m_i \ll T. \end{cases} \quad (1.52)$$

This means that we can write $e^{\mu_i/T} = n_i/n_i^{(0)}$, further simplifying the last line of Eq. (1.48) to

$$e^{-(E_A + E_B)/T} \left\{ \frac{n_C n_D}{n_C^{(0)} n_D^{(0)}} - \frac{n_A n_B}{n_A^{(0)} n_B^{(0)}} \right\}. \quad (1.53)$$

And one more definition to reach our goal, define the thermally averaged cross section

$$\begin{aligned} \langle \sigma v \rangle \equiv & \frac{1}{n_A^{(0)} n_B^{(0)}} \int \frac{d^3 p_A}{(2\pi)^3 2E_A} \int \frac{d^3 p_B}{(2\pi)^3 2E_B} \int \frac{d^3 p_C}{(2\pi)^3 2E_C} \int \frac{d^3 p_D}{(2\pi)^3 2E_D} e^{-(E_1+E_2)/T} \\ & (2\pi)^4 \delta^3(p_A + p_B - p_C - p_D) \delta(E_A + E_B - E_C - E_D) |\mathcal{M}|^2. \end{aligned} \quad (1.54)$$

Putting everything together, the final form of the Boltzmann equation for this section is

$$a^{-3} \frac{d(n_A a^3)}{dt} = n_A^{(0)} n_B^{(0)} \langle \sigma v \rangle \left\{ \frac{n_C n_D}{n_C^{(0)} n_D^{(0)}} - \frac{n_A n_B}{n_A^{(0)} n_B^{(0)}} \right\}. \quad (1.55)$$

This equation vanishes when the two terms inside curly brackets in the right hand side cancel, this special case corresponds to

$$\frac{n_C n_D}{n_C^{(0)} n_D^{(0)}} = \frac{n_A n_B}{n_A^{(0)} n_B^{(0)}}, \quad (1.56)$$

better known as the chemical equilibrium equation.

1.3.3 Freeze-Out

Consider the annihilation of two dark matter particles χ into two light particles l . The light particles are assumed to be in complete equilibrium, *i.e.* $n_l = n_l^{(0)}$.

Using Eq. (1.55) we have

$$a^{-3} \frac{d(n_\chi a^3)}{dt} = \langle \sigma v \rangle \left\{ \left(n_\chi^{(0)} \right) - n_\chi^2 \right\}. \quad (1.57)$$

Define $Y \equiv n_\chi/T^3$, and replace it inside the left hand side derivative, this leaves a factor of $(aT)^3$, that we can eliminate since temperature scales as a^{-1} . Now we have an equation for Y

$$\frac{dY}{dt} = T^3 \langle \sigma v \rangle \left\{ Y_{eq}^2 - Y^2 \right\}. \quad (1.58)$$

with $Y_{eq} = n_\chi^{(0)}/T^3$. For dark matter produced during the radiation-dominated era we have $a \propto t^{1/2}$, then $H = 1/(2t)$. Since $a^{-1} \propto T$, then $T(t) \propto t^{-1/2}$. Let's define a new time variable in terms of the mass of χ

$$x \equiv m_\chi/T, \quad \frac{dx}{dt} = Hx, \quad (1.59)$$

where the second expression follows from using the time dependence of T as given above. We will use $H = H(m_\chi)/x^2$. We rewrite the equation for Y using the new variable x as

$$\frac{dY}{dx} = -\frac{m_\chi^3 \langle \sigma v \rangle}{H(m_\chi)x^2} \left\{ Y^2 - Y_{eq}^2 \right\}. \quad (1.60)$$

As the universe cools down, x grows and Y_{eq} becomes exponentially suppressed. Eventually, the χ particles will be too far to interact, thus freezing-out and remaining as cosmological relics. The final freeze-out abundance is defined as $Y_\infty \equiv Y(x = \infty)$. As Y_{eq} becomes more suppressed, the right hand side of Eq. (1.60) will become mostly dominated by Y

$$\frac{dY}{dx} \approx -\frac{m_\chi^3 \langle \sigma v \rangle}{H(m_\chi)x^2} Y^2. \quad (1.61)$$

This is easily integrated from the epoch of freeze-out x_f to a later time $x = \infty$, yielding

$$\frac{1}{Y_\infty} - \frac{1}{Y_f} = \frac{m_\chi^3 \langle \sigma v \rangle}{H(m_\chi) x_f} \quad (1.62)$$

where usually $Y_f \gg Y_\infty$, allowing us to approximate

$$Y_\infty \approx \frac{H(m_\chi) x_f}{m_\chi^3 \langle \sigma v \rangle}. \quad (1.63)$$

After freeze-out, the particle density for χ is proportional to a^{-3} , meaning that the number density is multiplied by $m_\chi (a_1/a_0)^3$ to give the present energy density, where a_1 is the expansion rate at a time where Y has reached Y_∞ . The resulting energy density is

$$\rho_\chi = m_\chi Y_\infty T_0^3 \left(\frac{a_1 T_1}{a_0 T_0} \right)^3 \approx \frac{m_\chi Y_\infty T_0^3}{30}. \quad (1.64)$$

To find the contribution from dark matter to the critical density we only need to divide the previous result by the critical density ρ_c

$$\Omega_\chi = \frac{H(m_\chi) x_f T_0^3}{30 m_\chi^2 \langle \sigma v \rangle \rho_c} = \left[\frac{4\pi^3 g_*(m_\chi)}{45 M_P^2} \right]^{1/2} \frac{x_f T_0^3}{30 \langle \sigma v \rangle \rho_c} \quad (1.65)$$

where $H = [4\pi^3 g_*(T) T^4 / (45 M_P^2)]^{1/2}$ with $T = m_\chi$ and $g_*(T)$ is the effective number of relativistic degrees of freedom

$$g_* = \sum_{i=\text{bosons}} g_i + \frac{7}{8} \sum_{i=\text{fermions}} g_i. \quad (1.66)$$

When we construct a particular model we will calculate a $\langle \sigma v \rangle$ specific to our setup. Using the equations presented in this section, we calculate the relic density

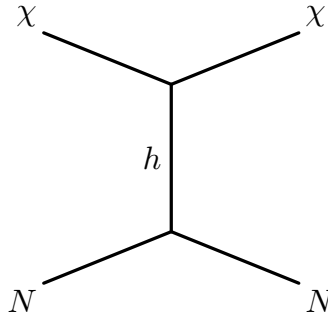


Figure 1.1: Effective interaction between dark matter and nucleons caused by the Higgs coupling with dark matter.

for the dark matter candidate in our model. Then we compare our result with measurements from the CMB to constraint our parameter space.

1.3.4 Direct Detection

Experimentally speaking, the most interesting feature of WIMP dark matter is the possibility of direct detection. Two of the most relevant experiments trying to directly detect dark matter are the *Large Underground Xenon experiment* (LUX) [20] and the *XENON dark matter research project* [21]. Both experiments use a large volume of liquid xenon inside a time projection chamber. Inside the chamber, a strong electric field is applied to catch any electron produced by the scattering of a dark matter particle with nucleons.

The dark matter models that will be presented here use Higgs portal interactions to connect dark matter with standard model particles. The coupling of a pair of dark matter particles with the standard model Higgs will allow the scattering of dark matter with quarks, which we interpret as an effective scattering with nucleons.

The effective scattering in both models has a factor

$$\sigma_{SI}(\chi N \rightarrow \chi N) \propto \sin^2 2\theta \frac{(m_\eta^2 - m_h^2)^2}{m_\eta^4 m_h^4} \left(\frac{m_N m_\chi}{m_N + m_\chi} \right)^2 \quad (1.67)$$

where m_η is the mass of a scalar that appears in the model, m_h is the Higgs scalar mass ~ 125 GeV, m_N is the nucleon mass ~ 1 GeV and θ is an angle that parameterizes the deviation from the standard model introduced by the new scalar. Current observations limit this deviation to $\sin^2 \theta < 0.1$.

At the moment of writing, there has been no direct detection of a dark matter particle. However, as experiments improve their setup, they keep pushing down the upper bound for the scattering between dark matter and nucleons. The challenge with every new model of WIMP dark matter is to remain in the zone not yet excluded by current experiments.

Chapter 2

A Permutation on Hybrid Natural Inflation ¹

In this chapter we analyze a model of hybrid natural inflation based on the smallest non-Abelian discrete group S_3 . Leading invariant terms in the scalar potential have an accidental global symmetry that is spontaneously broken, providing a pseudo-Goldstone boson that is identified as the inflaton. The S_3 symmetry restricts both the form of the inflaton potential and the couplings of the inflaton field to the waterfall fields responsible for the end of inflation. We identify viable points in the model parameter space. Although the power in tensor modes is small in most of the parameter space of the model, we identify parameter choices that yield potentially observable values of r without super-Planckian initial values of the inflaton field.

¹Work previously published in C. D. Carone, J. Erlich, M. Sher and R. Ramos, Phys. Rev. D **90** (2014), no. 6, 063521.

2.1 Introduction

Measurements of the anisotropy in the cosmic microwave background (CMB) have led to the development of a “standard model” of cosmology, with a cosmological constant, cold dark matter and a spectrum of initial CMB fluctuations that seed large scale structure [9]. It is widely believed that these initial fluctuations arise from an inflationary epoch, resulting in a nearly scale-invariant spectrum. More precise measurements of the CMB fluctuations, including polarization measurements, have been carried out by experiments such as WMAP [10], PLANCK [11] and BICEP2 [22]. These measurements provide information about initial metric perturbations that can severely constrain (or rule out) various inflationary models.

In order to satisfy the limits on the size of the CMB anisotropy fluctuations, the scalar self-coupling constant of the inflaton field must be very small, typically less than 10^{-12} in most realistic models [23]. While such a small coupling could be assumed, it would be aesthetically more desirable if it arose naturally. This is the case for theories in which the inflaton is identified with the pseudo-Goldstone boson of a spontaneously broken approximate global symmetry. Such “natural inflation” scenarios were proposed first by Freese, Frieman and Olinto [24]. If the scale of spontaneous symmetry breaking is f and if there is an explicit breaking of the global symmetry via an anomaly, the inflaton potential takes the form

$$V = V_0 \left[1 \pm \cos(n\phi/f) \right], \quad (2.1)$$

where n is an integer. The model is consistent with measured values of the spectral index and its running, as well as constraints on the ratio of powers in tensor and

scalar modes [25]. A concern about natural inflation is that the value of f must be very close to or above the Planck scale, so that quantum-gravitational corrections to the potential are not automatically under control.

A model that can result in a lower value of f is “hybrid natural inflation” [26–29]. The original hybrid inflation model, proposed by Linde [30], has a second scalar field which couples to the inflaton and ends the inflationary epoch. As the inflaton slowly rolls, the parameters of the potential of the second scalar field change due to the coupling, and at some point the second scalar field acquires a vacuum expectation value, ending inflation. This second scalar field was referred to as the “waterfall” field. Hybrid natural inflation models are natural inflation models in which inflation is terminated due to the dynamics of such additional fields.

An important question in any model based on the natural inflation idea is the origin of the approximate global symmetry. Global symmetries are not believed to be fundamental (for example, they are typically violated by quantum gravitational effects [31]), so it is desirable to arrange that these symmetries arise by accident, as a consequence of the form of the leading terms in the potential; these terms are restricted by the continuous or discrete gauge symmetries of the theory. While discrete gauge symmetries can be thought of as discrete remnants of a spontaneously broken continuous gauge symmetry [32], they also can be defined consistently without such an embedding [33]; in either case, they are preserved by quantum gravitational effects. Cohn and Stewart [26, 27] showed that accidental global symmetries could easily be obtained in models with non-Abelian discrete gauge symmetries, and illustrated their point with hybrid models based on the discrete group $\Delta(96)$. They note that many other models based on smaller discrete

groups are likely possible. Nevertheless, the literature on such models is relatively sparse. Ross and Germán [28, 29] have explored hybrid natural inflation models based on the discrete group D_4 . In their model, the inflaton potential takes the form

$$V = V_0 \left[1 + a \cos(\phi/f) \right], \quad (2.2)$$

where a is a constant. This potential can generate phenomenologically acceptable inflation with f substantially smaller than the Planck mass, so that higher-order corrections are under control. Ross and Germán [28, 29] point out that potentials of the form Eq. (2.2) should be expected in similar models based on other non-Abelian discrete groups.

Given the promise of the models considered in Refs. [26–29], and motivated by minimality, we explore in this chapter a hybrid natural inflation model based on the smallest non-Abelian discrete group, the permutation group S_3 . The discrete symmetry restricts both the inflaton potential and the couplings of the inflaton to the waterfall fields. The S_3 charge assignments in our model satisfy the requirements for a discrete gauge symmetry, as set out in Ref. [33]. In Sec. 2.2, we review the group S_3 and its representations. The model is presented in Sec. 2.3. After reviewing inflationary parameters in Sec. 2.4, we study a typical point in model parameter space in quantitative detail in Sec. 2.5. Motivated by the potential signature in gravitational waves, we show in Sec. 2.6 that the model can yield a potentially observable tensor-to-scalar ratio, without requiring super-Planckian values of the inflaton field, and we explain why this is not in conflict with the Lyth bound [34]. In Sec. 2.7, we discuss the cutoff of inflation and reheating. Finally, in Sec. 2.8, we present our conclusions.

2.2 The Group S_3

We base our model on S_3 , the smallest non-Abelian discrete symmetry group. The group has six elements whose action can be identified with the permutation of three objects. A useful discussion of this symmetry in a model building context can be found in Ref. [35].

S_3 has three irreducible representations: a two-dimensional representation $\mathbf{2}$ and two one-dimensional representations, $\mathbf{1}_A$ and $\mathbf{1}_S$. The $\mathbf{1}_S$ representation is the trivial singlet. The rules for group multiplication are given by $\mathbf{1}_A \otimes \mathbf{1}_A = \mathbf{1}_S$, $\mathbf{1}_S \otimes \mathbf{1}_S = \mathbf{1}_S$, $\mathbf{1}_A \otimes \mathbf{1}_S = \mathbf{1}_A$ and $\mathbf{2} \otimes \mathbf{2} = \mathbf{2} \oplus \mathbf{1}_A \oplus \mathbf{1}_S$. The product of two doublet representations can be decomposed into its irreducible components using Clebsch-Gordan matrices. Let ψ and η represent two-component column vectors that transform as doublets under S_3 and let σ^a denote the Pauli matrices. The products $\psi^T C_{\mathbf{1}_S} \eta$ and $\psi^T C_{\mathbf{1}_A} \eta$ transform in the $\mathbf{1}_S$ and $\mathbf{1}_A$ representations, respectively, where

$$C_{\mathbf{1}_S} = \mathbb{1} \quad \text{and} \quad C_{\mathbf{1}_A} = i\sigma^2. \quad (2.3)$$

Similarly, we can construct a doublet

$$\begin{bmatrix} \psi^T C_{\mathbf{2}}^{(1)} \eta \\ \psi^T C_{\mathbf{2}}^{(2)} \eta \end{bmatrix} \sim \mathbf{2}, \quad (2.4)$$

where

$$C_{\mathbf{2}}^{(1)} = \sigma^3 \quad \text{and} \quad C_{\mathbf{2}}^{(2)} = -\sigma^1. \quad (2.5)$$

The model we present in the next section includes an S_3 doublet field $\phi = (\phi_1, \phi_2)^T$, so it is useful to enumerate the S_3 invariants that can be constructed

from products of ϕ , up to quartic order. The quadratic combination of fields that transforms in the $\mathbf{1}_S$ representation has the form

$$(\phi^2)_{\mathbf{1}_S} \equiv \phi^T C_{\mathbf{1}_S} \phi = \phi_1^2 + \phi_2^2. \quad (2.6)$$

While there are three $\mathbf{1}_S$ reps in the product $\mathbf{2} \otimes \mathbf{2} \otimes \mathbf{2} \otimes \mathbf{2}$, all such invariants constructed from a single ϕ have the same form,

$$(\phi^4)_{\mathbf{1}_S} = (\phi_1^2 + \phi_2^2)^2. \quad (2.7)$$

While Eqs. (2.6) and (2.7) follow from S_3 invariance, it is important to note that these expressions are also invariant under a continuous symmetry, $\text{SO}(2)$, under which the ϕ field is also a doublet. However, this accidental symmetry is broken by the S_3 cubic invariant

$$(\phi^3)_{\mathbf{1}_S} = \phi_1 (\phi_1^2 - 3\phi_2^2). \quad (2.8)$$

The model of the next section will identify the inflaton field θ with the pseudo-Goldstone boson of this accidental $\text{SO}(2)$ symmetry; the soft breaking of this symmetry by the cubic invariant will be used to generate the inflaton potential. Notice, if we parameterize

$$\phi = (\rho + v) \begin{bmatrix} \cos(\theta/v) \\ \sin(\theta/v) \end{bmatrix}, \quad (2.9)$$

where v is the scale of spontaneous symmetry breaking and ρ is the massive radial excitation, then Eqs. (2.6) and (2.7) are independent of θ , indicating that these

terms contribute nothing to the inflaton potential. (Note that in this parameterization the kinetic term for θ is canonically normalized.) On the other hand, Eq. (2.8) simplifies to

$$(\phi^3)_{\mathbf{1}_S} = (\rho + v)^3 \cos(3\theta/v), \quad (2.10)$$

which can be used to lift the flat direction. In the next section we show how these ingredients can be combined to produce a viable model of hybrid natural inflation.

2.3 The Model

In addition to the doublet field ϕ described in the previous section, our model includes two real scalars, χ_1 and χ_2 , each in the $\mathbf{1}_S$ representation of S_3 . We assume a \mathbb{Z}_2 symmetry under which both χ fields are odd, which eliminates unwanted linear terms that would otherwise give the χ_i vevs. The $\text{SO}(2)$ invariant terms in the potential

$$V_{\text{SO}(2)}(\phi, \chi_i) = -\frac{1}{2}m_\phi^2(\phi_1^2 + \phi_2^2) + \lambda_\phi(\phi_1^2 + \phi_2^2)^2 + \cdots \quad (2.11)$$

lead to the spontaneous breaking of the $\text{SO}(2)$ symmetry due to the negative mass squared term for ϕ . The terms not shown include various $\phi^2\chi^2$ couplings as well as the potential for the χ_i fields by themselves. It is not hard to see that it is possible to choose parameters such that ϕ^2 develops a vacuum expectation value, while the χ_i do not. The details are not crucial for our purposes because the $\text{SO}(2)$ invariant terms have no effect on the form of the inflaton potential. All that is relevant at this stage is that the spontaneous symmetry breaking is consistent

with the parameterization in Eq. (2.9), with the Goldstone boson θ identified as the inflaton.

In the spirit of a perturbative expansion, we now introduce smaller terms which violate the accidental $\text{SO}(2)$ symmetry. At the renormalizable level, we can include a term of the form $m_0 (\phi^3)_{\mathbf{1}_S}$; the dimensionful coefficient m_0 parameterizes the breaking of the $\text{SO}(2)$ symmetry. We could simply assume a small value of m_0 as a fine-tuning in the model (after all, we have to accept the same for the Higgs boson mass in any non-supersymmetric theory). However, we can do better if we allow an additional \mathbb{Z}'_2 symmetry under which the ϕ doublet and χ_1 are odd, and treat m_0 consistently as a soft \mathbb{Z}'_2 -breaking parameter. Since the \mathbb{Z}'_2 symmetry is restored in the limit of vanishing m_0 , there can be no large radiative corrections and a small m_0 will be natural following the criterion of t'Hooft [36]. We will adopt this assumption henceforth. The only other term that we include that violates the $\text{SO}(2)$ symmetry is of the form $\chi_1 \chi_2 (\phi^3)_{\mathbf{1}_S}$. Identifying the χ fields as the waterfall fields of a hybrid inflation model, such couplings are responsible for ending inflation in the model. In the present case, this $\text{SO}(2)$ breaking term is Planck suppressed for sub-Planckian field values.

We now consider the effective theory below the $\text{SO}(2)$ -breaking scale (the scale of the ρ mass). With the particle content and the symmetries of the theory as we have specified them, the scalar potential for the θ , χ_1 and χ_2 fields is somewhat cumbersome for a general analysis. We will therefore adopt a simplifying assumption in our parameter choices to demonstrate most simply that viable cosmological solutions exist. Additional solutions are possible for less restrictive choices of model parameters.

We study the following simplified form for the scalar potential:

$$\begin{aligned}
V(\theta, \chi_i) = & V_0 + c_1 \frac{v^3}{M_P} \chi_1 \chi_2 \cos(3\theta/v) - m_0 v^3 \cos(3\theta/v) \\
& + \frac{1}{2} m_\chi^2 (\chi_1^2 + \chi_2^2) + (\lambda \chi_1^4 + \lambda_{12} \chi_1^2 \chi_2^2 + \lambda \chi_2^4). \tag{2.12}
\end{aligned}$$

Here V_0 is a constant, c_1 , λ and λ_{12} are couplings, and m_χ is a common χ_i field mass. The second and third terms are SO(2)-breaking interactions discussed previously. For definiteness, we assume $c_1 > 0$. In contrast to the most general case, we have assumed symmetry under $\chi_1 \leftrightarrow \chi_2$. This simplifying assumption has no effect on the shape of the inflaton potential (which is obtained by setting $\chi_i = 0$), but substantially streamlines our presentation. If one relaxes this assumption, one has to contend with minimization conditions that are cubic; this complicates the analysis but does not affect our conclusions qualitatively. Note also that we have omitted the $(\chi_1^2 + \chi_2^2) \cos(3\theta/v)$ and $\chi_1 \chi_2^3 + \chi_2 \chi_1^3$ interactions, which are \mathbb{Z}'_2 odd. Since the \mathbb{Z}'_2 symmetry is broken only by m_0 , these are suppressed by m_0/M_P relative to the second and fifth terms in Eq. (2.12), respectively, making them negligible². We set the cosmological constant to zero at the global minimum of the potential by choice of the parameter V_0 .

Inflation occurs as the field θ slow rolls toward the origin, between initial and final field values that lie within the interval $0 < 3\theta/v < \pi$. During inflation, the effective χ_i masses are positive and the χ fields remain at the origin. Inflation

²If one prefers to dispense with the softly-broken \mathbb{Z}'_2 symmetry and allow m_0 to be fine-tuned, then these terms can be omitted as a parametric simplification. The effect of including a $c_2 \frac{v^3}{M_P} (\chi_1^2 + \chi_2^2) \cos(3\theta/v)$ term, with $c_2 > 0$, is to change Eq. (2.13) by replacing $c_1 \rightarrow c_1 - c_2$ and Eqs. (2.16) and (2.17) by $m_\chi^2 \rightarrow m_\chi^2 + 2c_2 \frac{v^3}{M_P}$. If one adds a $\lambda_3 (\chi_1^3 \chi_2 + \chi_2^3 \chi_1)$ term, then the only change in these equations is $\lambda_{12} \rightarrow \lambda_{12} - 2\lambda_3$. These changes do not affect our results qualitatively.

ends via the waterfall mechanism when θ is such that

$$c_1 \frac{v^3}{M_P} \cos(3\theta/v) > m_\chi^2. \quad (2.13)$$

At this point, the χ_i potential is destabilized and the χ fields develop vevs³. Within a Hubble time, the fields reach a global minimum, and inflation abruptly ends. Oscillations of the waterfall fields about this minimum leads to reheating. Given the inequality in Eq. (2.13), we find that the location of the degenerate global minima in our model are given by

$$\theta = 0, \quad (2.14)$$

$$\chi_1 = -\chi_2, \quad (2.15)$$

and

$$\chi_1^2 = \frac{1}{2(2\lambda + \lambda_{12})} \left[c_1 \frac{v^3}{M_P} - m_\chi^2 \right]. \quad (2.16)$$

Setting the cosmological constant to zero at any of these minima determines the constant V_0 in Eq. (2.12):

$$V_0 = m_0 v^3 + \frac{1}{4(2\lambda + \lambda_{12})} \left(c_1 \frac{v^3}{M_P} - m_\chi^2 \right)^2. \quad (2.17)$$

With this result in hand, the form of the inflaton potential during the period of slow roll is fixed in term of the model parameters:

$$V(\theta) = V_0 [1 - \xi \cos(3\theta/v)] \quad (2.18)$$

³As we will see in Sec. 2.5, $\cos(3\theta/v) > 0$ when inflation ends, as has been assumed in Eq. (2.13).

where $\xi \equiv m_0 v^3/V_0$ and V_0 is given by Eq. (2.17). Our parameter choices in the next sections have $\xi < 1$.

Eq. (2.18) is amenable to the standard analysis of a single-field inflation model until the end of inflation. We review the quantities of interest in such an analysis in the next section and explore numerical results for a number of benchmark points in our model's parameter space. For these points, we will also present estimates to justify that the shut-off of inflation via the waterfall mechanism is sufficiently fast.

2.4 Inflation Parameters

In terms of the inflaton potential $V(\theta)$, the slow-roll parameters may be written [11]

$$\epsilon \equiv \frac{M_P^2}{16\pi} \left(\frac{V'}{V} \right)^2, \quad \eta \equiv \frac{M_P^2}{8\pi} \frac{V''}{V} \quad \text{and} \quad \gamma \equiv \frac{M_P^4}{64\pi^2} \frac{V'V'''}{V^2}. \quad (2.19)$$

In a generic single-field model, $\epsilon = 1$ is usually chosen to define the end of inflation; in the present case, ϵ remains small throughout the period of slow roll until inflation is terminated by the destabilization of the effective χ potential. The number of e -folds of inflation N may be expressed as [9]

$$N = \frac{2\sqrt{\pi}}{M_P} \int_{\theta_f}^{\theta_i} \frac{1}{\sqrt{\epsilon}} d\theta, \quad (2.20)$$

where θ_i and θ_f are the initial and final inflaton field values, respectively. We will evaluate this quantity in our model to assure that sufficient inflation is achieved.

A number of cosmic microwave background parameters can be expressed conveniently in terms of the slow roll parameters, as we now summarize [11, 37]. All are evaluated at values of the inflaton field corresponding to ~ 60 e -folds before the end of inflation, when scales of order the current Hubble radius exited the horizon. The amplitude of the tensor power spectrum in the slow-roll approximation is

$$\Delta_T^2(k) = \frac{128}{3} \frac{V}{M_P^4}, \quad (2.21)$$

while the amplitude of the scalar power spectrum is

$$\Delta_R^2(k) = \frac{128\pi}{3M_P^6} \frac{V^3}{V'^2} = \frac{8}{3M_P^4} \frac{V}{\epsilon}. \quad (2.22)$$

The ratio of the tensor to scalar amplitudes is then

$$r = 16\epsilon. \quad (2.23)$$

The scalar spectral index and its running are given by

$$n_s(k) = 1 - 6\epsilon + 2\eta \quad \text{and} \quad n_r = 16\epsilon\eta - 24\epsilon^2 - 2\gamma. \quad (2.24)$$

The predictions following from our model for the parameters summarized in this section can easily be computed starting with Eqs. (2.17) and (2.18). For example, the slow roll parameters take the form:

$$\epsilon = \frac{9\xi^2 M_P^2 \sin^2(3\theta/v)}{16\pi v^2 \left(1 - \xi \cos(3\theta/v)\right)^2}, \quad (2.25)$$

$$\eta = \frac{9\xi M_P^2 \cos(3\theta/v)}{8\pi v^2 \left(1 - \xi \cos(3\theta/v)\right)}, \quad (2.26)$$

$$\gamma = -\frac{81\xi^2 M_P^4 \sin^2(3\theta/v)}{64\pi^2 v^4 \left(1 - \xi \cos(3\theta/v)\right)^2}. \quad (2.27)$$

The parameters n_s , n_r , r and Δ_R^2 can then be evaluated using these expressions, with θ set to θ_i as determined from Eq. (2.20) with $N = 60$. We will follow this procedure in our quantitative analysis in the following section. The measured values of the cosmological parameters that we use in this analysis are $n_s = 0.9603 \pm 0.0073$, $n_r = -0.013 \pm 0.009$, $r < 0.12$ (95% C.L.) and $\Delta_R^2 = 2.2 \times 10^{-9}$ [11]. Note that the recent observation by the BICEP2 experiment of B-mode polarization in the CMB, would imply $r = 0.20^{+0.07}_{-0.05}$ if the signal is interpreted as cosmological in origin [22]. However, the contribution of foreground dust to the BICEP2 signal is currently uncertain, so one cannot draw a reliable conclusion on the value of r from this measurement at present [38, 39].

2.5 Numerical Analysis

In this section, we present the numerical analysis corresponding to a typical, benchmark point in the model parameter space. We will find in this example that the primordial gravitational wave signal is small. In the next section, we show that for a careful choice of parameters, a larger value of r can be obtained.

Working with the generic potential, Eq. (2.18), let us focus first on two quantities: the spectral index,

$$n_s - 1 = -\frac{9}{16\pi} \frac{M_p^2}{v^2} \left\{ \frac{2\xi^2 [2 + \sin^2(3\theta_i/v)] - 4\xi \cos(3\theta_i/v)}{[1 - \xi \cos(3\theta_i/v)]^2} \right\}, \quad (2.28)$$

and the amplitude of the scalar power spectrum,

$$\Delta_R^2 = \frac{128\pi}{27} \frac{V_0 v^2}{M_p^6} \frac{1}{\xi^2} \frac{[1 - \xi \cos(3\theta_i/v)]^3}{\sin^2(3\theta_i/v)}. \quad (2.29)$$

Both are evaluated at the initial field value θ_i , corresponding to 60 e -folds before the end of inflation. The number of e -folds, following from Eq. (2.20), is given by

$$N = \frac{8\pi}{9} \frac{v^2}{M_P^2} \frac{1}{\xi} \left[(1 - \xi) \ln \left(\frac{\sin(3\theta_i/v)}{\sin(3\theta_f/v)} \right) - \ln \left(\frac{1 + \cos(3\theta_i/v)}{1 + \cos(3\theta_f/v)} \right) \right]. \quad (2.30)$$

Let us define $x_{i,f} \equiv \cos(3\theta_{i,f}/v)$, as well as

$$N_0 \equiv \frac{1}{\left[\frac{9}{4\pi} \frac{M_P^2}{v^2} \xi \right]} \quad \text{and} \quad y \equiv \frac{\sqrt{V_0}}{M_p v}, \quad (2.31)$$

and temporarily work in units where $M_p = 1$. Working in the approximation $\xi \ll 1$, which will be accurate for the parameter choices that we consider, we choose $N = 60$, $n_s = 0.9603$ and $\Delta_R = 4.69 \times 10^{-5}$. Then, Eqs. (2.28), (2.29) and (2.30) lead to the constraints:

$$0.9603 = 1 + \frac{1}{N_0} x_i \quad (2.32)$$

$$4.69 \times 10^{-5} = \frac{2\sqrt{6}}{\sqrt{\pi}} \frac{y N_0}{\sqrt{1 - x_i^2}} \quad (2.33)$$

$$60 = 2N_0 \ln \left[\sqrt{\frac{(1 - x_i)(1 + x_f)}{(1 + x_i)(1 - x_f)}} \right]. \quad (2.34)$$

The parameter x_f is set by the scale m_χ and can be chosen freely, provided that the magnitude of the cosine is less than one. For this example, we choose $x_f = 0.8$.

Now the three equations above can be solved for the three unknowns, N_0 , x_i and y . We find

$$\begin{aligned}x_i &= -0.64, \\N_0 &= 16, \\y &= 8.0 \times 10^{-7}.\end{aligned}\tag{2.35}$$

Once v is specified, we can solve for the parameters V_0 and m_0 (the latter given by the definition of ξ). In this example, we choose $v = M_P/100$. Then we find (including the input mass scales, for comparison)

$$\begin{aligned}M_P &= 1.2 \times 10^{19} \text{ GeV}, \\v &= M_P/100, \\V_0 &= (1.1 \times 10^{15} \text{ GeV})^4, \\m_0 &= 6.7 \text{ TeV}.\end{aligned}\tag{2.36}$$

In our fundamental theory, Eq. (2.12), V_0 is fixed by Eq. (2.17). We find that the value for V_0 shown in Eq. (2.36) is obtained for the dimensionless parameter choices⁴ $\lambda = 0.1$, $\lambda_{12} = 0.2$ and $c_1 = 0.051$. Notice that none of the fundamental dimensionless couplings is forced to be unnaturally small, unlike the non-supersymmetric model based on the group D_4 that appeared in Ref. [28]; the D_4 symmetry in that proposal allows marginal $\text{SO}(2)$ -violating quartic self-couplings for the inflaton doublet, which necessitates a fine-tuning, while the S_3 symmetry prevents such operators and avoids this outcome. Given our choice of x_f , it follows

⁴Given our normalization of the quartic couplings, perturbativity requires that they be $\ll (4\pi)^2/4! \approx 6.6$, which is easily satisfied.

from Eq. (2.13) that $m_\chi = 2.5 \times 10^{15}$ GeV. Since this is a non-supersymmetric model, tuning of scalar masses is unavoidable; however, the χ mass is at a relatively high scale, so the largest tuning required is still that of the Higgs boson mass, as in the standard model.

Now we can summarize the values of the remaining cosmological parameters:

$$\begin{aligned}\epsilon &= 7.9 \times 10^{-8}, \\ r &= 1.3 \times 10^{-6}, \\ n_r &= 1.1 \times 10^{-3}.\end{aligned}\tag{2.37}$$

These are consistent with the current bounds, assuming that one conservatively accepts the Planck upper bound on r . An observable primordial gravitational wave signal, if confirmed, would rule out this parameter choice. Therefore, we next consider how one could obtain a solution with larger r .

2.6 Enhancing Primordial Gravity Waves

In the slow-roll approximation, by Eqs. (2.19) and (2.23),

$$r = 16 \epsilon = \frac{M_P^2}{\pi} \left(\frac{V'}{V} \right)^2.\tag{2.38}$$

On the other hand, the scalar spectral index was given in Eq. (2.24),

$$n_s(k) = 1 - 6\epsilon + 2\eta,\tag{2.39}$$

with value $n_s = 0.9603 \pm 0.0073$, from Ref. [11]. In order to increase r with fixed n_s in our model, we need to increase the values of both ϵ and η at the time that the fluctuations were created, which we take to be 60 e -folds prior to the end of inflation. We must therefore increase $|V'/V|$ while V''/V becomes less negative; this suggests that the inflaton in our model should minimize $|\cos(3\theta_i/v)|$ in order to obtain large r . Although we find that it is challenging to obtain 60 e -folds of inflation while satisfying observational constraints beginning with such small magnitude of $\cos(3\theta_i/v)$, we find nonetheless that there are points in parameter space where a primordial gravitational wave signal is large enough to be potentially observable in upcoming experiments. These points require a relatively small separation between v and M_P , pushing the limits of effective field theory.

The Lyth bound [34] relates the number of e -folds of inflation to the change in the inflaton field θ during the same period, and suggests that in a wide class of models it is not possible to obtain a sizable gravitational wave signal without a change in the inflaton field during inflation that is much larger than M_P . Such large field values would be problematic for the effective-field-theory interpretation of the model. Using the inflaton equation of motion and the relations for the power spectra of scalar and tensor modes in the slow-roll approximation, one obtains the relation [34],

$$\left(\frac{d\theta}{dN}\right)^2 = \frac{M_P^2}{64\pi} r. \quad (2.40)$$

If r is roughly constant during the last 60 e -folds of inflation, then one obtains,

$$\Delta\theta = \frac{1}{8\sqrt{\pi}} N \sqrt{r} M_P, \quad (2.41)$$

which exceeds M_P for $N\sqrt{r} > 8\sqrt{\pi}$. In particular, this will be the case if $N = 60$ and r is of a typical observable value, for example $r \sim 0.1$. We refer to Eq. (2.41) as the Lyth bound. Hybrid natural inflation models, including the one presented here, can evade the Lyth bound if the inflaton rolls from a steep point in the potential to near the bottom of the potential prior to the end of inflation [40, 41], as sketched in Fig. 2.1. In that case r varies significantly during inflation, which violates the assumption of nearly constant r that fed into the bound.

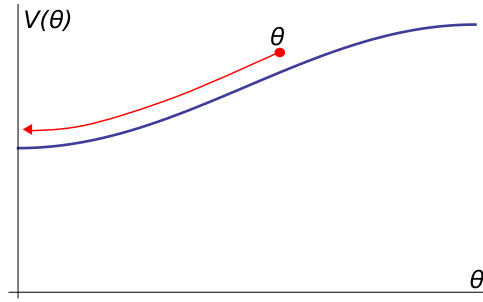


Figure 2.1: The Lyth bound is evaded if the inflaton slowly rolls from a steep point in the potential to near the minimum before the waterfall fields turn on.

In order to obtain 60 e -folds of inflation in this enhanced-gravity-wave scenario, we need inflation to end near the bottom of the inflaton potential, which is possible if the waterfall fields have large diagonal masses m_χ . After fixing the parameters to the well-measured values of Δ_R and n_s , we find that the less-well-measured running of the scalar tilt, $n_r = -0.013 \pm 0.009$ from the Planck experiment [11], in fact provides the greatest obstacle to rolling from near the steepest point of the potential. A viable parameter choice within 2σ of the measured n_r is

obtained by setting $x_f = 0.995$ and $v = M_P/2$, in which case we find⁵

$$\begin{aligned}x_i &= -0.32, \\N_0 &= 9.3, \\y &= 1.70 \times 10^{-6}.\end{aligned}\tag{2.42}$$

The physical mass scales in this case are given by

$$\begin{aligned}M_P &= 1.2 \times 10^{19} \text{ GeV}, \\v &= M_P/2, \\V_0 &= (1.12 \times 10^{16} \text{ GeV})^4, \\m_0 &= 2.6 \times 10^6 \text{ GeV}.\end{aligned}\tag{2.43}$$

In terms of the fundamental potential, Eq. (2.12), the scale V_0 can be reproduced in this case with the choices $\lambda = 0.1$, $\lambda_{12} = 0.2$ and $c_1 = 0.0017$. In that case, from Eq. (2.13) we find $m_\chi = 1.8 \times 10^{17} \text{ GeV}$.

The cosmological parameters evaluated at $\theta = \theta_i$ are now

$$\begin{aligned}\epsilon &= 8.9 \times 10^{-4}, \\r &= 0.014, \\n_r &= 4.8 \times 10^{-3}.\end{aligned}\tag{2.44}$$

⁵For this point in parameter space, there is a more substantial difference in the second significant digit between the exact results and those obtained using the small- ξ approximations in Eqs. (2.32), (2.33) and (2.34). Hence, we show the exact results in this section.

For this point in parameter space, a primordial gravitational wave signal could be within the reach of future CMB polarization measurements. With the same value of x_f but with $v = M_P/3$ rather than $M_P/2$, r decreases to 0.0066. We have assumed that the cutoff of the theory is M_P , where quantum gravity effects are expected to become strong, rather than the reduced Planck mass $M_* = M_P/\sqrt{8\pi}$ that normalizes the gravitational coupling. If we assume $v = M_*/2$ with the same value of x_f as above, we obtain $r = 0.00061$. For comparison, the upcoming PIPER experiment expects a sensitivity to measure r as low as 0.007 [42].

2.7 Inflation Shut-off and Reheating

In this section, we consider the end of inflation and reheating. We first present estimates that indicate the end of inflation happens abruptly⁶, less than a Hubble time after the χ fields develop vacuum expectation values.

Our estimates follow the arguments of Ref. [30]. Consider the evolution of the inflaton field θ during $\Delta t = H^{-1}$ after the critical time t_c , where Eq. (2.13) is an exact equality. At the very end of slow roll, $3H\dot{\theta} \approx -V'(\theta_f)$; hence the change in the inflaton field during the subsequent Δt is given by

$$\Delta\theta = -\frac{3M_P^2}{8\pi v} \frac{\xi \sin(3\theta_f/v)}{[1 - \xi \cos(3\theta_f/v)]}. \quad (2.45)$$

At t_c , the χ mass matrix has a zero eigenvalue, so the magnitude of the negative mass squared term that emerges Δt later is determined by $\Delta\theta$. To assure a rapid evolution of the χ fields, we require that the magnitude of this negative squared

⁶For alternatives to this requirement, see Ref. [43].

mass is larger than H^2 ,

$$3|c_1|\frac{v^2}{M_P}\sin(3\theta_f/v)|\Delta\theta| > H^2, \quad (2.46)$$

which, in the notation of the previous section, leads to the inequality

$$\frac{27}{64\pi^2}|c_1|\xi(1-x_f^2)\frac{v}{M_P} > \frac{V_0}{M_P^4}. \quad (2.47)$$

(Here and below we work to lowest order in $\xi \ll 1$.) In addition, the non-zero χ vevs after t_c generate a contribution to the θ mass squared which we also require to be greater than H^2 ,

$$9|c_1|\frac{v}{M_P}\langle\chi_1\chi_2\rangle > H^2, \quad (2.48)$$

which reduces to

$$\frac{27}{16\pi}\frac{c_1^2}{2\lambda+\lambda_{12}}(1-x_f)\left(\frac{v}{M_P}\right)^4 > \frac{V_0}{M_P^4}. \quad (2.49)$$

For the two points in parameter space studied in Secs. 2.5 and 2.6, respectively, we find numerically that the inequalities in Eqs. (2.47) and (2.49) are satisfied by between four and six orders of magnitude. This suggests that the fields will be driven to their global minimum sufficiently quickly, bringing inflation to an end.

The reheat temperature is sensitive to whether there is substantial preheating and depends on details of the couplings of the waterfall fields to matter, but for an estimate we assume reheating through a Higgs portal due to the quartic coupling,

$$V_{\chi^2 H^2} = \frac{\lambda_{\chi H}}{2}(\chi_1^2 + \chi_2^2)H^\dagger H \supset \frac{\lambda_{\chi H}}{2}\chi^2 H^\dagger H, \quad (2.50)$$

where the waterfall field $\chi \equiv (\chi_1 - \chi_2)/\sqrt{2}$ oscillates during reheating about the minimum of $V(\theta, \chi_i)$, which was determined in Eq. (2.16). We neglect the mixing with the orthogonal combination of $(\chi_1 + \chi_2)/\sqrt{2}$ and the inflaton field θ in this simplified analysis. The Higgs-portal coupling contains the term $\lambda_{\chi H} \langle \chi \rangle \chi H^\dagger H$, where $\langle \chi \rangle/\sqrt{2} = \langle \chi_1 \rangle = -\langle \chi_2 \rangle$, with the $\langle \chi_i \rangle$ determined by Eq. (2.16). This coupling leads to the χ decay rate,

$$\Gamma_\chi = \frac{\lambda_{\chi H}^2 \langle \chi_1 \rangle^2}{4\pi m_{\chi \text{eff}}}. \quad (2.51)$$

The effective χ mass at the minimum of the potential is given by,

$$m_{\chi \text{eff}}^2 = \frac{2c_1 v^3}{M_P} - 2m_\chi^2. \quad (2.52)$$

In most scenarios the reheat temperature is within an order of magnitude of [44]

$$T_{rh} \sim \sqrt{M_P \Gamma_\chi} = \frac{\lambda_{\chi H}}{4} \sqrt{\frac{M_P m_{\chi \text{eff}}}{(2\lambda + \lambda_{12})\pi}}. \quad (2.53)$$

With parameters as in Sec. 2.5 and Sec. 2.6 we find a generically high reheat temperature⁷ $T_{rh} \sim 10^{17} \lambda_{\chi H}$ GeV.

2.8 Conclusions

We have analyzed a model of inflation based on the non-Abelian discrete group S_3 . The mass term and quartic self-coupling of a doublet of scalar fields

⁷Note that the coupling $\lambda_{\chi H}$ first affects the flatness of the inflaton effective potential at two-loops, but only if a Planck-suppressed inflaton-Higgs coupling is present. Such a coupling can be taken small independently so that the range of $\lambda_{\chi H}$ is not restricted from this consideration. All other effects on the inflaton potential involving $\lambda_{\chi H}$ occur at three or more loops.

preserve an accidental $\text{SO}(2)$ symmetry. The $\text{SO}(2)$ is spontaneously broken, giving rise to a pseudo-Goldstone boson which plays the role of the inflaton, as in natural inflation. After the inflaton rolls sufficiently, the coupling of the inflaton to two additional scalar fields generates an instability in a linear combination of those fields, ending inflation and reheating the universe as in hybrid inflation. We studied constraints on the model due to the slow-roll conditions, the requirement of at least 60 e -folds of inflation, the measured magnitude of cosmic density perturbations, the measured scalar spectral index and its running. The model has a viable parameter space with technically natural couplings, and can accommodate potentially observable power in tensor modes without super-Planckian field values during inflation, with $r \sim 0.01$.

Our work has been motivated in part by the minimality of S_3 , which is the smallest possible non-Abelian discrete gauge group. However, it also is worth pointing out that the group S_3 has been used successfully in flavor model building [35]. Such models include substantial scalar sectors (the flavons) that are restricted by the discrete symmetry. It would be interesting in future work to see if the model described here could be incorporated into the flavor-symmetry-breaking sector of a flavor model involving S_3 symmetry.

Chapter 3

Flavored Axion-Monodromy inflation ¹

The hierarchy of fermion masses in the standard model may arise via the breaking of discrete gauge symmetries. The renormalizable interactions of the flavor-symmetry-breaking potential can have accidental global symmetries that are spontaneously broken, leading to pseudo-goldstone bosons that may drive inflation. In this chapter we consider two-field, axion-monodromy inflation models in which the inflaton is identified with a linear combination of pseudo-goldstone bosons of the flavor sector. We show that the resulting models are nontrivially constrained by current cosmological data as well as the requirements of viable flavor model building.

¹Work previously published in C. D. Carone, R. Ramos and Z. Wang, Phys. Rev. D **92**, no. 11, 116011 (2015).

3.1 Introduction

The prevailing approach to solving the horizon and flatness problems of conventional Big Bang cosmology is inflation, a period in which the universe underwent exponential expansion due to the effects of the nearly constant energy density provided by a scalar field [3–5]. Models of inflation are often studied in terms of the properties of the inflaton potential, with somewhat less focus on other roles the inflaton might play in extensions of the standard model. If the inflaton has no purpose other than to provide the source of the energy density that drives inflation, then model building becomes isomorphic to studying ways of generating different functional forms for the inflaton potential. These possibilities, now cataloged (see for example [45]), differ in their detailed predictions for the spectrum of fluctuations in the microwave background that are observed in experiments like Planck [11] and BICEP2 [22].

In this chapter, we consider a scenario in which the inflaton is an integral component of an extension of the standard model that aims to address one of its substantial mysteries: the hierarchy of elementary fermion masses. Models of flavor based on horizontal discrete symmetries postulate that these symmetries are broken via a set of fields, called flavons, that couple to standard model fermions through higher-dimension operators. Discrete flavor symmetries can often lead to accidental continuous global symmetries among the renormalizable terms of the flavon potential. In the present work, we consider the possibility that the inflaton may be identified as a linear combination of the approximate goldstone bosons that arise when these accidental symmetries are spontaneously broken. We will ultimately be interested in two-field models of inflation, for reasons described

below, which distinguishes the present work from the relatively sparse literature that explores the use of flavon fields for a similar purpose [46].

Consider the simplest possibility, a \mathbf{Z}_N flavor symmetry under which a single flavon field Φ transforms as $\Phi \rightarrow \omega\Phi$, where $\omega = \exp(2\pi i/N)$. If the fermions of the standard model are charged under the discrete group, then a tree-level Yukawa coupling that would otherwise be forbidden can arise via a higher-dimension operator. For example, for a down-type quark, one might have

$$\frac{1}{M_F^p} \bar{Q}_L H \phi^p D_R + \text{h.c.} , \quad (3.1)$$

where H is the standard model Higgs doublet, M_F is the flavor scale, and p is an integer. The Yukawa coupling is associated with the ratio $(\langle\phi\rangle/M_F)^p$ which can be much less than one; operators with different values of p can easily provide a hierarchical pattern of entries in the associated Yukawa matrix. If less than the Planck scale, the scale M_F is identified with that of new heavy states that account for the origin of the higher-dimension operators. However, a simpler assumption, that we adopt henceforth, is that the scale M_F is the reduced Planck scale M_* ; the desired operators appear as part of the most general set that are allowed by the local symmetries of the theory, as one expects based on our current understanding of quantum gravity [31]. An immediate implication of our assumptions is that the vacuum expectation value (vev) $\langle\Phi\rangle < M_*$, which will provide an important constraint in our attempt to identify the inflaton with a part of the field Φ .

To obtain an inflaton potential that is sufficiently flat, we require that the goldstone boson degree-of-freedom receives no contributions to its potential from renormalizable terms involving Φ . Let us therefore assume that $N \geq 5$. The

renormalizable terms in the potential are simply

$$V(\Phi) = -m_\Phi^2 \Phi^\dagger \Phi + \frac{\lambda_\Phi}{2} (\Phi^\dagger \Phi)^2. \quad (3.2)$$

Terms such as $(\Phi^4 + \text{h.c.})$ are forbidden by the \mathbf{Z}_N symmetry. Using the nonlinear decomposition

$$\Phi = \frac{\phi + f}{\sqrt{2}} \exp(i\theta/f) \quad (3.3)$$

where $f/\sqrt{2} \equiv \langle \Phi \rangle$, one sees immediately that $V(\Phi)$ is independent of θ , *i.e.*, the potential $V(\theta)$ is exactly flat. The potential in Eq. (3.2) has an accidental global U(1) symmetry and the field θ is the goldstone boson that results from its spontaneous breaking. Global symmetries are not respected by quantum gravitational corrections, so it is no surprise that there are Planck suppressed corrections,

$$\mathcal{L} \supset \frac{c_0}{2} \frac{1}{M_*^{N-4}} \Phi^N + \text{h.c.}, \quad (3.4)$$

that generate a potential for θ , where c_0 is an unknown order-one coefficient. Planck-suppressed operators that directly break the discrete flavor symmetry are not present since we assume in this example (and will require in all our models henceforth) that we work with discrete gauge symmetries, which satisfy appropriate anomaly cancellation conditions and are immune to quantum gravitational corrections. For the reader who is unfamiliar with discrete gauge symmetries, we review the basic issues relevant to our model building in Appendix B.

The operator in Eq. (3.4) leads to the θ potential

$$V(\theta) = c_0 M_*^4 \left(\frac{\langle \Phi \rangle}{M_*} \right)^N \left[1 - \cos(N\theta/f) \right], \quad (3.5)$$

where we have added a constant so that $V(0) = 0$. This is nothing more than the potential of “Natural Inflation” scenarios [23, 24]. However, this potential is not adequate for our purposes. It is well known that if one requires that Natural Inflation provides $\sim 50 - 60$ e-folds of inflation and predicts a spectral index n_s within the range allowed by current Planck data, then f must be well above the Planck scale [47]. For our present application, this would imply that $\langle\phi\rangle/M_*$ is not a small flavor-symmetry-breaking parameter and we lose the ability to predict standard model Yukawa couplings in a controlled approximation.

We therefore must consider other ways of generating potentials for the pseudo-goldstone inflaton that allow a sub-Planckian decay content f . The options assuming a single field inflation model are limited. For example, models of “multi-natural” inflation [48], in which one arranges for additional sinusoidal terms in the potential, can accommodate a sub-Planckian flavon vev, but tend to predict $n_s = 0.95$ in this limit [48], at the very edge of the 95% exclusion region following from Planck data. A different class of models that can more easily provide cosmological predictions consistent with Planck data are two-field models of the axion monodromy type [49–56]. We will show that these can be adapted for the present purpose.

The two pseudo-goldstone fields can have their origin if there are two flavon fields, Φ and χ , that transform under the discrete group $\mathbf{Z}_p^\Phi \times \mathbf{Z}_r^\chi$. We assume that each field transforms only under one of the \mathbf{Z}_N factors,

$$\Phi \rightarrow \omega_\Phi \Phi \quad \text{and} \quad \chi \rightarrow \omega_\chi \chi, \quad (3.6)$$

where $\omega_\Phi = \exp(2\pi i/p)$ and $\omega_\chi = \exp(2\pi i/r)$, where p and r are integers. For $p \geq 5$ and $r \geq 5$, the renormalizable terms in the potential are

$$V(\Phi, \chi) = -m_\Phi^2 \Phi^\dagger \Phi + \frac{\lambda_\Phi}{2} (\Phi^\dagger \Phi)^2 - m_\chi^2 \chi^\dagger \chi + \frac{\lambda_\chi}{2} (\chi^\dagger \chi)^2 + \lambda_p \Phi^\dagger \Phi \chi^\dagger \chi, \quad (3.7)$$

where λ_p is a portal-type coupling. There is no difficulty in choosing parameters such that each field develops a vev. This potential has an accidental $U(1) \times U(1)$ global symmetry that is spontaneously broken. Extending our previous parameterization, we write

$$\Phi = \frac{\phi_0 + f_\theta}{\sqrt{2}} \exp(i\theta/f_\theta) \quad \text{and} \quad \chi = \frac{\chi_0 + f_\rho}{\sqrt{2}} \exp(i\rho/f_\rho). \quad (3.8)$$

Spontaneous symmetry breaking renders the fields ϕ_0 and χ_0 massive so that they are decoupled from the inflation dynamics. The potential for the goldstone bosons $V(\rho, \theta)$ that follows from Eq. (3.7) is exactly flat.

We will discuss later how to generate a potential for ρ and θ of the following axion-monodromy form

$$V(\rho, \theta) = \Lambda_1^4 \left[1 + \cos \left(\frac{\rho}{f_\rho} \right) \right] + \Lambda_2^4 \left[1 - \cos \left(\frac{n\rho}{f_\rho} - \frac{\theta}{f_\theta} \right) \right], \quad (3.9)$$

where n is an integer. The first few terms in the expansion of the first cosine factor have the same form as $-m_r^2 r^2/2 + \lambda_r r^4/4!$, the shift-symmetry-breaking potential $W(r)$ assumed in the Dante's Waterfall scenario discussed in Ref. [50]. In that work, $W(r)$ was assumed to be generated by non-perturbative effects associated with moduli stabilization in string theory, as for example in Ref. [51]. In this chapter, we only consider field theoretic origins of the potential, where the emergence

of the functional form given in Eq. (3.9) is readily obtained. For the purposes of graphical display, if one plots the potential as if ρ and θ were polar coordinates, one would find a “hill” generated by the first cosine factor, circumscribed by a descending spiral “trench” generated by the second. Inflationary trajectories track the minimum of the trench. As θ advances by $2\pi f_\theta$ along the trench, the ρ coordinate does not return to the same value; this monodromy allows for large numbers of e-folds to be achieved within a bounded, sub-Planckian region of field space. We assume that the decay constant f_θ satisfies

$$\frac{f_\theta}{\sqrt{2}} = \lambda M_* \approx 0.22 M_*, \quad (3.10)$$

where λ is a flavor-symmetry-breaking parameter of the same size as the Cabibbo angle. This will allow us to identify the field Φ (and perhaps in some models both Φ and χ) as flavons that can be used in flavor model building. We will see that the discrete symmetry $\mathbf{Z}_p^\Phi \times \mathbf{Z}_r^\chi$ serves four purposes: (i) it assures that there are goldstone bosons that have no potential generated by renormalizable couplings, (ii) it will serve as a flavor symmetry to create a hierarchy of standard model fermion Yukawa couplings, (iii) it will lead to the correct pattern of couplings in a new gauge sector that provides for the desired form of the inflaton potential, Eq. (3.9), and (iv) it will keep quantum gravitational corrections to the potential highly suppressed.

This chapter is organized as follows. In the next section, we discuss the inflationary dynamics that follows from the potential given in Eq. (3.9). We identify solutions in which inflation ends when single-field slow-roll conditions are violated and other solutions where the termination of inflation is analogous to a

hybrid model [30]. In Sec. 3.3, we consider model building issues, in particular, how the discrete symmetries of the theory play an important role in assuring that we obtain the proper potential, and how the same symmetries can be used to produce a plausible model of standard model fermion masses. In the final section, we summarize our conclusions.

3.2 Inflationary Trajectories

In this section, we consider inflationary trajectories in the two-field potential given by Eq. (3.9), that are compatible with flavor model-building requirement Eq. (3.10). We give two example solutions that differ qualitatively in how inflation ends. Note that a more general potential that subsumes Eq. (3.9) was studied in a different context in Ref. [57]; the types of trajectories described therein are consistent qualitatively with those presented here.

3.2.1 Termination Without a Waterfall.

For our first solution, we make the parameter choice $f_\rho = f_\theta \equiv f_1$ and also define $f_1/n \equiv f_2$. We assume $f_1 \gg f_2$, which is equivalent to $n \gg 1$. The potential Eq. (3.9) then takes the form

$$V(\rho, \theta) = \Lambda_1^4 \left[1 + \cos \left(\frac{\rho}{f_1} \right) \right] + \Lambda_2^4 \left[1 - \cos \left(\frac{\rho}{f_2} - \frac{\theta}{f_1} \right) \right]. \quad (3.11)$$

The second cosine term creates a series of trenches on the surface of the potential defined by the first cosine term. If the field θ is plotted as a polar coordinate, the trenches form spirals originating at $\rho = 0$. As in Ref. [50], it is convenient to work

in the rotated field basis $\rho = c \tilde{\rho} + s \tilde{\theta}$ and $\theta = c \tilde{\theta} - s \tilde{\rho}$ with

$$c = \frac{f_1}{\sqrt{f_1^2 + f_2^2}} \quad \text{and} \quad s = \frac{f_2}{\sqrt{f_1^2 + f_2^2}}. \quad (3.12)$$

This allows us to rewrite the potential as

$$V(\tilde{\rho}, \tilde{\theta}) = \Lambda_1^4 \left[1 + \cos \left(\frac{c\tilde{\rho} + s\tilde{\theta}}{f_1} \right) \right] + \Lambda_2^4 \left[1 - \cos \left(\frac{\tilde{\rho}}{f} \right) \right], \quad (3.13)$$

where $f = f_1 f_2 / \sqrt{f_1^2 + f_2^2}$. The modulations in the potential due to the $\cos(\tilde{\rho}/f)$ term create the trench, whose location is given by $\partial V / \partial \tilde{\rho} = 0$, or

$$\sin \left(\frac{\tilde{\rho}}{f} \right) - s c \frac{\Lambda_1^4}{\Lambda_2^4} \sin \left(\frac{c\tilde{\rho} + s\tilde{\theta}}{f_1} \right) = 0. \quad (3.14)$$

The inflaton is the linear combination of the fields that slowly rolls along the trench; inflation terminates when the slow-roll conditions are violated. With the assumptions made throughout this chapter, the inflaton will be well approximated by the linear combination

$$\tilde{\theta} = s \rho + c \theta, \quad (3.15)$$

where c and s are given in Eq. (3.12). For the solutions considered in this subsection, the stability condition $\partial^2 V / \partial \tilde{\rho}^2 > 0$ will hold throughout this trajectory.

To study inflationary observables, we first consider a good approximation to the single-field inflaton potential, which holds for our choice of parameters and can be studied analytically, and then discuss an exact numerical approach that we use to confirm the validity of our results. Let us define $\kappa \equiv s c (\Lambda_1^4 / \Lambda_2^4)$ and consider parameter choices where $\kappa \ll 1$. It follows from Eq. (3.14) that to good

approximation

$$\tilde{\rho}/f \approx 2\pi j, \quad (3.16)$$

where j is an integer. Given our assumption that $f_1 \gg f_2$, it follows from Eqs. (3.13)-(3.16) that $\partial^2 V(\tilde{\rho}, \tilde{\theta})/\partial \tilde{\rho}^2 > 0$, confirming that the trench is stable. Substituting Eq. (3.16) into our original potential yields

$$V(\tilde{\theta}) = \Lambda_1^4 \left[1 + \cos \left(\delta + \tilde{\theta}/f_0 \right) \right], \quad (3.17)$$

where $\delta = 2\pi s c j$ and $f_0 = f_1/s$. Setting $j = 0$ is equivalent to redefining the origin of field space, so we will ignore δ henceforth. We note that the present approximation scheme differs from the one used in Ref. [50], in which one would expand the sinusoidal functions in Eq. (3.14) to linear order in their arguments, but is nonetheless accurate as we confirm numerically later. We note that $s \ll 1$ in the limit $n \gg 1$, so that the derived quantity f_0 can be super-Planckian even when the decay constants f_1 and f_2 are not.

We compare the predictions of the model to the latest results from the Planck Collaboration [11]. The slow roll parameters are defined by

$$\epsilon = \frac{1}{2} \left(\frac{V'}{V} \right)^2, \quad \eta = \frac{V''}{V} \quad \text{and} \quad \gamma = \frac{V'V'''}{V^2}, \quad (3.18)$$

where the primes refer to derivatives with respect to the inflaton field and we work in units where the reduced Planck mass $M_* \equiv M_P/\sqrt{8\pi} = 1$. In the present case, these are given by

$$\epsilon = \frac{1}{2f_0^2} \tan^2[\tilde{\theta}/(2f_0)], \quad (3.19)$$

$$\eta = -\frac{1}{f_0^2} \frac{\cos(\tilde{\theta}/f_0)}{1 + \cos(\tilde{\theta}/f_0)}, \quad (3.20)$$

$$\gamma = -\frac{1}{f_0^4} \tan^2[\tilde{\theta}/(2f_0)]. \quad (3.21)$$

Inflation ends when $\epsilon(\tilde{\theta}_f) = 1$. The initial value of the inflaton, $\tilde{\theta}_i$ is determined by the requirement that we achieve a desired number of e-folds of inflation, given in general by

$$N = \int_{\tilde{\theta}_i}^{\tilde{\theta}_f} \frac{1}{\sqrt{2\epsilon}} d\tilde{\theta} = 2f_0^2 \ln \left[\frac{\sin[\tilde{\theta}_f/(2f_0)]}{\sin[\tilde{\theta}_i/(2f_0)]} \right]. \quad (3.22)$$

We set $N = 60$ in the numerical results that follow. We evaluate the slow-roll parameters and the potential $V(\tilde{\theta})$ at $\tilde{\theta}_i$ in determining the spectral index $n_s = 1 - 6\epsilon + 2\eta$, the ratio of tensor-to-scalar amplitudes $r = 16\epsilon$, the running of the spectral index $n_r = 16\epsilon\eta - 24\epsilon^2 - 2\gamma$ and the scalar amplitude $\Delta_R^2 = V/(24\pi^2\epsilon)$. From Eqs. (3.19)-(3.21), it follows that

$$n_s = 1 + \frac{1}{f_0^2} \left(1 - 2 \sec^2[\tilde{\theta}_i/(2f_0)] \right), \quad (3.23)$$

$$r = \frac{8}{f_0^2} \tan^2[\tilde{\theta}_i/(2f_0)], \quad (3.24)$$

$$n_r = -\frac{2}{f_0^4} \tan^2[\tilde{\theta}_i/(2f_0)] \sec^2[\tilde{\theta}_i/(2f_0)], \quad (3.25)$$

$$\Delta_R^2 = \frac{1}{12\pi^2} \Lambda_1^4 f_0^2 \left(1 + \cos[\tilde{\theta}_i/f_0] \right)^3 \csc^2[\tilde{\theta}_i/f_0]. \quad (3.26)$$

To illustrate a viable solution, consider the parameter choice (again, in units where $M_* = 1$)

$$f_1 = 0.22\sqrt{2}, \quad (3.27)$$

$$f_2 = f_1/21, \quad (3.28)$$

$$\Lambda_1 = \Lambda_2 = 0.006, \quad (3.29)$$

which corresponds to $n = 21$ and $\kappa \approx 1/21$. We find that the initial and final fields for the inflaton trajectory are given by

$$(\tilde{\rho}, \tilde{\theta})_i = (6.04 \times 10^{-4}, 6.74) \quad \text{and} \quad (\tilde{\rho}, \tilde{\theta})_f = (1.50 \times 10^{-4}, 19.14), \quad (3.30)$$

respectively. Using this value for $\tilde{\theta}_i$, we find the following set of cosmological parameters:

$$n_s = 0.96, \quad (3.31)$$

$$r = 0.060, \quad (3.32)$$

$$n_r = -0.00046, \quad (3.33)$$

$$\Delta_R^2 = 2.2 \times 10^{-9}. \quad (3.34)$$

Fig. 3.1 displays the path followed by the inflaton during the 60 e-folds of inflation for this particular solution. The predictions in Eq. (3.34) are consistent with the results from the Planck experiment [11]: $n_s = 0.968 \pm 0.006$, $r < 0.12$ (95% C.L.), $n_r = -0.003 \pm 0.007$ and $\Delta_R^2 = 2.19 \pm 0.08 \times 10^{-9}$. (The value of Δ_R^2 , also called A_s , was taken from the first column of Table 3 in Ref. [11].)

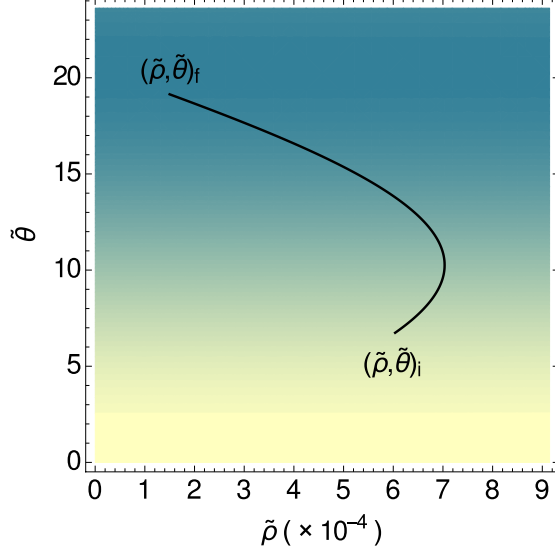


Figure 3.1: Path followed by the inflaton during 60 e-folds of inflation corresponding to the solution of Sec. 3.2.1, in units where $M_* = 1$. The background is a density plot where darker zones have lower values of the potential than lighter ones.

We may check the validity of the results in this section by numerically evaluating the slow-roll parameters in the two-field problem. Let a represent the linear combination of the fields that evolves along the minimum of the trench. Given that $da = \sqrt{d\tilde{\rho}^2 + d\tilde{\theta}^2}$ along the trench, it follows that we can write the n^{th} derivative of the potential with respect to a as

$$\frac{d^n V}{da^n} = \left[\left(1 + \frac{d\tilde{\rho}}{d\tilde{\theta}} \right)_{tr}^{-1/2} \frac{d}{d\tilde{\theta}} \right]^n V \left(\tilde{\theta}, \tilde{\rho}(\tilde{\theta})_{tr} \right), \quad (3.35)$$

where the subscript “tr” indicates quantities evaluated along $\tilde{\rho}(\tilde{\theta})_{tr}$, the solution to Eq. (3.14). Note that as the quantity da is defined above, the kinetic terms for a are canonically normalized. The slow roll parameters can be evaluated

numerically according to Eq. (3.35). We find in this case that $n_s = 0.96$, $r = 0.060$, $n_r = -0.00046$ and $\Delta_R^2 = 2.2 \times 10^{-9}$, in agreement with the results in Eq. (3.34).

3.2.2 Termination With a Waterfall.

For different choices of the model parameters, inflation will end before $\epsilon = 1$ is reached, at a point where there is no longer a solution to Eq. (3.14). At this point, the stability condition $\partial^2 V / \partial \tilde{\rho}^2 > 0$ is also not satisfied, and the fields evolve rapidly in a direction orthogonal to the original trajectory [50]. If one visualizes the motion by plotting the fields as polar coordinates, the evolution corresponds to a transition from spiraling to rapid motion in the radial direction, eventually ending at a global minimum. In Ref. [50] this was called the waterfall, in analogy to the behavior of hybrid inflation models [30], where stability in one field direction can be a function of the value of a second field.

Given an input of model parameters, we determine the final inflaton field value a_f by solving

$$\left. \frac{\partial^2 V}{\partial \tilde{\rho}^2} \right|_{tr} = 0, \quad (3.36)$$

and then the initial value a_i from

$$N = \int_{a_i}^{a_f} \left| \frac{V}{V'} \right| da. \quad (3.37)$$

where the primes refer to derivatives evaluated numerically according to Eq. (3.35), and a ($\approx \tilde{\theta}$) is the canonically normalized inflaton field. Again, we set $N = 60$. To illustrate a solution that ends with the waterfall behavior, consider the parameter

choices

$$f_1 = 0.22\sqrt{2}, \quad (3.38)$$

$$f_2 = f_1/17, \quad (3.39)$$

$$\Lambda_1 = 3.38 \times 10^{-3}, \quad (3.40)$$

$$\Lambda_2 = 1.61 \times 10^{-3}. \quad (3.41)$$

which corresponds to $n = 17$ and $\kappa = 1.13$. We find that the initial and final fields for the inflaton trajectory are given by

$$(\tilde{\rho}, \tilde{\theta})_i = (6.83 \times 10^{-3}, 1.63) \quad \text{and} \quad (\tilde{\rho}, \tilde{\theta})_f = (0.0281, 5.2970), \quad (3.42)$$

respectively. Using this value for $\tilde{\theta}_i$, we find the following set of cosmological parameters:

$$n_s = 0.96, \quad (3.43)$$

$$r = 0.0078, \quad (3.44)$$

$$n_r = -7.2 \times 10^{-5}, \quad (3.45)$$

$$\Delta_R^2 = 2.2 \times 10^{-9}. \quad (3.46)$$

These are consistent with the ranges allowed by Planck, as quoted in the previous subsection. That Eq. (3.44) is much smaller than Eq. (3.32) is consistent with the observation of Ref. [57] that trajectories terminating at a saddle point of the potential can have significantly smaller r than those terminating near minima. Note that our solutions here and in the previous subsection do not involve fine-

tuning; for example, we have checked in the present case that varying the initial value of $\tilde{\theta}$ at the 1% level only results in a change at the 2% level in the observables described above. The complete inflaton trajectory, extending beyond the point where Eq. (3.14) is no longer satisfied, can be found by solving the coupled equations of motion

$$\begin{aligned}\ddot{\rho} + 3H\dot{\rho} + \frac{\partial V}{\partial \rho} &= 0, \\ \ddot{\theta} + 3H\dot{\theta} + \frac{\partial V}{\partial \theta} &= 0,\end{aligned}\tag{3.47}$$

where H is the Hubble parameter. The result is shown in Fig. 3.2, assuming the initial field values $\rho(0) = 0.103$ and $\theta(0) = 1.63$ (equivalent to Eq. (3.42)) and $\dot{\rho}(0) = \dot{\theta}(0) = 0$. The qualitative form of the solution does not depend strongly on the choice of the initial first time derivative, provided that the slow-roll conditions are satisfied. One can see from the plot that the bottom of the trench given by Eq. (3.14), denoted by the thick red line, approximates the actual trajectory, given by the thin green line, very well. The inflaton eventually oscillates about and then settles at the global minimum of the potential.

3.3 Models

3.3.1 Origin of the Potential

The successful inflation potentials presented in the previous section correspond to a potential of the form given in Eq. (3.9). Here we consider the possibility that this potential arises via the effects of anomalies associated with new gauge groups.

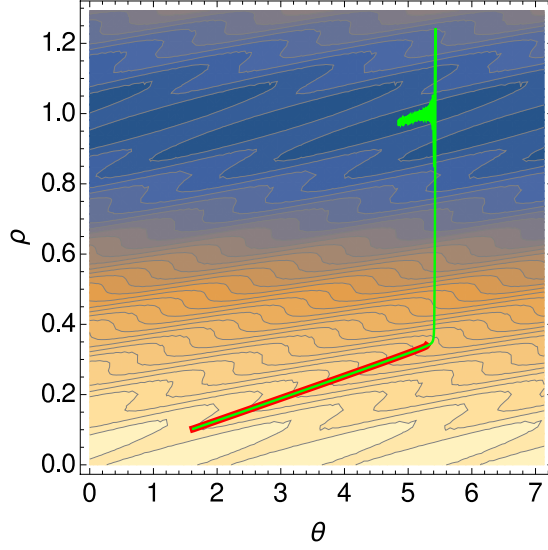


Figure 3.2: Inflaton trajectory, in ρ - θ space, overlaid on a contour plot of the potential, in units where $M_* = 1$. The bottom of the trench is indicated by the thick red line while the inflation trajectory is denoted by the thin green line.

Hence, we extend the standard model gauge group by the additional factors $SU(N_1) \times SU(N_2)$, and introduce the fermions $A_L \sim A_R \sim (\mathbf{N}_1, \mathbf{1})$ and $B_L^{(i)} \sim B_R^{(i)} \sim C_L \sim C_R \sim (\mathbf{1}, \mathbf{N}_2)$. We would like the Lagrangian to contain the following interactions

$$\mathcal{L} \supset h_1 \bar{A}_R A_L \chi + \sum_{i=1}^n h_2^{(i)} \bar{B}_R^{(i)} B_L^{(i)} \chi + h_3 \bar{C}_R C_L \Phi^* + \text{h.c.} \quad . \quad (3.48)$$

Here, the h_j 's are Yukawa couplings and the terms shown generate heavy fermion masses when the Φ and χ fields develop vevs. The accidental global $U(1)$ symmetries are each chiral when appropriate charges are assigned to the A , B and C fermions. However, these symmetries are anomalous with respect to the new

gauge groups. Triangle diagrams lead to the interactions [52]

$$\frac{g_1^2}{32\pi^2} \left(\frac{\rho}{f_\rho} \right) F_1 \tilde{F}_1 + \frac{g_2^2}{32\pi^2} \left(\frac{n\rho}{f_\rho} - \frac{\theta}{f_\theta} \right) F_2 \tilde{F}_2. \quad (3.49)$$

Note that the interactions in Eq. (3.48) are of exactly the same form as Eq. (2.1) of Ref. [52], so that the $F\tilde{F}$ interactions that are relevant in our case can be obtained by adjusting for the multiplicity of the given fermion field (either 1 or n), and taking into account that χ contains $\exp(i\rho/f_\rho)$ while Φ^* contains $\exp(-i\theta/f_\theta)$. With the $F\tilde{F}$ interactions included in the action, the potential is generated non-perturbatively by integrating over instanton gauge field configurations [58]. This leads to the form [52]

$$V(\rho, \theta) = \Lambda_1^4 \left[1 - \cos \left(\frac{\rho}{f_\rho} \right) \right] + \Lambda_2^4 \left[1 - \cos \left(\frac{n\rho}{f_\rho} - \frac{\theta}{f_\theta} \right) \right], \quad (3.50)$$

with the scales Λ_1 and Λ_2 identified with the scale of strong dynamics for each $SU(N)$ factor. (We assume N_1 and N_2 are chosen so that each group is asymptotically free, and that the gauge couplings in the ultraviolet are chosen so that any desired values of Λ_1 and Λ_2 can be achieved.) Redefining the origin of field space via

$$\rho \rightarrow \rho + \pi f_\rho \quad \text{and} \quad \theta \rightarrow \theta + n\pi f_\theta \quad (3.51)$$

puts the potential in the form that we previously assumed in Eq. (3.9). Note that the new gauge groups may be spontaneously broken at a scale well below Λ_1 and Λ_2 without affecting our conclusions.

The interactions given in Eq. (3.48) are clearly not generic. In the absence of our discrete charge assignments for Φ and χ , there would be no reason for the

Φ field to avoid coupling to the A and B -type fermions directly, nor would there be any prohibition of explicit fermion mass terms. Hence, this sector is suggestive of additional symmetries even had we not put them forward immediately as a starting assumption in our model building. Given the transformation properties of Φ and χ fields under the $\mathbf{Z}_p^\Phi \times \mathbf{Z}_r^\chi$ symmetry, Eq. (3.6), we can account for the desired pattern on couplings in Eq. (3.48) by choosing

$$A_R \rightarrow \omega_\chi A_R, \quad B_R^{(i)} \rightarrow \omega_\chi B_R^{(i)}, \quad C_L \rightarrow \omega_\Phi C_L, \quad (3.52)$$

with the remaining heavy fermions taken as singlets under the discrete group. However, we must now enlarge the fermion content to assure that discrete gauge anomalies are cancelled (see Appendix B), and do so in a way that assures that the additional fermions can become massive. To demonstrate that this can be accomplished, let us consider an example suggested by one of our previous cosmological solutions, discussed in Sec. 3.2.1, corresponding to the potential in Eq. (3.9) with $n = 21$. Let us choose $p = r = 21$. First, we note that there are 21 B -type fermions transforming each with \mathbf{Z}_{21}^χ charge $+1$, where we specify the charge Q by defining the group element to be $\exp(2i\pi Q/21)$. This implies that the \mathbf{Z}_{21}^χ -SU(N_2)² discrete anomaly cancellation condition would be satisfied by the B particle content alone. The A and C fermions, on the other hand, lead to anomalies, so we include additional fermions with matching gauge quantum numbers and the discrete transformation rules

$$\begin{aligned} A_R^{(i)} &\rightarrow \omega_\chi^{10} A_R^{(i)}, & A_L^{(i)} &\rightarrow A_L^{(i)} & (i = 1 \dots 2) \\ C_L^{(i)} &\rightarrow \omega_\Phi^{10} C_L^{(i)}, & C_R^{(i)} &\rightarrow C_R^{(i)} & (i = 1 \dots 2) \end{aligned} \quad (3.53)$$

which allow the anomaly cancellation conditions to be satisfied. Finally, we note that these fields will develop masses as a result of Planck-suppressed operators, for example, $\bar{A}_R^{(i)} \chi^{10} A_L^{(i)} / M_*^9 + \text{h.c.}$ and $\bar{C}_L^{(i)} \Phi^{10} C_R^{(i)} / M_*^9 + \text{h.c.}$, which lead to masses of order $\lambda^{10} M_* \sim 10^{11}$ GeV.

The discrete symmetry that we have assumed to assure the form of couplings in Eq. (3.48) also leads to a suppression of direct Planck suppressed corrections to the potential. Since quantum gravitational effects must respect the discrete gauge symmetry, the lowest order operators that will correct the potential have the form Φ^{21} / M_*^{17} or χ^{21} / M_*^{17} ; the scale of these corrections are of order $\lambda^{21} M_*^4 \sim 10^{-14} M_*^4$, negligible compared to the values of Λ_1 and Λ_2 that we found previously to be of order $10^{-3} M_*$.

3.3.2 Standard Model Flavor

The fields Φ and χ can now be utilized in constructing models of standard model fermion masses. These fields will appear in higher-dimension operators that generate the small entries of the standard model Yukawa matrices. Given our choice $\langle \Phi \rangle / M_* = \langle \chi \rangle / M_* = \lambda$, the size of these entries will be determined by powers of the Cabibbo angle λ . In this subsection, we present one example in which the desired set of higher-dimension operators is obtained via the same discrete symmetries that were used to obtain the inflaton potential. We focus on the $n = p = r = 21$ model just discussed, in which the Φ and χ fields each transform under a separate \mathbf{Z}_{21} symmetry. Of course, other choices of the symmetry group are possible, and the present choice does not suggest a unique set of fermion charge assignments (since there are many possible Yukawa textures

Q_{1L}	Q_{2L}	Q_{3L}	u_R^c	c_R^c	t_R^c	d_R^c	s_R^c	b_R^c
6	5	3	2	-1	-3	-1	-2	-2

L_{1L}	L_{2L}	L_{3L}	e_R^c	μ_R^c	τ_R^c	ν_{1R}^c	ν_{2R}^c	ν_{3R}^c
0	0	0	5	3	1	-3	-3	-3

Table 3.1: \mathbf{Z}_{21}^Φ charge assignments q , where the group transformation is defined by $\exp(2i\pi q/21)$. The Higgs doublet is a singlet under the flavor symmetry.

that are viable). The example we give here will suffice by serving as a proof of principle².

The simplest incorporation of the $n = 21$ model in a flavor sector is via the identification of \mathbf{Z}_{21}^Φ as the flavor symmetry and Φ as the sole flavon field. The charge assignments of the standard model fermions and a set of right-handed neutrinos are given in Table 3.1. Entries of the Yukawa matrices arise from \mathbf{Z}_{21}^Φ -invariant higher dimension operators. For example, the 1-1 entry in the up-sector Yukawa matrix involves the fields $\overline{Q}_{1L}Hu_R$, which has flavor charge -8 . This arises at lowest order via

$$\frac{1}{M_*^8} \overline{Q}_{1L} H \Phi^8 u_R + \text{h.c.}, \quad (3.54)$$

and hence the corresponding Yukawa matrix entry is of order λ^8 . Since ω^8 and ω^{-13} are identical, there is another possible operator, $\overline{Q}_{1L} H \Phi^{*13} u_R / M_*^{13} + \text{h.c.}$, but it is of higher order and can be neglected. We may populate the remaining entries of the quark and charged lepton Yukawa matrices in a similar manner. We

²It should also be clear that one could alternatively construct a model starting with the $n = 17$ potential that we discussed earlier, but there are no new qualitative insights gained by presenting two very similar examples.

find

$$Y_u = \begin{pmatrix} \lambda^8 & \lambda^5 & \lambda^3 \\ \lambda^7 & \lambda^4 & \lambda^2 \\ \lambda^5 & \lambda^2 & 1 \end{pmatrix}, Y_d = \begin{pmatrix} \lambda^5 & \lambda^4 & \lambda^4 \\ \lambda^4 & \lambda^3 & \lambda^3 \\ \lambda^2 & \lambda & \lambda \end{pmatrix}, Y_e = \begin{pmatrix} \lambda^5 & \lambda^3 & \lambda \\ \lambda^5 & \lambda^3 & \lambda \\ \lambda^5 & \lambda^3 & \lambda \end{pmatrix}, \quad (3.55)$$

where order one coefficients in each entry have been suppressed. These achieve the desired ratios $m_u/m_t \sim \lambda^8$, $m_c/m_t \sim \lambda^4$, $m_d/m_b \sim \lambda^4$, and $m_s/m_b \sim \lambda^2$, with the charged lepton Yukawa mass eigenvalues comparable in size to those of the down quark sector. It is not hard to verify that the choice of right-handed neutrino charge assignments leads via the see-saw mechanism to a neutrino mass matrix of the form $[\langle H \rangle^2 / \Lambda_R] Y_\nu$, where Λ_R is the right-handed neutrino mass scale, $\langle H \rangle$ is the standard model Higgs vev, and Y_ν is a matrix in which each entry is of order λ^0 times a function of (typically many) undetermined order one coefficients. These can be chosen to obtain the desired phenomenology without unnaturally large or small values of the individual coefficients³.

Finally, we must check that the standard model fermion charge assignments in this model satisfy the linear Ibáñez-Ross anomaly cancellation conditions for the non-Abelian gauge groups and gravity. Summing the \mathbf{Z}_{21}^Φ charges times the appropriate multiplicity factors for the color SU(3), weak SU(2), and gravitational anomalies gives 21, 42 and 63, respectively. These results mod 21 are zero,

³It is not necessarily the case that an alternative model that predicts the neutrino mass hierarchy via powers of λ is more desirable than this example. The reason is that the predictions for neutrino mass matrix entries in such a model also come multiplied by functions of products of a number of the order one operator coefficients. This can spoil the naive λ power counting without any individual operator coefficient being unnaturally small or large. This is a problem that is unique to the neutrino sector in such models when the mass matrix arises via the seesaw mechanism.

indicating that the discrete gauge anomaly cancellation conditions discussed in Appendix B remain satisfied.

3.4 Conclusions

Models of standard model flavor that are based on discrete gauge symmetries can have accidental continuous global symmetries that are spontaneously broken. We have argued that a linear combination of the approximate goldstone bosons that may arise in these models can serve plausibly as the inflaton in two-field models of inflation based on the axion monodromy idea. These models can accommodate the current Planck data on the microwave background [11] while allowing the flavor-symmetry-breaking vacuum expectation values (vevs) to remain sub-Planckian. This is important in the present work since the ratios of the flavon vevs to the reduced Planck scale serve as small flavor-symmetry-breaking parameters in our models, which allows one to predict the standard model Yukawa coupling entries in a controlled approximation. In addition to making correct Yukawa coupling predictions possible, the discrete symmetries of the theory also maintain the correct pattern of the interactions in a new gauge sector, leading to the desired form of the inflaton potential; they also keep the quantum gravitational corrections to the potential well under control. The literature on models of standard model fermion masses is vast and it is imaginable that more economical and compelling examples of flavor-sector inflation models are yet to be found. The present work suggests that exploring the full landscape of such models may be a fertile direction for future investigation.

Chapter 4

Classical Scale-Invariance, the Electroweak Scale and Vector Dark Matter ¹

In this chapter we consider a classically scale-invariant extension of the standard model in which a dark, non-Abelian gauge symmetry is spontaneously broken via the Coleman-Weinberg mechanism. Higgs portal couplings between the dark and standard model sectors provide an origin for the Higgs mass squared parameter and, hence, the electroweak scale. We find that choices for model parameters exist in which the dark gauge multiplet is viable as dark matter.

¹Work previously published in C. D. Carone and R. Ramos, Phys. Rev. D **88**, 055020 (2013).

4.1 Introduction

Over the past decade, solutions to the hierarchy problem have been dominated by an appealing theoretical paradigm: partners to standard model particles are postulated to cancel the quadratic divergence that otherwise affects the Higgs boson squared mass. These partners can have spins that differ from those of their standard model counterparts, as in the minimal supersymmetric standard model (MSSM) [59], or the same spins, as in little Higgs models [60]. They can be associated with states in Hilbert space of positive norm, as in the preceding two examples, or states of negative norm, as in the Lee-Wick standard model [61]. A point of commonality in all these scenarios is the requirement that the partner particles appear at or near the electroweak scale, which one might reasonably identify with the Higgs field vacuum expectation value (VEV), $v = 246$ GeV. Searches at the Large Hadron Collider (LHC) for new particles around this energy scale have, aside from the Higgs boson, produced null results [62].

Of course, all the scenarios described in the preceding paragraph have a decoupling limit, and it is a matter of taste how much fine-tuning one is willing to tolerate before concluding that a given proposal is disfavored. One might hope that the planned energy upgrade at the LHC will provide more definitive results. Nevertheless, the absence of even small indirect effects of partner particles in the current LHC data motivates us to study alternative paradigms. Here, we consider a scenario first discussed by Bardeen [63], and studied recently by many others [64–68, 81], that the standard model may possess a softly broken classical scale invariance that protects it from unwanted quadratic divergences. Such a scenario can be realized if the standard model Lagrangian has no dimensionful parameters and the Higgs mass arises via dimensional transmutation. This can

occur if the Higgs field couples to a new strongly interacting sector, as explored in Refs. [69]. (For a much earlier example of a classically scale-invariant theory in which the Higgs boson mass is determined via dimensional transmutation in a strongly interacting sector, see Ref. [70].) Alternatively, the Higgs boson mass can arise in a classically scale-invariant theory that is weakly coupled via the Coleman-Weinberg (CW) mechanism [71]. It is well known that the CW mechanism applied to the standard model alone leads to a Higgs boson mass that is much smaller than the electroweak gauge boson masses, and hence is not viable. However, Refs. [64–66, 81] demonstrate explicitly that modest extensions of the standard model can avoid this problem. It is this general approach that we pursue in the model building discussed in this chapter.

The argument of Bardeen has been rephrased a number of times in Refs. [65, 66], with additional justification and emphasis varying from paper to paper (see also a summary given in a talk by Lykken [72]). Rather than repeating this discussion, we refer the reader to these references; here we make only a few comments. In order for an extension of the standard model to be classically scale invariant and free of quadratic divergences, one first assumes that the tree-level Higgs mass term is absent and that there are no higher mass scales associated with new heavy particle thresholds, as would be the case, for example, in a grand unified theory. The latter requirement precludes a conventional seesaw mechanism for the generation of small neutrino masses, so we will simply assume that neutrinos have Dirac mass terms with small Yukawa couplings. As in the charged fermion sector, small neutrino masses are then technically natural [36] since chiral symmetries are restored in the limit of vanishing Yukawa couplings. As flavor physics is not the focus of the present work, this assumption will suffice for the

present purposes. If one then works with a regulator that does the least violence to the classical symmetry (namely, dimensional regularization), then one observes that a Higgs mass squared generated radiatively in the infrared is only multiplicatively renormalized [66]; this indicates that it too is technically natural. The only remaining assumption is that quantum gravitational physics does not spoil this outcome even though it is associated with a dimensionful scale, *viz.*, the Planck scale $M_{Pl} = 1.22 \times 10^{19}$ GeV (or alternatively, the reduced Planck scale, $M_* = 2.43 \times 10^{18}$ GeV). Our current uncertainty about the nature of quantum gravity makes this at most a plausible working assumption, but one that leads to a relatively restrictive framework for low-energy model building. Such models can be more readily put to direct experimental tests.

The model we study is one in which the standard model is extended by an additional $SU(2)_D$ gauge group and a complex scalar doublet Φ that transforms only under this new gauge symmetry. The subscript represents the word “dark”, since the new gauge sector only communicates with the standard model via a coupling between Φ and the standard model Higgs doublet field H ,

$$\lambda_p \Phi^\dagger \Phi H^\dagger H, \tag{4.1}$$

where λ_p is typically small. This is the well-known Higgs portal, one of the small number of possible renormalizable couplings between standard model fields and a new sector of particles that are singlets under the standard model gauge group. In the present case, the dark sector is scale invariant at tree level and undergoes spontaneous symmetry breaking via the Coleman-Weinberg mechanism. Hence, the vev $\langle \Phi \rangle \equiv v_D/\sqrt{2}$, which provides an origin for the Higgs boson mass scale via

Eq. (4.1), is determined by dimensional transmutation. The $SU(2)_D$ gauge group is spontaneously broken, leading to a degenerate triplet of massive gauge bosons A^a , $a = 1 \dots 3$, with masses $m_A \equiv g_D v_D/2$, where g_D is the $SU(2)_D$ gauge coupling. These spin-one states are stable and are potential dark matter candidates. One of the results we present in this chapter is that there are parameter choices consistent with viable Coleman-Weinberg symmetry breaking as well as the correct relic density of the $SU(2)_D$ gauge multiplet.

The motivation for the work we present on this model can also be framed in the context of the existing related literature. Let us give three different rationales that may appeal to readers with different theoretical tastes:

i.) The use of the Higgs portal as a means for communicating Coleman-Weinberg symmetry breaking in a dark sector to the standard model has been discussed recently in the context of Abelian dark gauge groups in Refs. [66]. Our work considers the phenomenology in a model based on a non-Abelian dark gauge group, a natural alternative possibility.

ii.) The possibility that dark matter may be spin-one is well known, and the case in which the dark matter is a massive $SU(2)$ gauge multiplet has been considered in Refs. [73]. In this scenario, called Hidden Vector Dark Matter, the doublet field Φ together with the H are assumed to have the most general scalar potential. Our work studies the Coleman-Weinberg limit of the potential, leading to a model that is parametrically simpler and whose phenomenology is more constrained.

iii.) There has been interest in dark matter models in which the dark matter candidate can annihilate predominantly into lighter, unstable intermediate particles. These “secluded dark matter” scenarios [74] are less constrained by direct

dark matter searches, since the annihilation cross section and the dark matter-nucleon elastic scattering cross section are determined by different combinations of couplings. Our work studies a simple model that falls into this interesting category.

This chapter is organized as follows. In Sec. 4.2, we define the model and our conventions. In Sec. 4.3, we consider phenomenological constraints on the model, including vacuum stability, perturbativity, and some aspects of Higgs boson physics. In Sec. 4.4, we consider the parameter ranges in which the model can provide a viable vector dark matter candidate. In Sec. 4.5, we summarize our conclusions.

4.2 The Model

The gauge symmetry of the model is $G_{\text{SM}} \times \text{SU}(2)_D$, where G_{SM} is the standard model gauge group. The standard model particle content is assumed to include three right-handed neutrinos so that neutrino Dirac masses are possible, for the reasons described in the introduction. In addition, the model includes a complex scalar doublet under $\text{SU}(2)_D$. No fermions transforming under the dark gauge group are present, so the model is free of gauge anomalies.

At tree-level, the scalar potential is given by

$$V(\Phi, H) = \frac{1}{2}\lambda(\Phi^\dagger\Phi)^2 - \lambda_p(H^\dagger H)(\Phi^\dagger\Phi) + \frac{1}{2}\lambda_H(H^\dagger H)^2, \quad (4.2)$$

where H is the standard model Higgs doublet field. Mass terms for the Φ and H fields are omitted, in accordance with the assumption of classical scale invariance.

Note that Eq. (4.2) can be rewritten

$$V(\Phi, H) = \frac{1}{2}\lambda_H \left(H^\dagger H - \frac{\lambda_p}{\lambda_H} \Phi^\dagger \Phi \right)^2 + \frac{1}{2} \left(\lambda - \frac{\lambda_p^2}{\lambda_H} \right) (\Phi^\dagger \Phi)^2, \quad (4.3)$$

from which one can read off the tree-level vacuum stability conditions

$$\lambda_H > 0 \quad \text{and} \quad \lambda \lambda_H > \lambda_p^2. \quad (4.4)$$

We will refer to these conditions again later in our analysis.

Given the absence of dimensionful couplings, it is not surprising that minimization of Eq. (4.2) gives $\langle \Phi \rangle = \langle H \rangle = 0$. This outcome, however, does not persist when quantum corrections to $V(\Phi, H)$ are taken into account [71]. We include the one-loop contributions to the effective potential that involve the $\text{SU}(2)_D$ gauge bosons and the top quark. For the numerical values of the couplings that are relevant in our later analysis, these represent the leading corrections. Defining the classical fields ϕ and σ by

$$\Phi = \frac{1}{\sqrt{2}} \begin{pmatrix} 0 \\ \phi \end{pmatrix} \quad \text{and} \quad H = \frac{1}{\sqrt{2}} \begin{pmatrix} 0 \\ \sigma \end{pmatrix}, \quad (4.5)$$

the one-loop effective potential may be written

$$\begin{aligned} V(\phi, \sigma)^{\overline{\text{MS}}} &= \frac{1}{8}\lambda\phi^4 + \frac{9}{1024\pi^2}g_D^4\phi^4 \left(\ln \frac{g_D^2\phi^2}{4\mu^2} - \frac{3}{2} \right) - \frac{1}{4}\lambda_p\sigma^2\phi^2 \\ &+ \frac{1}{8}\lambda_H\sigma^4 - \frac{3}{64\pi^2}h_t^4\sigma^4 \left(\ln \frac{h_t^2\sigma^2}{2\mu^2} - \frac{3}{2} \right), \end{aligned} \quad (4.6)$$

where h_t is the top quark Yukawa coupling. In Eq. (4.6) we work in the $\overline{\text{MS}}$ scheme and μ is the renormalization scale. We extremize the potential by evaluating

$$\frac{\partial V}{\partial \phi} = \frac{\partial V}{\partial \sigma} = 0, \quad (4.7)$$

with V and the couplings contained therein evaluated at the renormalization scale $\mu = \langle \sigma \rangle \equiv v$. (Note that we use this potential only to relate couplings defined at the electroweak scale and vevs that do not differ wildly from the same scale. For this purpose, renormalization group improvement is not necessary to achieve reliable results.) This leads to two constraints on the solution with nonvanishing $\langle \phi \rangle$ and $\langle \sigma \rangle$,

$$\lambda_H = \lambda_p \frac{\langle \phi \rangle^2}{\langle \sigma \rangle^2} - \frac{3}{8\pi^2} h_t^4 \left[1 - \ln \left(\frac{h_t^2}{2} \right) \right], \quad (4.8)$$

$$\lambda = \frac{9}{128\pi^2} g_D^4 \left[1 - \ln \left(\frac{g_D^2 \langle \phi \rangle^2}{4 \langle \sigma \rangle^2} \right) \right] + \lambda_p \frac{\langle \sigma \rangle^2}{\langle \phi \rangle^2}. \quad (4.9)$$

We fix $\langle \sigma \rangle \equiv v = 246$ GeV, as indicated earlier, while $h_t = \sqrt{2}m_t/v$ follows numerically from the $\overline{\text{MS}}$ value of the top quark mass, $m_t = 160_{-4}^{+5}$ GeV [37]. Thus far, Eqs. (4.8) and (4.9) imply that one can take the free parameters of the model to be g_D , λ_p and $\langle \phi \rangle$.

We know, however, that one parametric degree of freedom is fixed by the requirement that one of the two scalar mass eigenstates must correspond to the Higgs boson observed at the LHC. To proceed, we consider the scalar mass squared

matrix that follows from Eqs. (4.6), (4.8) and (4.9):

$$M^2 = \begin{bmatrix} \langle\phi\rangle^2\lambda_p + \Delta m^2 & -\lambda_p\langle\sigma\rangle\langle\phi\rangle \\ -\lambda_p\langle\sigma\rangle\langle\phi\rangle & \frac{9}{128\pi^2}g_D^4\langle\phi\rangle^2 + \lambda_p\langle\sigma\rangle^2 \end{bmatrix}. \quad (4.10)$$

Here, $\Delta m^2 = -3h_t^4\langle\sigma\rangle^2/(8\pi^2)$ is the shift in the Higgs boson mass in the standard model due to the top quark loop correction. For given input values of (g_D, λ_p) , we solve for $\langle\phi\rangle$ numerically by identifying either eigenvalue of Eq. (4.10) with the Higgs boson mass $m_h = 125$ GeV. The two choices correspond to either $m_\eta > m_h$ or $m_\eta < m_h$, where we let η represent the other scalar mass eigenstate. We define the mixing angle θ by

$$\begin{pmatrix} \cos\theta & -\sin\theta \\ \sin\theta & \cos\theta \end{pmatrix} \begin{pmatrix} h \\ \eta \end{pmatrix} = \begin{pmatrix} \sigma_0 \\ \varphi \end{pmatrix}, \quad (4.11)$$

where φ and σ_0 are the physical fluctuations about the vevs: $\phi = \langle\phi\rangle + \varphi$ and $\sigma = \langle\sigma\rangle + \sigma_0$. It follows that $\tan 2\theta = 2M_{12}^2/(M_{11}^2 - M_{22}^2)$, where M_{ij}^2 are the elements of the matrix in Eq. (4.10).

The phenomenology of the model may now be specified in terms of a two-dimensional parameter space, the (g_D, λ_p) plane. We begin isolating interesting regions of this parameter space in the next section.

4.3 Phenomenological Constraints

Given our assumption that there are no new, physical mass scales between the weak and Planck scales, we first require that viable points in parameter space do not lead to Landau poles below M_* in any of the couplings. This precludes

the possibility that a Landau pole is a symptom of omitted new physics that is associated with an intermediate mass scale. Of course, before a Landau pole is reached, a given coupling will become nonperturbatively large, and one cannot be sure that it actually blows up. We simply impose the requirement that λ , λ_H and λ_p remain each smaller than 3 below $\mu = M_*$. We find that the allowed parameter space of the model is not significantly enlarged for larger choices of this numerical limit, since couplings that exceed it tend to do so very quickly. To proceed, we numerically evaluate the following one-loop renormalization group equations (RGEs),

$$16\pi^2 \frac{d\lambda}{dt} = 12\lambda^2 + 4\lambda_p^2 - 9g_D^2\lambda + \frac{9}{4}g_D^4, \quad (4.12)$$

$$\begin{aligned} 16\pi^2 \frac{d\lambda_H}{dt} &= 12\lambda_H^2 + 4\lambda_p^2 + \frac{9}{4} \left(\frac{3}{25}g_1^4 + \frac{2}{5}g_1^2g_2^2 + g_2^4 \right) \\ &\quad - \left(\frac{9}{5}g_1^2 + 9g_2^2 \right) \lambda_H + 12h_t^2\lambda_H - 12h_t^4, \end{aligned} \quad (4.13)$$

$$16\pi^2 \frac{d\lambda_p}{dt} = \lambda_p \left(6\lambda - 4\lambda_p + 6\lambda_H + 6h_t^2 - \frac{9}{2}g_2^2 - \frac{9}{10}g_1^2 - \frac{9}{2}g_D^2 \right), \quad (4.14)$$

$$16\pi^2 \frac{dg_D}{dt} = -\frac{43}{6}g_D^3. \quad (4.15)$$

Here h_t , g_1 , g_2 and g_3 are evolved according to the one-loop standard model RGEs

$$16\pi^2 \frac{dh_t}{dt} = \left[-\frac{17}{20}g_1^2 - \frac{9}{4}g_2^2 - 8g_3^2 + \frac{9}{2}h_t^2 \right] h_t, \quad (4.16)$$

$$16\pi^2 \frac{dg_i}{dt} = b_i g_i^3, \quad (4.17)$$

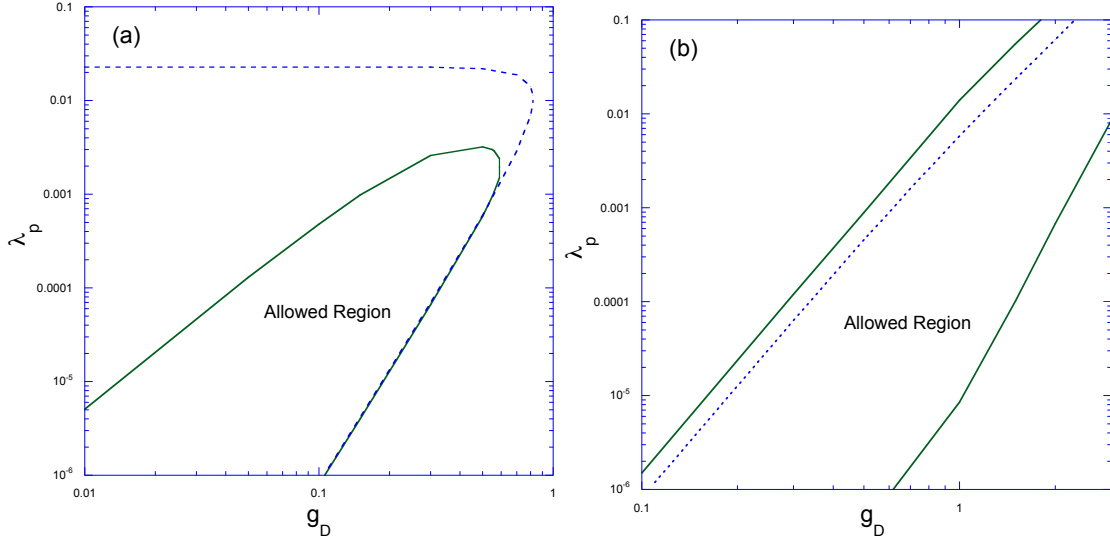


Figure 4.1: Regions of the g_D - λ_p plane that are consistent with the perturbativity and vacuum stability constraints discussed in the text. In (a), $m_\eta < m_h$, while in (b), $m_\eta > m_h$. The regions above and to the right of the dashed line in (a) and above the dashed line in (b) correspond to $\sin^2 \theta > 0.1$.

where $b_i = (\frac{41}{10}, -\frac{19}{6}, -7)$ and we use the SU(5) normalization of hypercharge. In addition to the assignment of initial conditions described in Sec. 4.2, we take $\alpha_1^{-1}(m_Z) = 59.02$, $\alpha_2^{-1}(m_Z) = 29.58$ and $\alpha_3^{-1}(m_Z) = 8.36$ [37]. Defining the parameter $t = \ln(\mu/m_Z)$, we evaluate the RGE's between $t = 0$ and $t_* = \ln(M_*/m_Z) \approx 37.8$, ignoring threshold corrections at the weak scale. We note that our requirement that the couplings remain bounded everywhere in this interval may be overly conservative, since (as theories of TeV-scale gravity have illustrated) the cut off at which gravitational physics becomes relevant may in fact be substantially smaller than M_* .

We are also now equipped to determine the vacuum stability of the model at each point in parameter space. In the standard model, one runs the Higgs quartic coupling to higher renormalization scales and determines whether there are points where the coupling becomes negative. This result implies that the

effective potential becomes unbounded from below. In two-Higgs doublet models, the standard approach is also to run the couplings of the tree-level potential, and to check that the tree-level stability conditions remain satisfied. The justification for this procedure is discussed in some detail in Ref. [75]. Applying this approach to the present model, we require at large renormalization scales that Eq. (4.4) remain satisfied. As discussed in Ref. [76], we do not expect these conditions to be satisfied at small scales, since we know that at small t the tree-level potential is *not* stable; the one-loop corrections are necessary ingredients for obtaining vacuum stability in this region. Given a choice of the two free parameters, the values and signs of all the remaining couplings are determined. Hence, our scan over parameter space will include all possible values of the electroweak-scale couplings that are phenomenologically viable. We then require that Eq. (4.4) remain satisfied over some range $t_0 < t < t_*$ with t_0 sufficiently larger than zero to eliminate cases in which the potential turns over and becomes unbounded from below at large field values. For definiteness, we take $t_0 = 5$ in computing our numerical results; our conclusions are not sensitive to the precise value of t_0 . The allowed regions that remain after the constraints of perturbativity and vacuum stability are imposed are shown in Fig. 4.1. There is no simple qualitative explanation for the shapes of these regions. Eqs. (4.8) and (4.9) as well as the RGEs are nonlinear; at some points in parameter space, λ_H reaches a Landau pole before M_* , while at nearby points one of the other couplings is first to become unacceptably large or leads to a violation of a stability condition. Note that we do not extend these plots to smaller values of g_D , since we will find that relatively large values of the couplings are required to obtain the desired dark vector annihilation cross section. This will be discussed in the next section.

The remaining issue we wish to address in this section is Higgs boson physics. The fact that the scalar mass eigenstates are mixtures of σ_0 and φ , where σ_0 would otherwise correspond to the standard model Higgs field, suggests that the model could lead to observable deviations of Higgs properties away from their standard model expectations. The production cross section times branching fractions of the Higgs-like eigenstate are proportional to $\cos^2 \theta$ times their standard model values. Current LHC bounds imply that this proportionality factor can be no smaller than ≈ 0.7 [77, 87]. Moreover, if the mixing is large, then the otherwise “dark” Higgs η would develop large enough couplings to the visible sector to be detected in Higgs boson searches at the LHC². In this case, the partial widths to standard model quarks, leptons and gauge bosons are $\sin^2 \theta$ times the value for a standard model Higgs. Ignoring possible decay to two standard model Higgs, one would expect that the branching fractions for the η state to be the same as a standard model Higgs boson, but the production cross section suppressed by a factor of $\sin^2 \theta$. LHC heavy Higgs search bounds can all be evaded for $\sin^2 \theta \lesssim 0.1$ [78]. Hence, we show in Fig. 4.1 the regions in which $\sin^2 \theta$ exceeds this value. The true constraint is actually weaker (since the LHC bound is not as restrictive as 0.1 for all scalar boson masses) but the distinction is not important here since the difference this produces in the allowed parameter region of Fig. 4.1 is relatively small.

²For an interesting exception to this statement, see Ref. [79]

4.4 Vector Dark Matter

Let us now consider the $SU(2)_D$ gauge boson interactions in the model,

$$\mathcal{L}_{SU(2)_D} = -\frac{1}{4} \left(F_{\mu\nu}^a \right)^2 + |D_\mu \Phi|^2, \quad (4.18)$$

where $F_{\mu\nu}^a = \partial_\mu A_\nu^a - \partial_\nu A_\mu^a + g_D \epsilon^{abc} A_\mu^b A_\nu^c$ and $D_\mu = \partial_\mu - ig_D T^a A_\mu^a$. The second term of (4.18) contains interactions between φ and the A^a gauge fields:

$$\mathcal{L}_{SU(2)_D} = -\frac{1}{4} \left(F_{\mu\nu}^a \right)^2 + \frac{1}{2} |\partial_\mu \varphi|^2 + \frac{1}{8} g_D^2 A_\mu^a A^{a\mu} (v_D + \varphi)^2. \quad (4.19)$$

Eq. (4.19) exhibits a non-anomalous $SO(3)$ symmetry under which the three gauge bosons transform as a triplet; the other particles in the model are singlets under this symmetry. As pointed out in Refs. [73], this $SO(3)$ symmetry is responsible for preserving the stability of the dark gauge boson multiplet. If higher-dimension operators were present, this symmetry could be broken, leading to a decaying dark matter scenario; this possibility is discussed in the second paper of Ref. [73]. Such dimensionful operators cannot be introduced here due to the assumption of classical scale invariance. After re-expressing φ and σ_0 in terms of the mass eigenstates h and η , one may isolate the leading diagrams that are responsible for dark gauge boson annihilation; in the case of small mixing angle θ (which is the relevant limit, given the results of the previous section), one obtains a reasonable approximation by considering the diagrams shown in Fig. 4.2. These diagrams are relevant provided that the second Higgs field η remains in thermal equilibrium with the ordinary standard model particle content up to the point at which dark gauge boson freeze-out occurs. We will come back to this point later. For the

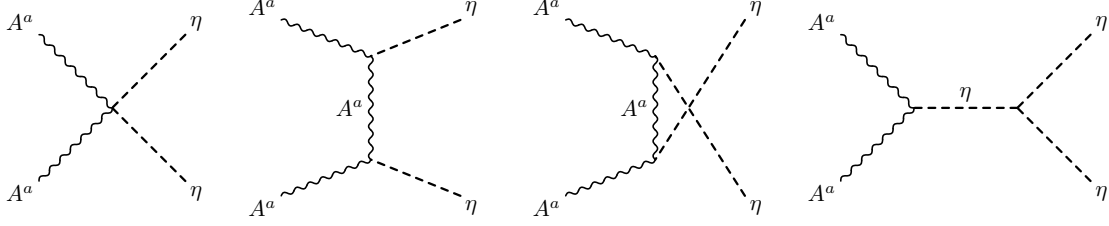


Figure 4.2: Dark gauge boson annihilation diagrams included in the relic density estimate presented in the text.

purposes of our relic density estimate, we omit diagrams that change dark matter number by only one unit, i.e., $AA \rightarrow A\eta$, the same assumption made in the first paper of Ref. [73]. For the parameter region in which we obtain the desired $\Omega_D h^2$, the Higgs portal coupling $\lambda_P \gtrsim 0.001$; in the second paper of Ref. [73], it was found for similar Higgs portal couplings that the omitted diagrams did not substantially affect the relic density estimate; we leave their inclusion, as well as sub-leading diagrams that change dark matter number by two units, for a more detailed analysis in future work.

We find that the thermally averaged annihilation cross section times relative velocity that follows from Fig. 4.2 is

$$\begin{aligned}
 \langle \sigma_{\text{ann}} v \rangle = & \frac{g_D^4 \cos^4 \theta}{192\pi m_A^2} \sqrt{1 - \frac{m_\eta^2}{m_A^2}} \left[\left(\frac{3}{2} \frac{\lambda \langle \varphi \rangle^2 \cos^2 \theta}{(4m_A^2 - m_\eta^2)} + \frac{1}{2} \right)^2 \right. \\
 & - \frac{4}{3} \left(\frac{m_A^2}{m_\eta^2 - 2m_A^2} \right)^2 \left(8 - 6 \frac{m_\eta^2}{m_A^2} + \frac{m_\eta^4}{m_A^4} \right) \left(\frac{3}{2} \frac{\lambda \langle \varphi \rangle^2 \cos^2 \theta}{(4m_A^2 - m_\eta^2)} + \frac{1}{2} \right) \\
 & \left. + \frac{4}{3} \left(\frac{m_A^2}{m_\eta^2 - 2m_A^2} \right)^2 \left(6 - 4 \frac{m_\eta^2}{m_A^2} + \frac{m_\eta^4}{m_A^4} \right) \right]. \quad (4.20)
 \end{aligned}$$

From this result, the freeze-out temperature and relic density are numerically calculated. With $x \equiv m_A/T$, we find numerically that the freeze-out temperature

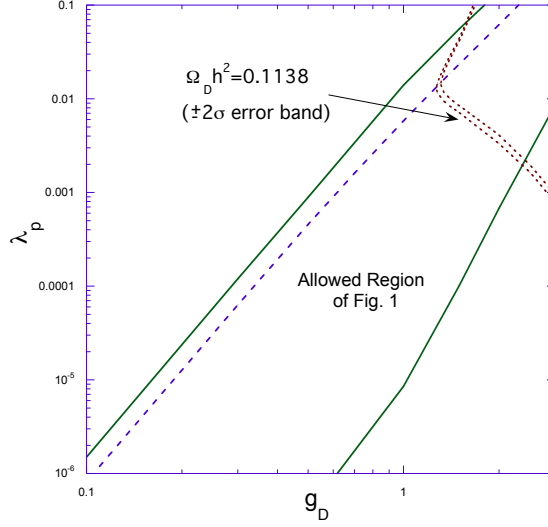


Figure 4.3: Band where the dark gauge multiplet provides the dark matter relic density within $\pm 2\sigma$ experimental uncertainty.

is typically in the range $x_F \approx 26 - 27$. The relic density is given by

$$\Omega_D h^2 \approx 3 \cdot \frac{(1.07 \times 10^9 \text{ GeV}^{-1}) x_F}{\sqrt{g_*(x_F)} M_{Pl} \langle \sigma v \rangle_F} \quad (4.21)$$

where the factor of 3 takes into account the size of the $SU(2)_D$ gauge multiplet. As a point of reference, we note that if all species are dynamical and in equilibrium, one would find $g_* = 122$; we take into account the temperature dependence of g_* in our numerical analysis.

The region in parameter space where $0.1048 < \Omega_D h^2 < 0.1228$, the $\pm 2\sigma$ band for the WMAP result 0.1138 ± 0.0045 [10], is shown in Fig. 4.3, together with our previous constraints. In order to accommodate the observed relic density, the annihilation cross section must be sufficiently large, which in turn requires larger values of g_D and λ_p than allowed if $m_\eta < m_h$. Hence, our relic density results shown relative to the allowed parameter region of Fig. 4.1b.

We note that for all the allowed points in this band, the η remains in thermal equilibrium with the standard model particle bath at the time that the dark matter freezes out. The relevant constraint (following from decay and inverse decay) is $\Gamma_\eta > H(x_F)$, where Γ_η is the η decay width and H is the Hubble parameter [74]; we find that this inequality is satisfied by many orders of magnitude for allowed points in the $\Omega_D h^2$ band. Moreover, we find that the two-into-two process $\eta\eta \rightarrow hh$ is sufficient for maintaining η equilibrium by itself, for all points in the $\Omega_D h^2$ band that are also within the previously allowed region.

Finally, we check the compatibility of our results with current dark matter direct detection bounds. The dark matter-nucleon elastic scattering cross section is given by

$$\sigma(NA \rightarrow NA) = \frac{1}{64\pi} f^2 g_D^4 \sin^2 2\theta \frac{m_N^2}{m_A^2} \frac{\langle\varphi\rangle^2}{\langle\sigma\rangle^2} \frac{(m_\eta^2 - m_h^2)^2}{m_\eta^4 m_h^4} \left(\frac{m_N m_A}{m_N + m_A} \right)^2 \quad (4.22)$$

where m_N is the nucleon mass and f parameterizes the Higgs-nucleon coupling. In Table 4.1, we provide more detailed information on a sampling of points within the $\Omega_D h^2$ allowed band of Fig. 4.3, including the direct detection cross section. The table displays results for $f = 0.3$; for different choices of f , the results can be scaled according to Eq. (4.22). All the points shown are consistent with the bounds from the Xenon100 experiment [21]. We find the same to be true for all points in the $\Omega_D h^2$ allowed band above $g_D \approx 1.23$.

It is now easier to see why this model can be categorized as a secluded dark matter scenario [74]. The dark matter annihilates to an unstable mediator particle, η , at a rate controlled primarily by the coupling g_D . On the other hand, the direct detection cross section, Eq. (4.22), can be made small independently, by choosing

g_D	λ_p ($\times 10^{-3}$)	$\langle\varphi\rangle$ (GeV)	m_A (GeV)	m_η (GeV)	$\sin\theta$	$\sigma(AN)$ ($\times 10^{-45}$ cm ²)
1.4	9.127	1410	987	235	0.0802	1.279
1.5	7.689	1531	1148	292	0.0417	0.5176
2.0	3.609	2228	2228	752	0.0036	0.00972
2.5	1.795	3158	3947	1666	0.0005	0.00031
3.0	0.8606	4561	6841	3465	0.00008	0.00001

Table 4.1: Sample points with $\Omega_D h^2 = 0.1138$, the central WMAP value [10] used in Fig. 4.3. All points shown have an elastic scattering cross section $\sigma(AN)$ below the current Xenon100 direct detection bounds [21].

λ_p values at fixed g_D that produce small $\sin^2 2\theta$. Table 4.1 indicates this behavior as one moves along the $\Omega_d h^2$ band toward the right side of Fig. 4.3.

4.5 Conclusions

We have investigated an extension of the standard model that is classically scale-invariant and in which the electroweak scale arises via the Coleman-Weinberg mechanism [71]. Like similar models involving new Abelian gauge groups [66], our non-Abelian model communicates the dimensional transmutation that originates in a dark sector to standard model particles via the Higgs portal. We have shown that there are regions of the model parameter space in which the theory maintains vacuum stability and perturbativity between the electroweak and the Planck scales, and in which the modifications to the Higgs sector would not yet have been discerned at the LHC. We have also shown that the particular gauge extension we discuss provides a dark matter candidate, a multiplet of stable vector bosons which behaves in accord with secluded dark matter scenarios [74] that have been discussed in the literature.

We note that modifications of this model may also be of interest. For example, if one wanted a similar non-Abelian scenario with fermionic rather than vector dark matter, then one could introduce dark fermions that obtain masses only via spontaneous $SU(2)_D$ breaking (so as not to introduce any new fundamental mass scale) and provide a decay channel for the dark gauge boson multiplet. In such a scenario, a new fermion could be a potential dark matter matter candidate. And as indicated earlier, one might entertain weakening the constraints we've considered by taking the gravitational cut off of the theory to be lower than the conventional Planck scale. Many other variations of the model and the analysis are conceivable.

In light of the current LHC data, the origin of the electroweak scale and the nature of the hierarchy problem merit an exploration of the widest range of theoretical possibilities, including the classically scale-invariant scenarios that have re-emerged as a possibility in the recent literature [66] and motivate the present work. In a few years, the LHC may provide more definitive guidance on whether the one of the more popular theoretical proposals or a less expected paradigm is relevant in describing physics at the TeV scale.

Chapter 5

Dark Chiral Symmetry Breaking and the Origin of the Electroweak Scale ¹

In this chapter we study a classically scale-invariant model in which strong dynamics in a dark sector sets the scale of electroweak symmetry breaking. Our model is distinct from others of this type that have appeared in the recent literature. We show that the Higgs sector of the model is phenomenologically viable and that the spectrum of dark sector states includes a partially composite dark matter candidate.

¹Work previously published in C. D. Carone and R. Ramos, Phys. Lett. B **746**, 424 (2015).

5.1 Introduction

The Lagrangian of the standard model has precisely one dimensionful parameter, the squared mass of the Higgs doublet field. This mass sets the scale of electroweak symmetry breaking, which is communicated to the standard model fermions via their Yukawa couplings. The origin and stability of the hierarchy between the electroweak scale and the Planck scale has motivated many of the leading proposals for physics beyond the standard model. In this letter, we study the phenomenology of a specific model in which the Higgs mass squared arises as a result of strong dynamics in a dark sector. Other models of this type have been discussed in the recent literature [69, 80]; we explain how our model differs from those proposals below.

It is well known that the Yukawa coupling between a scalar ϕ and fermions can lead to a linear term in the scalar potential if the fermions condense. Such a term alters the potential so that the scalar develops a vacuum expectation value (vev). If the scalar squared mass term is absent, then the scale of the scalar vev is set entirely by that of the strong dynamics that produced the condensate. If these fields carry electroweak quantum numbers, then electroweak symmetry will be spontaneously broken. A simple model based on this idea was proposed by Carone and Georgi in Ref. [70]. In this letter, we consider a similar theory in which the scalar and fermions in question do not carry electroweak charges. The vev of ϕ does not break electroweak symmetry, but provides an origin for the Higgs squared mass via the Higgs portal coupling $\lambda_p \phi^\dagger \phi H^\dagger H$. As long as λ_p has the appropriate sign, electroweak symmetry breaking is triggered at a scale set by the strong dynamics of the dark sector.

The choice of a classically scale-invariant scalar potential can be justified by various arguments. We place them in two categories:

1. *The model is tuned.* Dimensionful parameters might not assume natural values as a consequence of the probability distribution over the string landscape, which is poorly understood. If one takes this point of view, it is not unreasonable to consider extensions of the standard model that are designed to address its deficiencies (for example, extensions that provide for viable dark matter physics) that appear tuned but are parametrically simple and can be easily tested in experiment. Our model is of this type and could easily be ruled out (or supported) by upcoming dark matter searches.

2. *The model is not tuned.* If there are no physical mass scales between the weak and Planck scales, then the only possible source of a Higgs quadratic divergences is from the cut off of the theory. Although field theoretic completions to low-energy effective theories lead generically to quadratic divergences proportional to the square of the cutoff [81], this may not be the case for quantum gravitational physics at the Planck scale [82]. As argued in Ref. [83], a space-time description itself may break down at this scale and one’s intuition based on quantum field theories may be flawed. If one takes this point of view, it is not unreasonable to assume that a Higgs mass generated via dimensional transmutation in the infrared is only multiplicatively renormalized [63] and to explore the phenomenological consequences. A significant number of recent papers have adopted this perspective [64–66, 69, 80, 81, 84].

The model we propose has a dark sector $SU(2)_L \times SU(2)_R$ chiral symmetry that is spontaneously broken by a fermion condensate triggered by strong dynamics. An $SU(2)_D$ subgroup of the global symmetry is gauged, and the dark

fermions have Yukawa couplings to a scalar that is a doublet under this gauge symmetry. The dark sector would be an electroweak neutral clone of the model in Ref. [70], except that a $U(1)$ gauge factor is replaced by a discrete subgroup to avoid a massless dark photon. The presence of an $SU(2)_D$ -doublet scalar immediately distinguishes the model from most related ones in the literature which employ a dark singlet to communicate dark sector strong dynamics through the Higgs portal [69]. We note that the model of Ref. [80] has the same dark sector global chiral symmetry as ours, but does not gauge any subgroup. This leads to a different particle spectrum and phenomenology. We also utilize a non-linear chiral Lagrangian approach, familiar from the study of technicolor and QCD, which provides a convenient framework for the systematic description of dark sector phenomenology at low energies.

This chapter is organized as follows: In the next section we define the model. In Sec. 3, we consider phenomenological constraints. In Sec. 4, we study the relic density and direct detection of the dark matter candidate in the model, which is a partially composite dark sector state. In Sec. 5, we present our conclusions.

5.2 The Model

The gauge group of the model is $G_{\text{SM}} \times SU(N) \times SU(2)_D$. The first factor refers to the standard model gauge group, while the second is responsible for confinement in the dark sector. The G_{SM} singlet fields (which we will call the dark sector, henceforth) are: a complex $SU(2)_D$ -doublet scalar ϕ , a left-handed $SU(2)_D$ -doublet fermion $\Upsilon_L \equiv (p_L, m_L)^T$ and two right-handed singlet fermions p_R and m_R . The fermions transform in the fundamental representation of the

$SU(N)$ group. The field content is analogous to that of the technicolor model in Ref. [70] with $SU(2)_W$ replaced by $SU(2)_D$ and $U(1)_Y$ replaced by a Z_3 factor. As we will see below, the latter choice is the simplest way to preserve a convenient analogy between the two theories while also eliminating an unwanted massless gauge field. The dark sector has a global $SU(2)_L \times SU(2)_R$ chiral symmetry that is spontaneously broken when the dark fermions condense

$$\langle \bar{p} p + \bar{m} m \rangle \approx 4\pi f^3, \quad (5.1)$$

where f is the dark pion decay constant. We refer to the unbroken $SU(2)$ subgroup of the global symmetry as dark isospin. Spontaneous chiral symmetry breaking results in an isotriplet of dark pions

$$\Pi = \sum_{a=1}^3 \pi^a \frac{\sigma^a}{2}, \quad (5.2)$$

where σ^a are the Pauli matrices. As in the chiral Lagrangian approach of Ref. [70], we adopt a nonlinear representation

$$\Sigma = \exp(2i\Pi/f), \quad (5.3)$$

which transforms under the global chiral symmetry as $\Sigma \rightarrow L\Sigma R^\dagger$, where L and R are the transformation matrices for $SU(2)_L$ and $SU(2)_R$, respectively. It will be convenient to define the following four-by-four matrix field

$$\Phi \equiv \left(i\sigma^2 \phi^* \mid \phi \right), \quad (5.4)$$

and the nonlinear field redefinition

$$\Phi = \frac{\sigma + f'}{\sqrt{2}} \Sigma' \quad (5.5)$$

with $\Sigma' = \exp(2i\Pi'/f')$. The kinetic terms for Φ and Σ are

$$\begin{aligned} \mathcal{L}_{KE} &= \frac{1}{2} \text{tr} \left(D_\mu \Phi^\dagger D^\mu \Phi \right) + \frac{f^2}{4} \text{tr} \left(D_\mu \Sigma^\dagger D^\mu \Sigma \right) \\ &= \frac{1}{2} \partial_\mu \sigma \partial^\mu \sigma + \frac{f^2}{4} \text{tr} \left(D_\mu \Sigma^\dagger D^\mu \Sigma \right) + \frac{(\sigma + f')^2}{4} \text{tr} \left(D_\mu \Sigma'^\dagger D^\mu \Sigma' \right). \end{aligned} \quad (5.6)$$

Here $D_\mu = \partial_\mu - ig_D A_\mu^a \frac{\sigma^a}{2}$, where A_μ^a is the $\text{SU}(2)_D$ gauge field. Study of the terms quadratic in the fields allows one to identify an unphysical linear combination of fields Π_u that becomes the longitudinal component of A_μ^a , and an orthogonal state π_p that is physical:

$$\pi_u = \frac{f\Pi + f'\Pi'}{\sqrt{f^2 + f'^2}}, \quad (5.7)$$

$$\pi_p = \frac{-f'\Pi + f\Pi'}{\sqrt{f^2 + f'^2}}. \quad (5.8)$$

The π_p multiplet will later be identified as the dark matter candidate in the theory.

Explicit breaking of the chiral symmetry originates from the Yukawa couplings. Assuming that the fields transform under the Z_3 symmetry as

$$\Upsilon_L \rightarrow \Upsilon_L, \quad \phi \rightarrow \omega \phi, \quad p_R \rightarrow \omega p_R, \quad m_R \rightarrow \omega^2 m_R, \quad (5.9)$$

where $\omega^3 = 1$, we find that the Yukawa couplings are given as in Ref. [70] by

$$-\mathcal{L}_y = y_+ \bar{\Upsilon}_L \tilde{\phi} p_R + y_- \bar{\Upsilon}_L \phi m_R + \text{h.c.} \quad (5.10)$$

Defining $\Upsilon_R \equiv (p_R, m_R)$ and the matrix $Y \equiv \text{diag}(y_+, y_-)$ this may be re-expressed as

$$-\mathcal{L}_y = \bar{\Upsilon}_L \Phi Y \Upsilon_R + \text{h.c.}, \quad (5.11)$$

which implies that we may treat (ΦY) as a chiral-symmetry-breaking spurion with the transformation property

$$(\Phi Y) \rightarrow L(\Phi Y)R^\dagger. \quad (5.12)$$

The lowest order term in the chiral Lagrangian that involves (ΦY) is

$$\mathcal{L} = c_1 4\pi f^3 \text{tr}(\Phi Y \Sigma^\dagger) + \text{h.c.} \quad (5.13)$$

where c_1 is expected to be of order unity by naive dimensional analysis [85]. This term determines the physical dark pion mass

$$m_\pi^2 = 2c_1 \sqrt{2} \frac{4\pi f}{f'} (f^2 + f'^2) y, \quad (5.14)$$

where $y \equiv (y_+ + y_-)/2$, as well as a linear term in the scalar potential

$$V_y(\sigma) = -8\sqrt{2}\pi c_1 f^3 y \sigma. \quad (5.15)$$

This term sets the scale of the dark scalar vev, which determines the induced mass term for the standard model Higgs doublet H via a coupling in the potential $V = V_0 + V_y$, where V_0 represents the scale-invariant terms:

$$V_0(\phi, H) = \frac{\lambda}{2} (H^\dagger H)^2 - \lambda_p (H^\dagger H) (\phi^\dagger \phi) + \frac{\lambda_\phi}{2} (\phi^\dagger \phi)^2. \quad (5.16)$$

In the ultraviolet (UV), before the dark fermions have condensed, vacuum stability of Eq. (5.16) requires that

$$\lambda > 0 \quad \text{and} \quad \lambda\lambda_\phi > \lambda_p^2. \quad (5.17)$$

Noting that $\phi^\dagger\phi = \text{tr}(\Phi^\dagger\Phi)/2 = (\sigma + f')^2/2$ and working in unitary gauge where $H = [0, (v + h)/\sqrt{2}]^T$, the potential may be re-expressed as

$$V(h, \sigma) = \frac{\lambda}{8}(v + h)^4 - \frac{\lambda_p}{4}(v + h)^2(\sigma + f')^2 + \frac{\lambda_\phi}{8}(\sigma + f')^4 - 8\sqrt{2}\pi c_1 f^3 y \sigma. \quad (5.18)$$

after the dark fermions have condensed. Minimization of Eq. (5.18) leads to the following expressions for the vevs v and f' :

$$v^3 = 2 \left(\frac{\lambda_p}{\lambda} \right)^{3/2} \left(\lambda_\phi - \frac{\lambda_p^2}{\lambda} \right)^{-1} 8\sqrt{2}\pi c_1 f^3 y, \quad (5.19)$$

$$f'^3 = 2 \left(\lambda_\phi - \frac{\lambda_p^2}{\lambda} \right)^{-1} 8\sqrt{2}\pi c_1 f^3 y. \quad (5.20)$$

Of course, we fix $v = 246$ GeV to obtain the correct electroweak gauge boson masses. The mass squared matrix in the (h, σ) basis is given by

$$M^2 = \begin{pmatrix} \lambda & -\sqrt{\lambda\lambda_p} \\ -\sqrt{\lambda\lambda_p} & \frac{1}{2} \left(\frac{3\lambda_\phi\lambda}{\lambda_p} - \lambda_p \right) \end{pmatrix} v^2, \quad (5.21)$$

which is positive definite for positive couplings with $\lambda\lambda_\phi > \lambda_p^2$.

One of the eigenvalues of this matrix corresponds to the squared mass of the higgs scalar observed at the LHC, $m_{h_0}^2 = (125.09 \text{ GeV})^2$ [86]. We call the

remaining mass eigenstate field η below, and define the mixing angle θ by

$$\begin{pmatrix} \cos \theta & -\sin \theta \\ \sin \theta & \cos \theta \end{pmatrix} \begin{pmatrix} h_0 \\ \eta \end{pmatrix} = \begin{pmatrix} h \\ \sigma \end{pmatrix}. \quad (5.22)$$

The value of the angle θ is given by $\tan 2\theta = 2M_{12}^2/(M_{11}^2 - M_{22}^2)$ where M_{jk}^2 are elements of the matrix in Eq. (5.21).

With the Higgs sector of the theory now defined, we proceed in the next section to study its phenomenology. The parameters that define the Higgs sector are y_+ , y_- , c_1 , λ , λ_p , λ_ϕ , f , f' and v . We set the order-one coupling $c_1 = 1$ for definiteness, and fix values for the Yukawa couplings assuming, for simplicity, that $y_+ = y_-$. The remaining six parameters are constrained by $v = 246$ GeV, $m_{h_0} = 125.09$ GeV, and the two minimization conditions given in Eqs. (5.20)-(5.19). This leaves two degrees of freedom. We choose the free parameters to be f and λ_p and map out the constraints on the model on the f - λ_p plane. This choice lends itself to easy physical interpretation since f parameterizes the scale of the dark sector strong dynamics, while λ_p indicates how strongly the dark sector couples to the visible one.

5.3 Phenomenological Constraints

We determine whether a given point on the f - λ_p plane is allowed by imposing the following constraints:

1. *Absence of Landau poles below the Planck scale.* The presence of such a Landau pole would suggest the onset of new physics at an intermediate scale, contradicting our initial assumptions. Since a coupling that blows up will become

non-perturbative first, we eliminate the possibility of Landau poles by imposing perturbativity constraints on the running couplings. For this purpose, we use the one-loop renormalization group equations (RGEs), which we provide in Appendix A. For the couplings λ , λ_p and λ_ϕ , one-loop corrections become equal in size to tree-level diagrams when, for example, $\lambda \approx 16\pi^2$; to avoid the complete breakdown of the perturbative expansion, we set a generous upper limit on each of these couplings to be one-third of this value, $16\pi^2/3$, evaluated at all scales between m_Z and the reduced Planck mass M_* . By similar reasoning, we place upper limits on the gauge and Yukawa couplings of $4\pi/\sqrt{3}$. For our numerical results, we choose a perturbative value of the $SU(2)_D$ gauge coupling (35% of $4\pi/\sqrt{3}$ in the example we present) that is large enough to assure that the isotriplet gauge multiplet is heavier than the physical pions π_p ; this will be required for our dark matter solutions, as discussed in the next section. We take the $SU(N)$ gauge coupling to be at our perturbativity limit, $4\pi/\sqrt{3}$, at m_Z and choose $N = 4$. Since the $SU(N)$ gauge coupling is asymptotically free in our theory, it remains perturbative for all scales higher than m_Z (where we evaluate the RGEs), but it blows up quickly below m_Z , consistent with our assumption of strong dynamics in the infrared.

2. *Vacuum stability.* The presence of the non-vanishing Higgs portal coupling requires that vacuum stability be studied in the context of a two-Higgs doublet model. In two-Higgs-doublet models, one can assure that the scalar potential remains bounded from below by taking the stability conditions derived from the tree-level potential and testing whether they continue to hold for values of the couplings evaluated at higher-renormalization scales, up to the Planck scale. The justification for this approach can be found in Ref. [75]. We implement this by

evaluating Eq. (5.17) using the one-loop renormalization group equations provided in Appendix A. The scale at which a vacuum instability first arises depends on the free parameters of the model. A given point in the f - λ_p plane satisfies the stability criterion if we find numerically that no violation of the stability conditions arises before the Planck scale. For the dark-matter allowed points described later, the Higgs quartic coupling at the weak scale is larger than its standard model value, which contributes to the model’s vacuum stability.

3. *Sufficiently standard-model-like Higgs boson.* Standard model Higgs boson couplings are altered in this model by a factor of $\cos^2 \theta$, which can be no smaller than 0.7 without spoiling global fits to Higgs data [87]. The η couplings to the visible sector are like those of the Higgs but suppressed by $\sin^2 \theta$; non-observation of the η in heavy Higgs search data from the LHC is assured for any η mass within the range experimentally studied, 145 – 710 GeV, provided that $\sin^2 \theta \lesssim 0.1$ [78]. For simplicity, we require that each point in the f - λ_p plane satisfy $\sin^2 \theta < 0.1$. Our final set of allowed points in parameter space discussed in Sec. 5.4 will correspond to η masses in the range 178 – 203 GeV, falling within the LHC range. Note that we do not consider potentially tighter mixing angle bounds on very light η from LEP2 since we will see later that this region of parameter space is excluded by our fourth constraint.

4. *Approximate chiral symmetry.* Our effective chiral Lagrangian is valid provided that sources of explicit chiral symmetry breaking are small compared to the chiral-symmetry-breaking scale $\Lambda_\chi \equiv 4\pi f$. We reject points in which the dark fermion masses m_\pm exceed one-third Λ_χ , or equivalently

$$\frac{1}{\sqrt{2}} y_\pm f' < \frac{4}{3} \pi f. \quad (5.23)$$

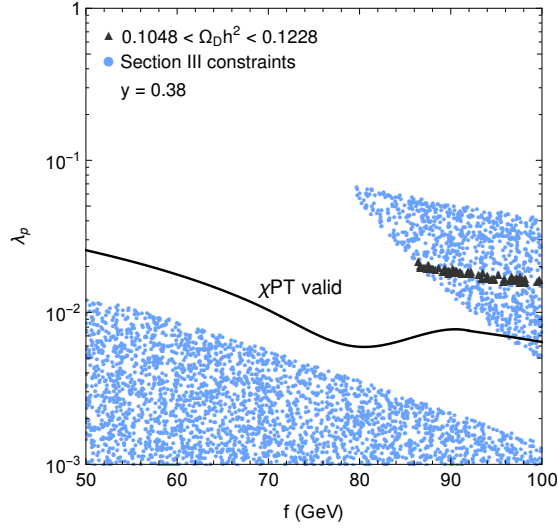


Figure 5.1: Regions of the parameter space consistent with perturbativity and stability constraints, as well as $\sin^2 \theta < 0.1$. Points above the solid black line are consistent with approximate dark sector chiral symmetry. Two branches of points correspond to $m_\eta > m_{h_0}$ (upper branch) and $m_\eta < m_{h_0}$ (lower branch). The triangular points in the upper branch are consistent with current dark matter constraints.

This assures that our initial assumption of an approximate $SU(2)_L \times SU(2)_R$ global symmetry remains valid.

We show results for a particular choice of y in Fig. 5.1. We have chosen to study values of f near or below the scale where the $SU(N)$ gauge coupling becomes strong. The shaded regions satisfy the first three of the constraints discussed in this section. The upper branch of points corresponds to an η heavier than the SM Higgs boson, while the lower branch corresponds to the opposite. The points which also satisfy our fourth constraint lie above the solid black line. We find that viable dark matter solutions exist only for $0.23 < y < 0.52$; we have picked an intermediate value of y as a representative choice. The dark matter results included in this figure will be discussed in the following section.

5.4 Dark Matter

The dark sector of the model includes stable dark pions and baryons, provided that the pions are lighter than the baryons and the $SU(2)_D$ gauge multiplet. In the case we consider, where $y_+ = y_-$, the stabilizing symmetry is the residual dark $SU(2)$ isospin, which is non-anomalous and unbroken by higher-dimension operators (which are absent by the assumed scale invariance of the theory). If y_+ and y_- are unequal, then only the lightest of the dark pion triplet would be stable; for simplicity, we consider the degenerate case here. The dark baryons are separately stable due to a conserved dark baryon number. However, estimating the dark baryon-anti-baryon annihilation cross section by scaling the analogous quantity measured experimentally in QCD, we find that that dark baryon contribution to the relic density is orders of magnitude smaller than that of the π_p for the parameter choices of relevance to our analysis².

The Higgs sector mixing angle θ is generally small, and we can estimate the annihilation cross section by the contributions that are lowest order in $\sin \theta$: this selects $\pi_p^a \pi_p^a \rightarrow \eta \eta$, where $\pi_p = \sum_{a=1}^3 \pi_p^a \sigma^a / 2$, with π_p defined in Eq. (5.8). The $\pi_p \pi_p \eta$ and $\pi_p \pi_p h_0$ vertices originate from Eq. (5.13):

$$\mathcal{L} \supset -\frac{m_\pi^2}{2f'} (\eta \cos \theta + h_0 \sin \theta) \pi_p^a \pi_p^a. \quad (5.24)$$

The first term contributes to the annihilation process of interest via t - and u -channel pion exchange diagrams. Working in the nonrelativistic limit, we find the

²We will see in our figures that the relevant π_p masses are comparable to the scale $\Lambda_\chi = 4\pi f$, which we expect to be of order the dark baryon masses; however, in the effective chiral Lagrangian, the baryon mass terms involve additional unknown parameters that we may choose to assure that the dark baryons are heavier than the π_p . We check directly that the $SU(2)_D$ gauge multiplet is also heavier.

thermally averaged annihilation cross section times velocity

$$\langle \sigma_{\text{ann}} v \rangle = \frac{1}{16\pi} \frac{m_\pi^6}{f'^4} \left(1 - \frac{m_\eta^2}{m_\pi^2} \right)^{1/2} \left[\frac{\cos^2 \theta}{m_\eta^2 - 2m_\pi^2} \right]^2, \quad (5.25)$$

with m_π^2 given by Eq. (5.14). Using this, we calculate the freeze-out temperature T_F and the dark matter relic density by standard methods [8]. Defining $x = m_\pi/T$ and taking into account the dark sector spectrum in evaluating $g_*(x)$, the number of relativistic degrees of freedom at the temperature T , we find freeze-out temperatures near $x_F \approx 26$. The relic density is given by

$$\Omega_D h^2 \approx 3 \cdot \frac{(1.07 \times 10^9 \text{ GeV}^{-1}) x_F}{\sqrt{g_*(x_F)} M_{\text{Pl}} \langle \sigma_{\text{ann}} v \rangle_F} \quad (5.26)$$

which we require to reproduce the WMAP result 0.1138 ± 0.0045 [88] within two standard deviations. In Fig. 5.1, the region consistent with π_p dark matter is the band of triangular points in the upper branch of otherwise allowed points. For our choice of $g_D \approx 2.54$, the $\text{SU}(2)_D$ gauge bosons are heavier than the π_p for each triangular point shown. We do not display results for other choices of y in the range $0.23 < y < 0.52$ which are similar qualitatively to the plot in Fig. 5.1. The main effect of increasing y over this range is to enlarge the upper branch of points while moving the solid black exclusion line upwards until it is roughly contiguous with the band preferred by dark matter considerations when $y = 0.52$.

Finally, we compare the direct detection predictions of the model with current experimental bounds. The π_p -nucleon spin-independent elastic scattering cross section is determined by t -channel h_0 and η exchange diagrams following from the

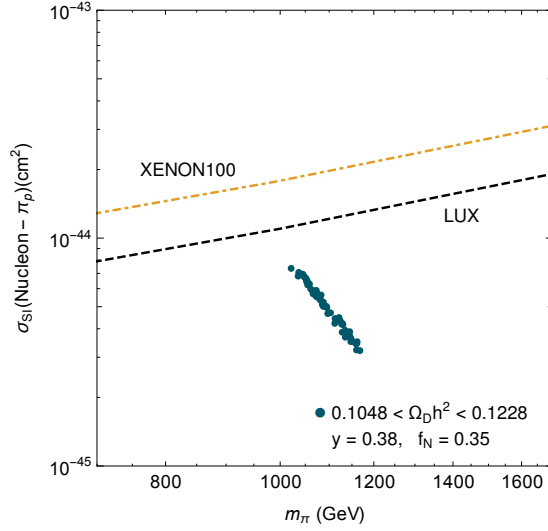


Figure 5.2: Dark pion-nucleon elastic scattering cross section for the points within the dark-matter-preferred band of Fig. 5.1. The current bounds from LUX [20] and XENON100 [21] are also shown.

vertices in Eq. (5.24). We find

$$\sigma_{SI}(\pi_p N \rightarrow \pi_p N) = \frac{f_N^2}{16\pi} \frac{m_\pi^2 m_N^2}{v^2 f'^2} \sin^2 2\theta \frac{(m_\eta^2 - m_{h_0}^2)^2}{m_\eta^4 m_{h_0}^4} \left(\frac{m_N m_\pi}{m_N + m_\pi} \right)^2, \quad (5.27)$$

where f_N parameterizes the Higgs-nucleon coupling and m_N is the nucleon mass. The value of $f_N = 0.35$ is used [89]. Results corresponding to the dark-matter-preferred band in Fig. 5.1 are shown in Fig. 5.2, which includes the current LUX [20] and XENON100 [21] bounds for comparison. All the points shown are currently allowed by direct search constraints, though they are in a region not far from the current bounds. This suggests that future results from the LUX experiment may begin to substantially restrict the preferred dark matter parameter space of the model.

5.5 Conclusions

We have studied a classically scale-invariant model that provides an origin for the electroweak scale via dark sector strong dynamics. The dark sector has a structure similar to the bosonic technicolor model proposed in Ref. [70]: a fermion condensate is responsible for the instability that leads to a scalar doublet acquiring a vev. In the model of Ref. [70], the fermion condensate and the scalar vev each contribute to the breaking of electroweak symmetries. Here, the analogous fields are electroweak singlets; the scalar vev breaks a dark $SU(2)$ gauge group and induces a mass term for the standard model Higgs doublet field via couplings in the Higgs potential. We found regions in the parameter space of the model where all the couplings can be run up to the Planck scale while remaining perturbative, where the scalar potential satisfies vacuum stability constraints, and where the Higgs boson is sufficiently standard-model-like to be consistent with existing collider data. In addition, we showed that the partially composite dark isotriplet bosons in the model can provide a viable dark matter candidate, providing the desired relic density while evading current direct detection bounds. In addition, the model predicts that the dark matter-nucleon elastic scattering cross section lies just beyond the current LUX bounds. Hence, the model may be ruled out, or given experimental support, as the LUX data set is enlarged.

Appendix A

RGEs

The RGEs used in the analysis of section 5.3 are as follows:

$$16\pi^2 \frac{d\lambda_\phi}{dt} = 4N\lambda_\phi (y_-^2 + y_+^2) - 4N (y_-^4 + y_+^4) - 9g_D^2\lambda_\phi + \frac{9}{4}g_D^4 + 4\lambda_p^2 + 12\lambda_\phi^2, \quad (\text{A.1})$$

$$16\pi^2 \frac{d\lambda}{dt} = \frac{9}{4} \left(\frac{2}{5}g_1^2g_2^2 + \frac{3}{25}g_1^4 + g_2^4 \right) - \lambda \left(\frac{9}{5}g_1^2 + 9g_2^2 \right) + 12\lambda y_t^2 + 12\lambda^2 + 4\lambda_p^2 - 12y_t^4 \quad (\text{A.2})$$

$$16\pi^2 \frac{d\lambda_p}{dt} = \left[2N (y_-^2 + y_+^2) + \frac{9}{2} \left(-\frac{1}{5}g_1^2 - g_2^2 - g_D^2 \right) + 6\lambda - 4\lambda_p + 6\lambda_\phi + 6y_t^2 \right] \lambda_p, \quad (\text{A.3})$$

$$16\pi^2 \frac{dy_t}{dt} = \left[-\frac{17}{20}g_1^2 - \frac{9}{4}g_2^2 - 8g_3^2 + \frac{9}{2}y_t^2 \right] y_t, \quad (\text{A.4})$$

$$16\pi^2 \frac{dy_-}{dt} = \left[\left(N + \frac{3}{2} \right) y_-^2 + \left(N - \frac{3}{2} \right) y_+^2 - \frac{9}{4}g_D^2 - \frac{3(N^2 - 1)}{N}g_N^2 \right] y_-, \quad (\text{A.5})$$

$$16\pi^2 \frac{dy_+}{dt} = \left[\left(N - \frac{3}{2} \right) y_-^2 + \left(N + \frac{3}{2} \right) y_+^2 - \frac{9}{4}g_D^2 - \frac{3(N^2 - 1)}{N}g_N^2 \right] y_+, \quad (\text{A.6})$$

$$16\pi^2 \frac{dg_D}{dt} = \left[\frac{N}{3} - \frac{43}{6} \right] g_D^3, \quad (\text{A.7})$$

$$16\pi^2 \frac{dg_N}{dt} = \left[\frac{4}{3} - \frac{11}{3}N \right] g_N^3, \quad (\text{A.8})$$

$$16\pi^2 \frac{dg_i}{dt} = b_i g_i^3. \quad (\text{A.9})$$

Here $t = \ln(\mu/m_Z)$, where μ is the renormalization scale, $b_i = (\frac{41}{10}, -\frac{19}{6}, -7)$, the SU(5) normalization for the hypercharge was used and g_N is the SU(N) gauge coupling.

Appendix B

Discrete Gauge Symmetries, Briefly

It is well known that continuous gauge symmetries are not violated by quantum gravitational effects. Under what circumstances is the same true for discrete symmetries? It was noted long ago by Ibáñez and Ross (IR) [32] that a discrete group that arises as a subgroup of a continuous gauge symmetry inherits this protection. While the full theory must satisfy the anomaly cancellation conditions relevant for the continuous gauge groups, IR determined the conditions that are relevant in the low-energy theory, below the scale at which the continuous gauge symmetries are broken. Since some of the fermions in the complete theory may become massive and decoupled when symmetry breaking occurs, the low-energy theory includes only part of the fermion content that contributes to anomaly cancellation in the full theory. The low-energy constraints should refer only to the light fermion content, which in the present context corresponds to models defined below the reduced Planck scale M_* . If the appropriate consistency conditions are

satisfied, the discrete gauge symmetry can be treated as fundamental, without reference to specific high-energy embeddings.

The constraints that we apply in our model building are the linear IR conditions involving non-Abelian gauge group factors; these follow from triangle diagrams involving two non-Abelian gauge group factors and one factor of the continuous gauge group in which the discrete symmetry is embedded. For example, the \mathbf{Z}_N -SU(M)² anomaly cancellation condition is [32]

$$\sum_i C_i q_i = \frac{1}{2} r N. \quad (\text{B.1})$$

Here r is an integer, q_i is the \mathbf{Z}_N charge of the i^{th} fermion (which transforms under \mathbf{Z}_N by $\exp[i2\pi q_i/N]$) and C_i is the Casimir invariant given by $\text{Tr}(T^a T^b) = C_i \delta^{ab}$, where the T^a are SU(M) generators in the representation of the i^{th} fermion. Since all the fermions in the model presented in Sec. 3.3 are in the fundamental representations of the relevant SU(M) gauge groups, $C_i = 1/2$; the linear IR conditions simply requires that the \mathbf{Z}_N charges of the fermions that transform under a specified SU(M) factor sum to an integer multiple of N . According to IR, when N is odd (relevant to the model of Sec. 3.3) the gravitational anomalies linear in \mathbf{Z}_N are cancelled when the sum of all the \mathbf{Z}_N charges are also an integer multiple of N . It is straightforward to verify that these conditions are satisfied by the charge assignments displayed in Table 3.1.

What about the other possible anomaly cancellation conditions? First, IR note that the linear conditions involving the Abelian gauge groups do not lead to any useful constraints on the low-energy theory [32]. Banks and Dine (BD) [33] later showed that the IR conditions non-linear in the discrete group make a tacit

assumption about the high-energy embedding of the theory, through the requirement that both the light and the heavy fermions have integer $U(1)$ charges. BD show that there are consistent, non-anomalous theories (ones in which the effective discrete symmetry at low energies is smaller than that of the full theory) in which the low-energy spectrum does not satisfy the non-linear IR constraints; their failure only implies the existence of heavy fermions with fractional charges. Thus, the non-linear IR conditions are not required for the consistency of the low-energy effective theory. BD note that the surviving discrete anomaly cancellation conditions are physically sensible: for example, the condition for the cancellation of the \mathbf{Z}_N - $SU(M)^2$ anomaly also guarantees that there are no t'Hooft interactions generated by $SU(M)$ instantons that would explicitly break the \mathbf{Z}_N symmetry. This physical constraint [90] is completely independent of the high-energy embedding.

BIBLIOGRAPHY

- [1] P. A. R. Ade *et al.* [Planck Collaboration], “Planck 2015 results. XIII. Cosmological parameters,” arXiv:1502.01589 [astro-ph.CO].
- [2] A. A. Penzias and R. W. Wilson, “A Measurement of excess antenna temperature at 4080-Mc/s,” *Astrophys. J.* **142**, 419 (1965). doi:10.1086/148307
- [3] A. H. Guth, “The Inflationary Universe: A Possible Solution to the Horizon and Flatness Problems,” *Phys. Rev. D* **23**, 347 (1981). doi:10.1103/PhysRevD.23.347
- [4] A. D. Linde, “A New Inflationary Universe Scenario: A Possible Solution of the Horizon, Flatness, Homogeneity, Isotropy and Primordial Monopole Problems,” *Phys. Lett. B* **108**, 389 (1982);
- [5] A. Albrecht and P. J. Steinhardt, “Cosmology for Grand Unified Theories with Radiatively Induced Symmetry Breaking,” *Phys. Rev. Lett.* **48**, 1220 (1982).
- [6] F. Zwicky, “On the Masses of Nebulae and of Clusters of Nebulae,” *Astrophys. J.* **86**, 217 (1937). doi:10.1086/143864
- [7] M. Kamionkowski, “WIMP and axion dark matter,” In **Trieste 1997, High energy physics and cosmology** 394-411 [hep-ph/9710467].

- [8] E. W. Kolb and M. S. Turner, “The Early Universe,” *Front. Phys.* **69**, 1 (1990).
- [9] S. Dodelson, “Modern Cosmology,” Amsterdam, Netherlands: Academic Pr. (2003) 440 p
- [10] G. Hinshaw *et al.* [WMAP Collaboration], “Nine-Year Wilkinson Microwave Anisotropy Probe (WMAP) Observations: Cosmological Parameter Results,” arXiv:1212.5226 [astro-ph.CO].
- [11] P. A. R. Ade *et al.* [Planck Collaboration], “Planck 2015 results. XX. Constraints on inflation,” arXiv:1502.02114 [astro-ph.CO].
- [12] Z. Ahmed *et al.* [BICEP3 Collaboration], “BICEP3: a 95GHz refracting telescope for degree-scale CMB polarization,” *Proc. SPIE Int. Soc. Opt. Eng.* **9153**, 91531N (2014) doi:10.1117/12.2057224 [arXiv:1407.5928 [astro-ph.IM]].
- [13] M. Trodden and S. M. Carroll, “TASI lectures: Introduction to cosmology,” astro-ph/0401547.
- [14] D. Baumann, “Inflation,” doi:10.1142/9789814327183_0010 arXiv:0907.5424 [hep-th].
- [15] V. C. Rubin, and N. Thonnard, N. and W. K. Ford, Jr., “Extended rotation curves of high-luminosity spiral galaxies. IV - Systematic dynamical properties, SA through SC” *Astrophys. J.* **225**, 107 (1978). doi:10.1086/182804

- [16] V. C. Rubin and W. K. Ford, Jr., “Rotation of the Andromeda Nebula from a Spectroscopic Survey of Emission Regions,” *Astrophys. J.* **159**, 379 (1970). doi:10.1086/150317
- [17] E. D. Loh and E. J. Spillar, “A measurement of the mass density of the universe,” *Astrophys. J.* **307**, L1 (1986). doi:10.1086/184717
- [18] M. Milgrom, “A Modification of the Newtonian dynamics as a possible alternative to the hidden mass hypothesis,” *Astrophys. J.* **270**, 365 (1983). doi:10.1086/161130
- [19] G. Bertone, “The moment of truth for WIMP Dark Matter,” *Nature* **468**, 389 (2010) doi:10.1038/nature09509 [arXiv:1011.3532 [astro-ph.CO]].
- [20] D. S. Akerib *et al.* [LUX Collaboration], “First results from the LUX dark matter experiment at the Sanford Underground Research Facility,” *Phys. Rev. Lett.* **112**, 091303 (2014) [arXiv:1310.8214 [astro-ph.CO]].
- [21] E. Aprile *et al.* [XENON100 Collaboration], “Dark Matter Results from 225 Live Days of XENON100 Data,” *Phys. Rev. Lett.* **109**, 181301 (2012) [arXiv:1207.5988 [astro-ph.CO]].
- [22] P. A. R. Ade *et al.* [BICEP2 Collaboration], “Detection of B-Mode Polarization at Degree Angular Scales by BICEP2,” *Phys. Rev. Lett.* **112**, 241101 (2014) [arXiv:1403.3985 [astro-ph.CO]].
- [23] F. C. Adams, J. R. Bond, K. Freese, J. A. Frieman and A. V. Olinto, “Natural inflation: Particle physics models, power law spectra for large scale structure, and constraints from COBE,” *Phys. Rev. D* **47**, 426 (1993) [hep-ph/9207245].

- [24] K. Freese, J. A. Frieman and A. V. Olinto, “Natural inflation with pseudo - Nambu-Goldstone bosons,” *Phys. Rev. Lett.* **65**, 3233 (1990).
- [25] K. Freese, C. Savage and W. H. Kinney, “Natural Inflation: The Status after WMAP 3-year data,” *Int. J. Mod. Phys. D* **16**, 2573 (2008) [arXiv:0802.0227 [hep-ph]].
- [26] J. D. Cohn and E. D. Stewart, “NonAbelian discrete gauge symmetries and inflation,” *Phys. Lett. B* **475**, 231 (2000) [hep-ph/0001333].
- [27] E. D. Stewart and J. D. Cohn, “Inflationary models with a flat potential enforced by nonAbelian discrete gauge symmetries,” *Phys. Rev. D* **63**, 083519 (2001) [hep-ph/0002214].
- [28] G. G. Ross and G. German, “Hybrid natural inflation from non Abelian discrete symmetry,” *Phys. Lett. B* **684**, 199 (2010) [arXiv:0902.4676 [hep-ph]].
- [29] G. G. Ross and G. German, “Hybrid Natural Low Scale Inflation,” *Phys. Lett. B* **691**, 117 (2010) [arXiv:1002.0029 [hep-ph]].
- [30] A. D. Linde, “Hybrid inflation,” *Phys. Rev. D* **49**, 748 (1994) [astro-ph/9307002].
- [31] R. Kallosh, A. D. Linde, D. A. Linde and L. Susskind, “Gravity and global symmetries,” *Phys. Rev. D* **52**, 912 (1995) [hep-th/9502069].
- [32] L. E. Ibanez and G. G. Ross, “Discrete gauge symmetry anomalies,” *Phys. Lett. B* **260**, 291 (1991).

- [33] T. Banks and M. Dine, “Note on discrete gauge anomalies,” *Phys. Rev. D* **45**, 1424 (1992) [hep-th/9109045].
- [34] D. H. Lyth, “What would we learn by detecting a gravitational wave signal in the cosmic microwave background anisotropy?,” *Phys. Rev. Lett.* **78**, 1861 (1997) [hep-ph/9606387].
- [35] L. J. Hall and H. Murayama, “A Geometry of the generations,” *Phys. Rev. Lett.* **75**, 3985 (1995) [hep-ph/9508296]; C. D. Carone, L. J. Hall and H. Murayama, “ $S(3)_3$ flavor symmetry and $p \rightarrow K^0 e^+$,” *Phys. Rev. D* **53**, 6282 (1996) [hep-ph/9512399]; “A Supersymmetric theory of flavor and R-parity,” *Phys. Rev. D* **54**, 2328 (1996) [hep-ph/9602364].
- [36] G. ’t Hooft, “Naturalness, chiral symmetry, and spontaneous chiral symmetry breaking,” *NATO Adv. Study Inst. Ser. B Phys.* **59**, 135 (1980).
- [37] J. Beringer *et al.* [Particle Data Group Collaboration], “Review of Particle Physics (RPP),” *Phys. Rev. D* **86**, 010001 (2012).
- [38] M. J. Mortonson and U. Seljak, “A joint analysis of Planck and BICEP2 B modes including dust polarization uncertainty,” arXiv:1405.5857 [astro-ph.CO].
- [39] R. Flauger, J. C. Hill and D. N. Spergel, “Toward an Understanding of Foreground Emission in the BICEP2 Region,” arXiv:1405.7351 [astro-ph.CO].
- [40] A. Hebecker, S. C. Kraus and A. Westphal, “Evading the Lyth Bound in Hybrid Natural Inflation,” *Phys. Rev. D* **88**, 123506 (2013) [arXiv:1305.1947 [hep-th]].

- [41] M. Carrillo-González, G. Germán-Velarde, A. Herrera-Aguilar, J. C. Hidalgo and R. Sussman, “Testing Hybrid Natural Inflation with BICEP2,” *Phys. Lett. B* **734**, 345 (2014) [arXiv:1404.1122 [astro-ph.CO]].
- [42] J. Lazear, P. A. R. Ade, D. Benford, C. L. Bennett, D. T. Chuss, J. L. Dotson, J. R. Eimer and D. J. Fixsen *et al.*, “The Primordial Inflation Polarization Explorer (PIPER),” arXiv:1407.2584 [astro-ph.IM].
- [43] S. Clesse, “Hybrid inflation along waterfall trajectories,” *Phys. Rev. D* **83**, 063518 (2011) [arXiv:1006.4522 [gr-qc]].
- [44] L. Kofman, A. D. Linde and A. A. Starobinsky, “Towards the theory of reheating after inflation,” *Phys. Rev. D* **56**, 3258 (1997) [hep-ph/9704452].
- [45] D. H. Lyth, “Particle physics models of inflation,” *Lect. Notes Phys.* **738**, 81 (2008) [hep-th/0702128].
- [46] S. Antusch, S. F. King, M. Malinsky, L. Velasco-Sevilla and I. Zavala, “Flavon Inflation,” *Phys. Lett. B* **666**, 176 (2008) [arXiv:0805.0325 [hep-ph]].
- [47] J. E. Kim, H. P. Nilles and M. Peloso, “Completing natural inflation,” *JCAP* **0501**, 005 (2005) [hep-ph/0409138].
- [48] M. Czerny and F. Takahashi, “Multi-Natural Inflation,” *Phys. Lett. B* **733**, 241 (2014) [arXiv:1401.5212 [hep-ph]].
- [49] L. McAllister, E. Silverstein and A. Westphal, “Gravity Waves and Linear Inflation from Axion Monodromy,” *Phys. Rev. D* **82**, 046003 (2010) [arXiv:0808.0706 [hep-th]].

- [50] C. D. Carone, J. Erlich, A. Sensharma and Z. Wang, “Two-field axion-monodromy hybrid inflation model: Dante’s Waterfall,” *Phys. Rev. D* **91**, no. 4, 043512 (2015) [arXiv:1410.2593 [hep-ph]].
- [51] M. Berg, E. Pajer and S. Sjors, “Dante’s Inferno,” *Phys. Rev. D* **81**, 103535 (2010) [arXiv:0912.1341 [hep-th]].
- [52] J. McDonald, “A Minimal Sub-Planckian Axion Inflation Model with Large Tensor-to-Scalar Ratio,” arXiv:1407.7471 [hep-ph];
- [53] J. McDonald, “Signatures of Planck Corrections in a Spiralling Axion Inflation Model,” arXiv:1412.6943 [hep-ph].
- [54] G. Barenboim and W. I. Park, “Spiral Inflation,” arXiv:1412.2724 [hep-ph]; “Spiral Inflation with Coleman-Weinberg Potential,” *Phys. Rev. D* **91**, no. 6, 063511 (2015) [arXiv:1501.00484 [hep-ph]].
- [55] T. Li, Z. Li and D. V. Nanopoulos, “Helical Phase Inflation via Non-Geometric Flux Compactifications: from Natural to Starobinsky-like Inflation,” arXiv:1507.04687 [hep-th]; “Helical Phase Inflation,” *Phys. Rev. D* **91**, no. 6, 061303 (2015) [arXiv:1409.3267 [hep-th]]; “Helical Phase Inflation and Monodromy in Supergravity Theory,” arXiv:1412.5093 [hep-th].
- [56] J. Erlich, J. Olsen and Z. Wang, “Multi-field inflation and the field-space metric,” arXiv:1509.06781 [hep-ph].
- [57] M. Peloso and C. Unal, “Trajectories with suppressed tensor-to-scalar ratio in Aligned Natural Inflation,” *JCAP* **1506**, no. 06, 040 (2015) [arXiv:1504.02784 [astro-ph.CO]].

- [58] R. D. Peccei and H. R. Quinn, “Constraints Imposed by CP Conservation in the Presence of Instantons,” *Phys. Rev. D* **16**, 1791 (1977).
doi:10.1103/PhysRevD.16.1791
- [59] See, for example, H. Baer and X. Tata, “Weak scale supersymmetry: From superfields to scattering events,” Cambridge, UK: Univ. Pr. (2006) 537 pp.
- [60] N. Arkani-Hamed, A. G. Cohen, E. Katz, A. E. Nelson, T. Gregoire and J. G. Wacker, “The Minimal moose for a little Higgs,” *JHEP* **0208**, 021 (2002) [hep-ph/0206020].
- [61] B. Grinstein, D. O’Connell and M. B. Wise, “The Lee-Wick standard model,” *Phys. Rev. D* **77**, 025012 (2008) [arXiv:0704.1845 [hep-ph]].
- [62] See, for example, the ATLAS Collaboration summary plots at:
<https://twiki.cern.ch/twiki/bin/view/AtlasPublic/CombinedSummaryPlots>
- [63] W. A. Bardeen, “On naturalness in the standard model,” FERMILAB-CONF-95-391-T, C95-08-27.3.
- [64] R. Hempfling, “The Next-to-minimal Coleman-Weinberg model,” *Phys. Lett. B* **379**, 153 (1996) [hep-ph/9604278]; W. -F. Chang, J. N. Ng and J. M. S. Wu, “Shadow Higgs from a scale-invariant hidden U(1)(s) model,” *Phys. Rev. D* **75**, 115016 (2007) [hep-ph/0701254 [HEP-PH]]; R. Foot, A. Kobakhidze, K. .L. McDonald and R. .R. Volkas, “Neutrino mass in radiatively-broken scale-invariant models,” *Phys. Rev. D* **76**, 075014 (2007) [arXiv:0706.1829 [hep-ph]]; “A Solution to the hierarchy problem from an almost decoupled hidden sector within a classically scale invariant theory,” *Phys. Rev. D* **77**, 035006 (2008) [arXiv:0709.2750 [hep-ph]]; T. Ham-

- bye and M. H. G. Tytgat, “Electroweak symmetry breaking induced by dark matter,” *Phys. Lett. B* **659**, 651 (2008) [arXiv:0707.0633 [hep-ph]]; S. Iso, N. Okada and Y. Orikasa, “Classically conformal B^- L extended Standard Model,” *Phys. Lett. B* **676**, 81 (2009) [arXiv:0902.4050 [hep-ph]]; M. Holthausen, M. Lindner and M. A. Schmidt, “Radiative Symmetry Breaking of the Minimal Left-Right Symmetric Model,” *Phys. Rev. D* **82**, 055002 (2010) [arXiv:0911.0710 [hep-ph]]; R. Foot, A. Kobakhidze and R. R. Volkas, “Stable mass hierarchies and dark matter from hidden sectors in the scale-invariant standard model,” *Phys. Rev. D* **82**, 035005 (2010) [arXiv:1006.0131 [hep-ph]]; L. Alexander-Nunneley and A. Pilaftsis, “The Minimal Scale Invariant Extension of the Standard Model,” *JHEP* **1009**, 021 (2010) [arXiv:1006.5916 [hep-ph]]; A. Farzinnia, H. -J. He and J. Ren, “Natural Electroweak Symmetry Breaking from Scale Invariant Higgs Mechanism,” arXiv:1308.0295 [hep-ph].
- [65] K. A. Meissner and H. Nicolai, “Conformal Symmetry and the Standard Model,” *Phys. Lett. B* **648**, 312 (2007) [hep-th/0612165]; “Effective action, conformal anomaly and the issue of quadratic divergences,” *Phys. Lett. B* **660**, 260 (2008) [arXiv:0710.2840 [hep-th]].
- [66] S. Iso and Y. Orikasa, “TeV Scale B-L model with a flat Higgs potential at the Planck scale - in view of the hierarchy problem -,” *PTEP* **2013**, 023B08 (2013) [arXiv:1210.2848 [hep-ph]]; C. Englert, J. Jaeckel, V. V. Khoze and M. Spannowsky, “Emergence of the Electroweak Scale through the Higgs Portal,” *JHEP* **1304**, 060 (2013) [arXiv:1301.4224 [hep-ph]].

- [67] M. Farina, D. Pappadopulo and A. Strumia, “A modified naturalness principle and its experimental tests,” arXiv:1303.7244 [hep-ph].
- [68] M. Heikinheimo, A. Racioppi, M. Raidal, C. Spethmann and K. Tuominen, “Dark Supersymmetry,” arXiv:1305.4182 [hep-ph].
- [69] M. Heikinheimo and C. Spethmann, “Galactic Centre GeV Photons from Dark Technicolor,” JHEP **1412**, 084 (2014) [arXiv:1410.4842 [hep-ph]]; J. Kubo, K. S. Lim and M. Lindner, “Gamma-ray Line from Nambu-Goldstone Dark Matter in a Scale Invariant Extension of the Standard Model,” JHEP **1409**, 016 (2014) [arXiv:1405.1052 [hep-ph]]; O. Antipin, M. Redi and A. Strumia, “Dynamical generation of the weak and Dark Matter scales from strong interactions,” JHEP **1501**, 157 (2015) [arXiv:1410.1817 [hep-ph]]; J. Kubo, K. S. Lim and M. Lindner, “Electroweak Symmetry Breaking via QCD,” Phys. Rev. Lett. **113**, 091604 (2014) [arXiv:1403.4262 [hep-ph]]; M. Holthausen, J. Kubo, K. S. Lim and M. Lindner, “Electroweak and Conformal Symmetry Breaking by a Strongly Coupled Hidden Sector,” JHEP **1312**, 076 (2013) [arXiv:1310.4423 [hep-ph]]; M. Heikinheimo, A. Racioppi, M. Raidal, C. Spethmann and K. Tuominen, “Physical Naturalness and Dynamical Breaking of Classical Scale Invariance,” Mod. Phys. Lett. A **29**, 1450077 (2014) [arXiv:1304.7006 [hep-ph]]; T. Hur and P. Ko, “Scale invariant extension of the standard model with strongly interacting hidden sector,” Phys. Rev. Lett. **106**, 141802 (2011) [arXiv:1103.2571 [hep-ph]].
- [70] C. D. Carone and H. Georgi, “Technicolor with a massless scalar doublet,” Phys. Rev. D **49**, 1427 (1994) [hep-ph/9308205].

- [71] S. R. Coleman and E. J. Weinberg, “Radiative Corrections as the Origin of Spontaneous Symmetry Breaking,” *Phys. Rev. D* **7**, 1888 (1973).
- [72] J. D. Lykken, “Higgs without SUSY,” talk presented at *The first three years of the LHC*, Mainz, March 18-22, 2013.
- [73] T. Hambye, “Hidden vector dark matter,” *JHEP* **0901**, 028 (2009) [arXiv:0811.0172 [hep-ph]]; C. Arina, T. Hambye, A. Ibarra and C. Weniger, “Intense Gamma-Ray Lines from Hidden Vector Dark Matter Decay,” *JCAP* **1003**, 024 (2010) [arXiv:0912.4496 [hep-ph]].
- [74] M. Pospelov, A. Ritz and M. B. Voloshin, “Secluded WIMP Dark Matter,” *Phys. Lett. B* **662**, 53 (2008) [arXiv:0711.4866 [hep-ph]].
- [75] E. Gildener and S. Weinberg, “Symmetry Breaking and Scalar Bosons,” *Phys. Rev. D* **13**, 3333 (1976); M. Sher, “Electroweak Higgs Potentials and Vacuum Stability,” *Phys. Rept.* **179**, 273 (1989); S. Nie and M. Sher, “Vacuum stability bounds in the two Higgs doublet model,” *Phys. Lett. B* **449**, 89 (1999) [hep-ph/9811234].
- [76] G. Kreyerhoff and R. Rodenberg, “Renormalization Group Analysis Of Coleman-Weinberg Symmetry Breaking In Two Higgs Models,” *Phys. Lett. B* **226**, 323 (1989).
- [77] P. P. Giardino, K. Kannike, M. Raidal and A. Strumia, “Is the resonance at 125 GeV the Higgs boson?,” *Phys. Lett. B* **718**, 469 (2012) [arXiv:1207.1347 [hep-ph]].

- [78] S. Chatrchyan *et al.* [CMS Collaboration], “Search for a standard-model-like Higgs boson with a mass in the range 145 to 1000 GeV at the LHC,” *Eur. Phys. J. C* **73**, 2469 (2013) [arXiv:1304.0213 [hep-ex]].
- [79] M. Heikinheimo, A. Racioppi, M. Raidal and C. Spethmann, “Twin Peak Higgs,” arXiv:1307.7146 [hep-ph].
- [80] T. Hur, D. W. Jung, P. Ko and J. Y. Lee, “Electroweak symmetry breaking and cold dark matter from strongly interacting hidden sector,” *Phys. Lett. B* **696**, 262 (2011) [arXiv:0709.1218 [hep-ph]].
- [81] G. Marques Tavares, M. Schmaltz and W. Skiba, “Higgs mass naturalness and scale invariance in the UV,” *Phys. Rev. D* **89**, no. 1, 015009 (2014) [arXiv:1308.0025 [hep-ph]].
- [82] S. Dubovsky, V. Gorbenko and M. Mirbabayi, “Natural Tuning: Towards A Proof of Concept,” *JHEP* **1309**, 045 (2013) [arXiv:1305.6939 [hep-th]].
- [83] W. Altmannshofer, W. A. Bardeen, M. Bauer, M. Carena and J. D. Lykken, “Light Dark Matter, Naturalness, and the Radiative Origin of the Electroweak Scale,” *JHEP* **1501**, 032 (2015) [arXiv:1408.3429 [hep-ph]].
- [84] J. Guo, Z. Kang, P. Ko and Y. Orikasa, “Accidental Dark Matter: Case in the Scale Invariant Local $B - L$ Models,” arXiv:1502.00508 [hep-ph].
H. Okada and Y. Orikasa, “Classically Conformal Radiative Neutrino Model with Gauged B-L Symmetry,” arXiv:1412.3616 [hep-ph].
S. Benic and B. Radovic, “Majorana dark matter in a classically scale invariant model,” *JHEP* **1501**, 143 (2015) [arXiv:1409.5776 [hep-ph]].
“Electroweak breaking and Dark Matter from the common scale,” *Phys. Lett. B* **732**, 91

(2014) [arXiv:1401.8183 [hep-ph]]; G. M. Pelaggi, “Predictions of a model of weak scale from dynamical breaking of scale invariance,” Nucl. Phys. B **893**, 443 (2015) [arXiv:1406.4104 [hep-ph]]. M. Lindner, S. Schmidt and J. Smirnov, “Neutrino Masses and Conformal Electro-Weak Symmetry Breaking,” JHEP **1410**, 177 (2014) [arXiv:1405.6204 [hep-ph]]; K. Kanike, A. Racioppi and M. Raidal, “Embedding inflation into the Standard Model - more evidence for classical scale invariance,” JHEP **1406**, 154 (2014) [arXiv:1405.3987 [hep-ph]]. A. Farzinnia and J. Ren, “Higgs Partner Searches and Dark Matter Phenomenology in a Classically Scale Invariant Higgs Boson Sector,” Phys. Rev. D **90**, no. 1, 015019 (2014) [arXiv:1405.0498 [hep-ph]]; C. Tamarit, “Higgs vacua with potential barriers,” Phys. Rev. D **90**, no. 5, 055024 (2014) [arXiv:1404.7673 [hep-ph]]; K. Allison, C. T. Hill and G. G. Ross, “Ultra-weak sector, Higgs boson mass, and the dilaton,” Phys. Lett. B **738**, 191 (2014) [arXiv:1404.6268 [hep-ph]]; H. Davoudiasl and I. M. Lewis, “Right-Handed Neutrinos as the Origin of the Electroweak Scale,” Phys. Rev. D **90**, no. 3, 033003 (2014) [arXiv:1404.6260 [hep-ph]]; V. V. Khoze, C. McCabe and G. Ro, “Higgs vacuum stability from the dark matter portal,” JHEP **1408**, 026 (2014) [arXiv:1403.4953 [hep-ph], arXiv:1403.4953]; M. Hashimoto, S. Iso and Y. Orikasa, “Radiative symmetry breaking from flat potential in various U(1)’ models,” Phys. Rev. D **89**, no. 5, 056010 (2014) [arXiv:1401.5944 [hep-ph]]; J. Guo and Z. Kang, “Higgs Naturalness and Dark Matter Stability by Scale Invariance,” arXiv:1401.5609 [hep-ph]; C. T. Hill, “Is the Higgs Boson Associated with Coleman-Weinberg Dynamical Symmetry Breaking?,” Phys. Rev. D **89**, no. 7, 073003 (2014) [arXiv:1401.4185 [hep-ph]]; S. Abel

and A. Mariotti, “Novel Higgs Potentials from Gauge Mediation of Exact Scale Breaking,” *Phys. Rev. D* **89**, no. 12, 125018 (2014) [arXiv:1312.5335 [hep-ph]]; M. Hashimoto, S. Iso and Y. Orikasa, “Radiative symmetry breaking at the Fermi scale and flat potential at the Planck scale,” *Phys. Rev. D* **89**, no. 1, 016019 (2014) [arXiv:1310.4304 [hep-ph]]; T. G. Steele, Z. W. Wang, D. Contreras and R. B. Mann, “Viable dark matter via radiative symmetry breaking in a scalar singlet Higgs portal extension of the standard model,” *Phys. Rev. Lett.* **112**, no. 17, 171602 (2014) [arXiv:1310.1960 [hep-ph]]; E. Gabrielli, M. Heikinheimo, K. Kannike, A. Racioppi, M. Raidal and C. Spethmann, “Towards Completing the Standard Model: Vacuum Stability, EWSB and Dark Matter,” *Phys. Rev. D* **89**, no. 1, 015017 (2014) [arXiv:1309.6632 [hep-ph]]; V. V. Khoze, “Inflation and Dark Matter in the Higgs Portal of Classically Scale Invariant Standard Model,” *JHEP* **1311**, 215 (2013) [arXiv:1308.6338 [hep-ph]]; T. Hambye and A. Strumia, “Dynamical generation of the weak and Dark Matter scale,” *Phys. Rev. D* **88**, 055022 (2013) [arXiv:1306.2329 [hep-ph]]; P. Humbert, M. Lindner and J. Smirnov, “The Inverse Seesaw in Conformal Electro-Weak Symmetry Breaking and Phenomenological Consequences,” arXiv:1503.03066 [hep-ph]; K. Endo and Y. Sumino, “A Scale-invariant Higgs Sector and Structure of the Vacuum,” arXiv:1503.02819 [hep-ph].

- [85] A. Manohar and H. Georgi, “Chiral Quarks and the Nonrelativistic Quark Model,” *Nucl. Phys. B* **234**, 189 (1984); H. Georgi and L. Randall, “Flavor Conserving CP Violation in Invisible Axion Models,” *Nucl. Phys. B* **276**, 241 (1986).

- [86] G. Aad *et al.* [ATLAS and CMS Collaborations], “Combined Measurement of the Higgs Boson Mass in pp Collisions at $\sqrt{s} = 7$ and 8 TeV with the ATLAS and CMS Experiments,” arXiv:1503.07589 [hep-ex].
- [87] J. R. Espinosa, C. Grojean, M. Muhlleitner and M. Trott, “First Glimpses at Higgs’ face,” JHEP **1212**, 045 (2012) [arXiv:1207.1717 [hep-ph]].
- [88] C. L. Bennett *et al.* [WMAP Collaboration], “Nine-Year Wilkinson Microwave Anisotropy Probe (WMAP) Observations: Final Maps and Results,” Astrophys. J. Suppl. **208**, 20 (2013) [arXiv:1212.5225 [astro-ph.CO]].
- [89] J. R. Ellis, A. Ferstl and K. A. Olive, “Reevaluation of the elastic scattering of supersymmetric dark matter,” Phys. Lett. B **481**, 304 (2000) [hep-ph/0001005].
- [90] J. Preskill, S. P. Trivedi, F. Wilczek and M. B. Wise, “Cosmology and broken discrete symmetry,” Nucl. Phys. B **363**, 207 (1991).

VITA

Raymundo Ramos

Name: Raymundo Alberto Ramos

Date and place of birth: January 5, 1988. Colima, COL, México

Address: Department of Physics, College of William and Mary,
300 Ukrop Way. Williamsburg, VA 23185

Phone: (757) 221-1986

Email: raramos@email.wm.edu

Education

- B.S. Physics, University of Colima, Mexico, 2010.
- M.S. Physics, College of William and Mary, 2013.
- Ph.D. Physics, College of William and Mary, 2016.

Research Experience

- 2009-2010: 1 year of undergraduate Research, School of Sciences, University of Colima, Advisor: Prof. Alfredo Aranda.
- 2010-2011: 1 year of graduate Research, School of Sciences, University of Colima, Advisor: Prof. Alfredo Aranda.

- Summer 2012: Summer Research, Department of Physics, College of William and Mary, Advisor: Prof. Christopher Carone.

Awards & Grants

- “Ruben Vizcarra Campos” Excellence Award, July 2008, July 2009.

Teaching Experience

- **Teaching Assistant.** Statistical Mechanics and Thermodynamics, Fall Semester 2011, College of William and Mary.
- **Teaching Assistant.** General Physics, Fall Semester 2011, College of William and Mary.
- **Teaching Assistant.** Introduction to Quantum Physics, Fall Semester 2012, College of William and Mary.
- **Teaching Assistant.** Introduction to Mathematical Physics, Spring Semester 2012, Spring Semester 2013, College of William and Mary.
- **Teaching Assistant.** General Physics - Honors, Spring Semester 2012, Spring Semester 2013, College of William and Mary.

Professional Development

- **VI Fundamental Physics School**, BUAP, Puebla, Mexico, May, 2010.

- **42nd SLAC Summer Institute**, SLAC National Accelerator Laboratory, Menlo Park, California, August, 2014.

Publications

1. A. Aranda, C. Bonilla, R. Ramos and A. D. Rojas, “Model of flavor with quaternion symmetry,” *Phys. Rev. D* **84**, 016009 (2011) [arXiv:1105.6373 [hep-ph]].
2. C. D. Carone and R. Ramos, “Classical scale-invariance, the electroweak scale and vector dark matter,” *Phys. Rev. D* **88**, 055020 (2013) [arXiv:1307.8428 [hep-ph]].
3. H. Davoudiasl, W. J. Marciano, R. Ramos and M. Sher, “Charged Higgs Discovery in the W plus ”Dark” Vector Boson Decay Mode,” *Phys. Rev. D* **89**, no. 11, 115008 (2014) [arXiv:1401.2164 [hep-ph]].
4. C. D. Carone, R. Ramos and M. Sher, “LHC Constraints on the Lee-Wick Higgs Sector,” *Phys. Lett. B* **732**, 122 (2014) [arXiv:1403.0011 [hep-ph]].
5. C. D. Carone, J. Erlich, M. Sher and R. Ramos, “Permutation on hybrid natural inflation,” *Phys. Rev. D* **90**, no. 6, 063521 (2014) [arXiv:1407.6017 [hep-ph]].
6. C. D. Carone and R. Ramos, “Dark chiral symmetry breaking and the origin of the electroweak scale,” *Phys. Lett. B* **746**, 424 (2015) [arXiv:1505.04448 [hep-ph]].

7. C. D. Carone, R. Ramos and Z. Wang, “Flavored axion-monodromy inflation,”
Phys. Rev.D **92**, no. 11, 116011 (2015) [arXiv:1509.08013 [hep-ph]].